EXPERIMENTAL INVESTIGATION OF THE HEAT TRANSFER CHARACTERISTICS OF A RADIO FREQUENCY SURGICAL PROBE

Richard Gordon Katz

NAVAL POSTGRADUATE SCHOOL
Monterey, California

THESIS

EXPERIMENTAL INVESTIGATION OF THE
HEAT TRANSFER CHARACTERISTICS OF A
RADIO FREQUENCY SURGICAL PROBE

by

Richard Gordon Katz

Thesis Advisor: Thomas E. Cooper

March 1973

Approved for public release; distribution unlimited.

Experimental Investigation of the Heat Transfer Characteristics of a Radio Frequency Surgical Probe

by

Richard Gordon Katz
Lieutenant Commander, United States Navy
B.S., United States Naval Academy, 1964

Submitted in partial fulfillment of the
requirements for the degree of

MASTER OF SCIENCE IN MECHANICAL ENGINEERING
and
MECHANICAL ENGINEER
from the
NAVAL POSTGRADUATE SCHOOL
March 1973

ABSTRACT

Liquid crystals, a material that exhibits brilliant changes in color over narrow temperature bands, have been successfully used to study the temperature field produced by spherical and cylindrical radio frequency surgical probes. An agar-water mixture was used to simulate tissue. Experimental temperature data were obtained by photographing the liquid crystal material through the clear agar. Comparison of experimental data with an existing theoretical solution was excellent, agreeing within 8% for the spherical probe. However, the cylindrical data and cylindrical theory agreed only to within 30%, the large discrepancy being attributed to edge effects.

TABLE OF CONTENTS

LIST OF ILLUSTRATIONS

NOMENCLATURE

Symbol	Description	Typical Units
A	Surface area	cm^2
$\mathring{A}$	Wavelength	Angstrom
b	Number of flow tubes	
C	Volumetric heat capacity	cal/cm^3 °C
°C	Temperature in degrees Centigrade	
D	Diameter	cm
E	Electric potential	volts
f	Frequency	hertz
G	Nondimensional power	
G'	Corrected nondimensional power	
$\mathcal{I}$	Current density	$amps/cm^2$
I	Radio frequency current	amps
i	Coordinate of nodal point along distance axis in finite difference formulation	
k	Thermal conductivity	W/m °K
L	Length	cm
M	Stability criterion for finite difference formulation	
m	Slope of nondimensional resistivity curve	
n	Coordinate of nodal point along time axis in finite difference formulation	
R	Nondimensional radius to an isotherm	
R_{10}	Ten ohm-ten watt resistor	

r_o	Probe radius	cm
r	Radius	cm
r_i	Isotherm radius	cm
T	Temperature	°C
t	Time	seconds
V	Voltage	volts
α	Thermal diffusivity	cm^2/sec
γ	Slope of dimensional resistivity curve	
η	Ratio of speed of light in air to that in water	
θ	Nondimensional temperature	
λ	Wavelength	Angstrom
ρ	Resistivity	ohm-cm
$\tilde{\rho}$	Nondimensional resistivity	
τ	Nondimensional time	
ϕ	General potential	
ω	Uncertainty	
∇	Del operator	

SUBSCRIPTS

o	Initial conditions
10	At the ten ohm resistor
cct	In the circuit
i	Of the ith component
p	From the photographs
cyl	With reference to the cylindrical probe
sphere	With reference to the spherical probe

NONDIMENSIONAL QUANTITIES

$$\theta = \frac{T - T_o}{T_o}$$ Temperature

$$\tau = \frac{\alpha t}{r_o^2}$$ Time

$$G_o = \frac{I^2 \rho_o r_o^2}{A^2 k T_o}$$ Power

$$R = \frac{r}{r_o}$$ Distance

$$\tilde{\rho} = \frac{\rho}{\rho_o} = 1 + m\theta$$ Resistivity

ACKNOWLEDGEMENT

The encouragement and guidance provided by Professor Thomas E. Cooper has been a valuable asset during this project. His advice and assistance are greatly appreciated. As valuable has been the support and confidence of my wife, Margie, to whom this thesis is dedicated.

I. INTRODUCTION

In neurosurgery, radio frequency current has been used to create lesions, thus alleviating conditions such as acute pain and Parkinsonism. A current emitting electrode, similar to a hypodermic needle, is inserted into the brain through the skull. An inactive electrode is placed elsewhere on the body in an area of high conductivity. Radio frequency current, at a low power level, is passed between the electrodes and electrical energy is transformed to heat in the tissue with the resultant rise in temperature destroying the tissue.

To accurately use the radio frequency technique, a surgeon must know the exact location of the electrode (probe) tip in the brain, the volume of tissue to be destroyed, the thermal and electrical properties of the tissue [1], and the temperature near the probe tip. Thermocouples and thermistors attached to the probe have been used to monitor probe tip temperatures [2, 3, 4]. However, these temperature sensors indicated the temperature of the probe, not the tissue temperature itself. Additionally, the sensors were nearly as large as the probe tip and may have distorted the thermal field by acting as thermal sinks. Without accurate knowledge of tissue temperature, tissue boiling occurred with attendant gas formation and tissue carbonization [4]. These effects resulted in irregular shaped lesions and unpredictable damage along the entrance path of the probe into the tissue.

The objectives of this thesis were twofold. First, to experimentally determine the thermal field produced by a radio frequency probe embedded in a resistive agar medium. Liquid crystals, a material that indicates temperature through a color change, were used as the temperature sensors.

The second objective was to compare experimental data with results predicted using a theoretical heat transfer model of the radio frequency probe [5]. The general theoretical model included the effects of tissue metabolism and blood profusion. These two effects have been excluded from the present investigation since the thermal field was generated in an inert gel-like substance.

The temperature fields produced by spherical and cylindrical radio frequency probes were successfully studied with the liquid crystal material. , The crystals, with their low thermal capacity [6], produced brilliant, undistorted, continuous displays of several selected isotherms surrounding the probes. Agreement between the theoretically predicted and experimentally measured values of temperature for the spherical probe was excellent (8%). Agreement between theory and experiment for the cylindrical probe was not good (30%). The large differences observed in the cylindrical case are attributed to edge effects. The theory assumed an infinitely long probe while the experiment employed probes with length to diameter ratios of 4, 10, and 20. The edge effects were clearly displayed by the liquid crystals.

II. HISTORICAL BACKGROUND

Use of radio frequency current to create physiologic lesions is not new. Carpenter and Whittier [7] describe early investigations into the uses of radio frequency current as a surgical tool. Aronow [1] was the first investigator of recent time to study the problem of radio frequency current in tissue. Lesion formation using radio frequency current is accomplished by inserting into the tissue a small hypodermic needle which is electrically insulated except at the tip. This electrode acts as the active, current emitting electrode. A larger, inactive electrode is placed elsewhere on the body. The path of current conduction, i.e. the body, acts as a leaky dielectric by dissipating electrical energy in the form of heat [1]. This Joulean heating effect results in a local rise in tissue temperature. When tissue temperature is increased to 55°C, tissue destruction occurs. Accurate prediction of when tissue in the probe tip region has reached this temperature has been a major problem with the radio frequency probe.

Excessive tip temperature causes gas formation and tissue carbonization which results in poor prediction of lesion size and additional damage along the path of electrode insertion [4]. Studies with thermocouples and thermistors have been conducted to correlate electrode temperature with lesion size [2, 3]. Since heating takes place in the tissue and not in the electrode, the sensors inside the probe tip indicate only that temperature rise caused by conduction from the tissue back into the electrode. This temperature rise may be less than the maximum tissue temperature. Therefore, reliable prevention of excessive tip temperature has been difficult. The same type of tissue temperature measurement problem occurs with the direct current probe, [5].

The direct current probe has a more serious liability than the tissue temperature measurement problem. Direct current has preferred paths in the body which results in irregular lesions. Death may occur if the direct current finds a path to the heart. Preferred paths in the body do not appear to be a problem with the radio frequency or the high resistance probe.

The high resistance probe consists of a high resistance iron-nickel alloy wrapped around a nonconductive rod. Electrical current is passed through the wire causing the probe to be heated. Groff's study of the high resistance probe [8] demonstrated the feasibility of producing controlled, predictable heated regions in agar. In opposition to the radio frequency probe, where heating occurs in the tissue, the high resistance probe itself generates heat. Thermal energy is then transferred to the tissue by conduction. Prediction of the magnitude of the temperature field produced by a high resistance probe thus requires knowledge of only the thermal properties of the medium. Another advantage of the high resistance probe is the fact that a surgeon may check for proper probe tip location before forming the lesion.

Probe tip location may be verified by raising the tissue temperature to 40-49°C using low current levels. Increasing temperature into this range blocks nerve functioning but does not cause permanent damage. This technique, equally applicable to the high resistance and the radio frequency probe, is especially helpful in treating Parkinsonism. As the temperature increases, shaking diminishes and stops when the probe tip has been properly located. Lesion formation is then accomplished by increasing the local tissue temperature to 55°C, being careful to prevent excessive tip temperatures that result in tissue boiling.

While the high resistance probe requires knowledge of only the thermal properties of tissue, the radio frequency probe requires knowledge of both thermal and electrical properties. Geddes and Baker [9] discuss difficulties in obtaining electrical properties of tissue. Since tissues are composed of cells, different properties may be exhibited depending on the cell orientation. Other factors influencing the electrical property values include age, history, and environment of the tissue. Tissue properties measured IN VITRO differ from those measured IN VIVO. Thermal properties, on the other hand, are reliably predicted based on the tissue water content [10]. The prediction of lesion size based on the magnitude and duration of radio frequency current and tissue electrical properties is, therefore, more complex when using the radio frequency probe than when using the high resistance probe.

III. THEORETICAL DEVELOPMENT

A. SPHERICAL PROBE

Consider a spherical probe, of radius r_o, which continuously emits radio frequency current, I, into a medium that is homogeneous and infinite in extent. Assume that the medium possesses electrical resistivity, ρ, thermal conductivity, k, and volumetric heat capacity, C. Gengler [5] has derived the basic equation which accounts for the thermal effects produced in the medium due to the Joulean heating effects of the radio frequency current:

$$\frac{1}{r^2}\,\frac{\partial\left[kr^2\,\frac{\partial T}{\partial r}\right]}{\partial r} + \frac{I^2\rho}{16\pi^2 r^4} = C\,\frac{\partial T}{\partial t} \qquad (1)$$

In the present investigation, the experimental test medium, an agar-water mixture, was found to exhibit an electrical resistivity that varied linearly with temperature:

$$\rho = \rho_o + \gamma(T - T_o) \qquad (2)$$

where the subscript indicates an initial, reference condition. Substitution of Equation (2) into Equation (1) yields:

$$\frac{1}{r^2}\,\frac{\partial\left[kr^2\,\frac{\partial T}{\partial r}\right]}{\partial r} + \frac{I^2\rho_o}{16\pi^2 r^4} + \frac{I^2\gamma\,(T - T_o)}{16\pi^2 r^4} = C\,\frac{\partial T}{\partial t} \qquad (3)$$

Assuming that k and C are constant, Equation (3) may be normalized by introducing the following non-dimensional quantities:

$$R = \frac{r}{r_o} \qquad \text{Distance}$$

$$\tau = \frac{kt}{Cr_o^2} = \frac{\alpha t}{r_o^2} \qquad \text{Time}$$

$$\theta = \frac{T - T_o}{T_o} \qquad \text{Temperature}$$

$$G_o = \frac{I^2 \rho_o r_o^2}{k T_o} \qquad \text{Power}$$

$$\tilde{\rho} = \frac{\rho}{\rho_o} = 1 + m\theta \qquad \text{Resistivity}$$

$$m = \frac{\gamma T_o}{\rho_o}$$

where $I = \frac{I}{4\pi r_o^2} = \frac{I}{A}$ the current flux.

Substitution into Equation (3) yields:

$$\frac{1}{R^2} \frac{\partial\left[R^2 \frac{\partial\theta}{\partial R}\right]}{\partial R} + \frac{G_o}{R^4}\left(1 + m\theta\right) = \frac{\partial\theta}{\partial\tau} \qquad (4)$$

The boundary and initial conditions are:

a) at the probe surface, there is no heat conduction back into the probe,

$$\left(\frac{\partial\theta}{\partial R}\right)_{R=1} = 0; \qquad (5)$$

b) the temperature field is undistorted at large distances from the probe,

$$R \to \infty, \ \theta \to 0; \qquad (6)$$

c) the medium is initially at uniform temperature,

$$\tau = 0, \ \theta = 0. \tag{7}$$

Equations (4), (5), (6), and (7) may be cast in explicit finite difference form as [5]

$$\frac{1}{\Delta R^2}\left[\left(1 - \frac{1}{i}\right)\theta_{i-1}^{n} + \left(1 + \frac{1}{i}\right)\theta_{i+1}^{n} - 2\theta_{i}^{n}\right] + \frac{G_o}{(i\Delta R)^4} + \frac{mG_o\theta_i^n}{(i\Delta R)^4} = \frac{\theta_i^{n+1} - \theta_i^n}{\Delta\tau} \tag{4a}$$

$$\theta_{i^*-1}^{n} = \theta_{i^*+1}^{n} \tag{5a}$$

$$\theta_{N-1}^{n} = \theta_{N+1}^{n} \tag{6a}$$

$$\theta_i^o = 0.0 \tag{7a}$$

where i and n define the coordinates of a nodal point in an R, τ network such that the nondimensional temperature at time $\tau = n\Delta\tau$ and radial location $R = i\Delta R$ is defined as θ_i^n ; i* is at R = 1; $i = i^*, i^* + 1, \ldots, N-1, N$. Solving Equation (4a) for θ_i^{n+1} yields:

$$\theta_i^{n+1} = \frac{\Delta\tau}{\Delta R^2}\left[\left(1 - \frac{1}{i}\right)\theta_{i-1}^n + \left(1 + \frac{1}{i}\right)\theta_{i+1}^n\right] + \theta_i^n\left(1 - 2\frac{\Delta\tau}{\Delta R^2} + \frac{\Delta\tau m G_o}{(i\Delta R)^4}\right) + \frac{\Delta\tau G_o}{(i\Delta R)^4}$$

Define $M = \Delta\tau/\Delta R^2$, then

$$\theta_i^{n+1} = M\left[\left(1 - \frac{1}{i}\right)\theta_{i-1}^n + \left(1 + \frac{1}{i}\right)\theta_{i+1}^n\right] + \theta_i^n\left(1 - 2M + \frac{Mm\Delta R^2 G_o}{(i\Delta R)^4}\right) + \frac{\Delta\tau G_o}{(i\Delta R)^4} \quad (8)$$

Since an explicit finite difference scheme has been employed, a stability criterion must be stated to limit the size of the time step based on the value of incremental distance (ΔR). Discussions of stability may be found in References 11 and 12. The stability criterion for this problem becomes

$$1 - 2M + \frac{Mm\Delta R^2 G_o}{(i\Delta R)^4} \geq 0$$

Solving for M and assuming the worse case,

$$M = \frac{1}{2 - \frac{m\Delta R^2 G_o}{(i\Delta R)^4}} \quad (9)$$

Since M was originally defined as $\Delta\tau/\Delta R^2$, choosing a value of ΔR^2 fixes the value of $\Delta\tau$.

Computer program I (Appendix E) was used to solve Equation (8) subject to boundary, initial, and stability conditions (Equations 5a, 6a, 7a, and 9). Reference 13 states that the error in an explicit difference approximation is on the order of ΔR^2. By varying the size of the ΔR increments and plotting temperature versus ΔR^2, it was possible to extrapolate the exact value of temperature. Figure 1 represents this technique, known as

Richardson's technique, for the spherical probe. It can be seen that using a value of $\Delta R = 0.1$ yielded theoretical results within 2% of the exact value.

B. CYLINDRICAL PROBE

Paralleling the development of the basic equations for the spherical probe, the equation for the cylindrical probe in nondimensional form is:

$$\frac{1}{R}\,\frac{\partial\left(R\,\frac{\partial\theta}{\partial R}\right)}{\partial R} + \frac{G_o}{R^2} = \frac{\partial\theta}{\partial\tau} \tag{10}$$

where $G_o = \dfrac{I^2\rho_o r_o^2}{kT_o}$

$$I = \frac{I}{A} = \frac{I}{2\pi r_o L}$$

Substituting $G = G_o(1 + m\theta)$ into Equation (10) and transforming to finite difference form yields:

$$\theta_i^{n+1} = M\left[\left(1 - \frac{1}{2i}\right)\theta_{i-1}^n + \left(1 + \frac{1}{2i}\right)\theta_{i+1}^n\right] + \theta_i^n\left(1 - 2M + \frac{mG_oM}{i^2}\right) + \frac{G_oM}{i^2} \tag{11}$$

The appropriate boundary conditions are:

$$\theta_{i^*-1}^n = \theta_{i^*+1}^n$$

$$\theta_{N-1}^n = \theta_{N+1}^n$$

$$\theta_i^o = 0.0$$

Figure 1
Richardson's Technique
applied to a spherical probe in
a medium with variable resistivity

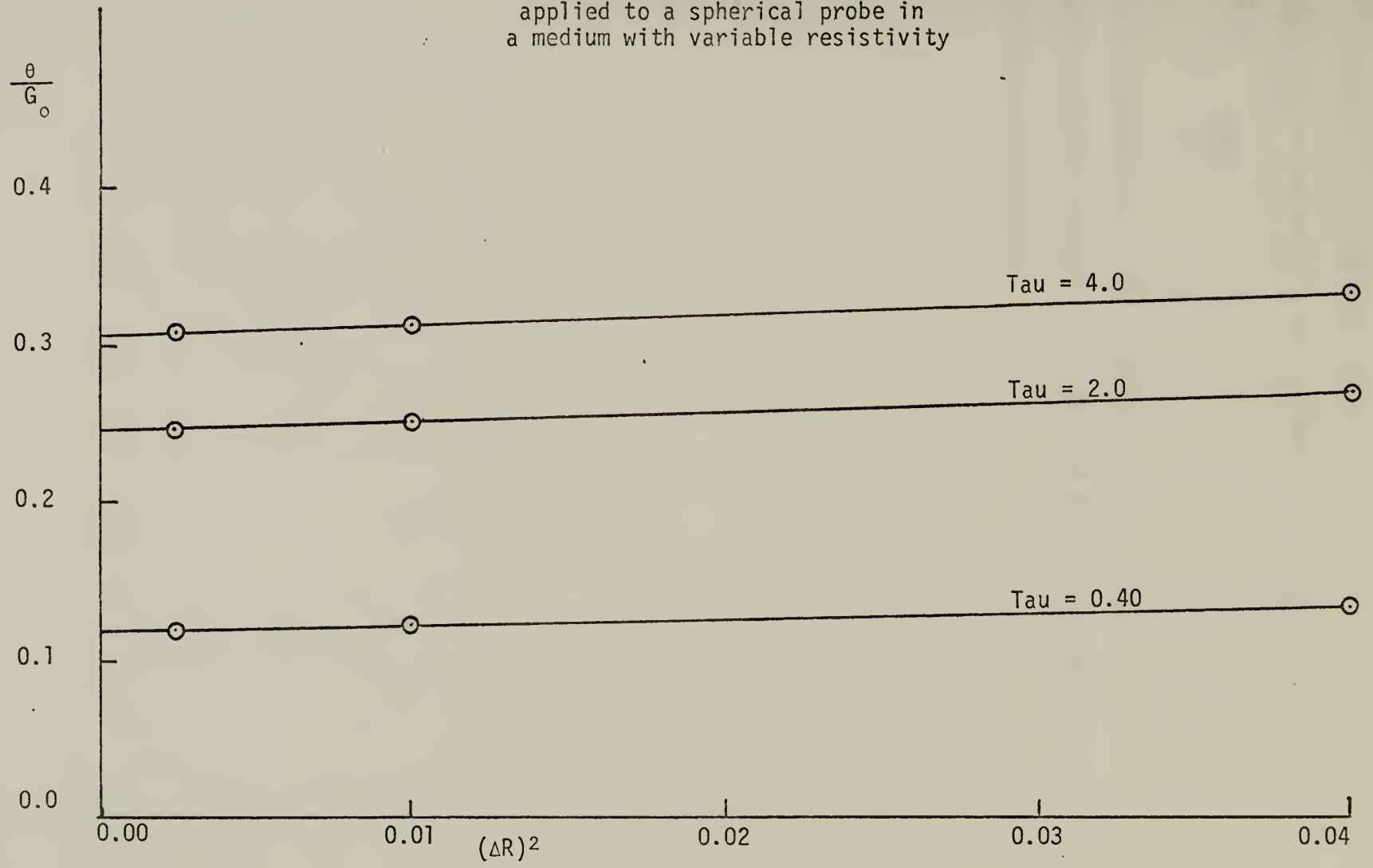

where i* corresponds to R = 1.0

$$i = i^*, i^* + 1, \ldots, N-1, N$$

The stability criterion for the cylindrical case is:

$$M = \frac{1}{2 - \frac{mG_o}{i^2}}$$

where M is defined as in the spherical case as $\Delta\tau/\Delta R^2$.

Computer program II (Appendix E) was used to generate the numerical solution to this problem.

IV. EXPERIMENT

A. EQUIPMENT

A radio frequency generator, Model RFG-2AV, manufactured by Radionics Incorporated of Burlington, Massachusetts, was used in the present investigation to generate radio frequency current. Output from the generator was a continuous, unmodulated sine wave at 500 kilohertz with a maximum power of 18 watts. Although the generator included a built-in radio frequency voltmeter and radio frequency milliammeter, two independent RMS meters were utilized in data collection to allow the use of more sensitive scales where required. Figure 2 displays the generator, voltmeters, and one of the experimental probe test cells used in the experiments. Figure 3 is a schematic of the circuitry used.

Both spherical and cylindrical radio frequency probe geometries were studied experimentally. An agar-water mixture (a gel-like substance) was used to simulate tissue. The mixture was contained in the test cells shown in Figure 4. In both cells, at least 25 probe radii separated the probe from the nearest solid boundary. Thus the cells could be considered as surfaces at infinity in relation to the probes. Plexiglass was used for the probe-agar cells due to its transparence and because it is a dielectric at the low power levels used during experimentation. Boundary conditions were changed from insulated surfaces to conductive surfaces by lining the inside surfaces of the cells with conductive foil. The current path was then from the probe, through the agar medium, to the foil with electrical energy dissipated as heat in the agar.

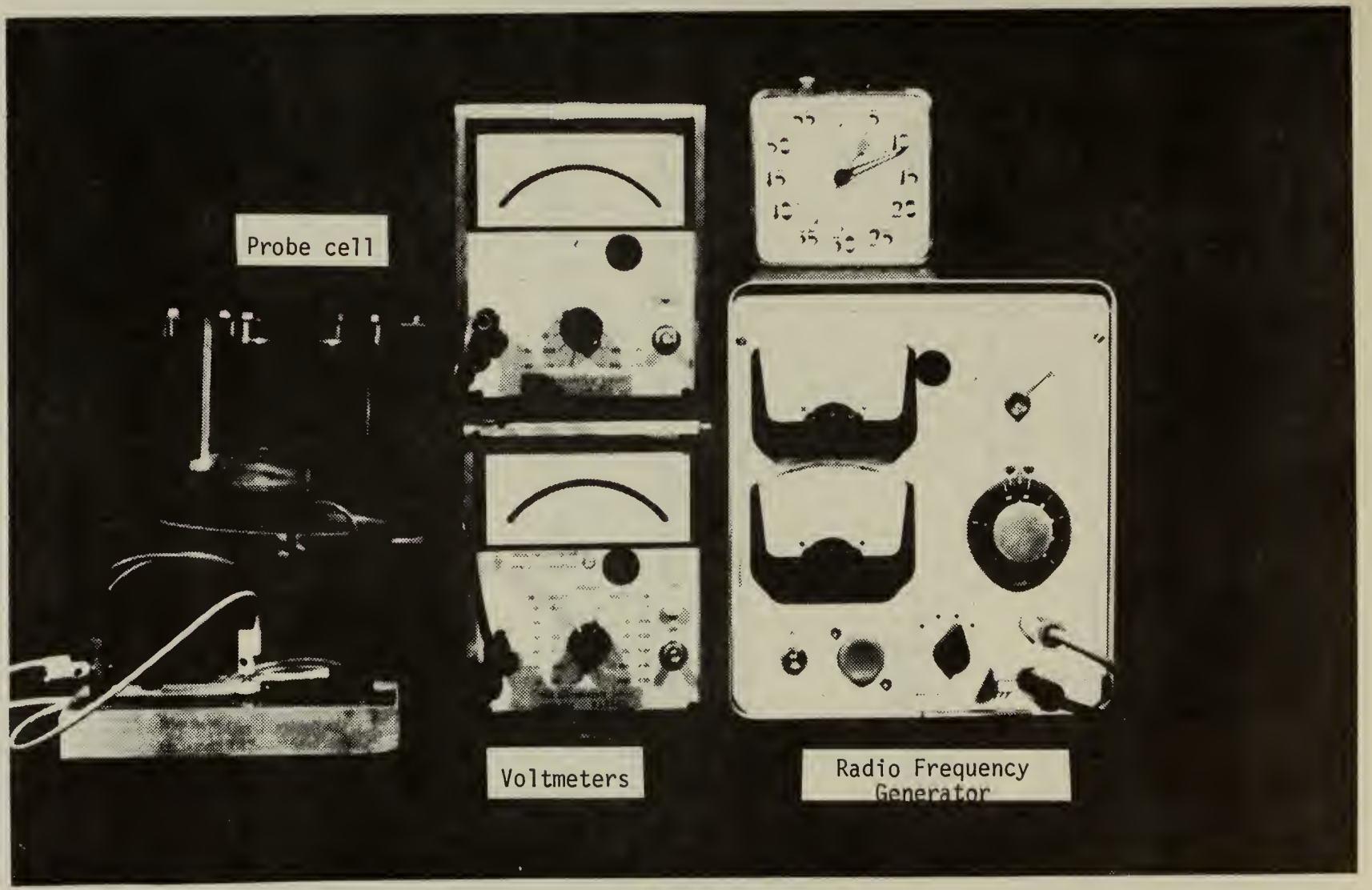

Figure 2. Experimental Equipment

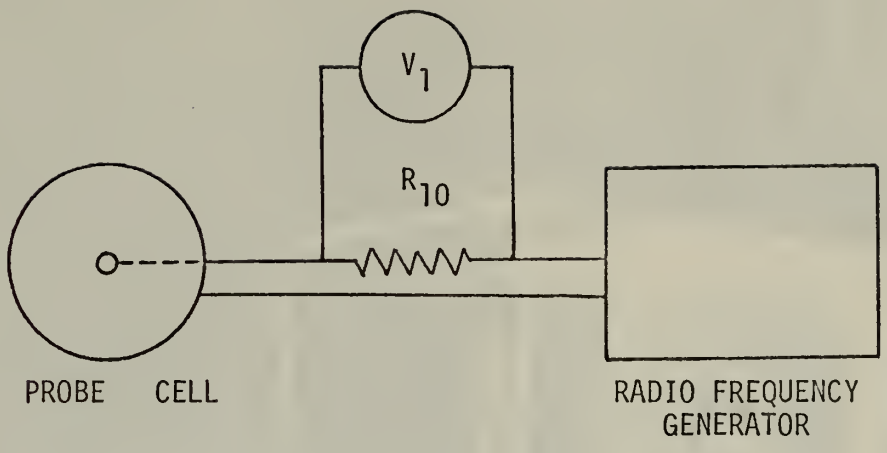

Voltmeter V_1 measured the voltage drop across the ten ohm resistor R_{10}. Circuit current was determined from the two quantities using Kirchoff's Law.

Circuitry for radio frequency probe experiments

Figure 3

Figure 4. Probe Test Cells

Local temperature increases in the agar were measured by use of liquid crystals. Appendix B presents a complete discussion of liquid crystals. Briefly, liquid crystals change color at specific temperatures, the particular temperature depending on the crystal in use. The color change thus allows a continuous display of isotherm fronts for the mapping of thermal regions.

In the experiments, liquid crystals manufactured by National Cash Register and Hoffman-LaRoche were used. The Hoffman-LaRoche liquid crystal, ROCHROME, was provided in the form of a tape which could be applied directly to the object under study. The National Cash Register liquid crystals were obtained in liquid form. The crystals are actually encapsulated in spheres 5 to 30 microns in diameter, thus preventing contamination of the crystal. Due to this encapsulation procedure, it was possible to mix different liquid crystals together without changing the characteristics of any single crystal. Several distinct sets of isotherms were viewed since the liquid crystals mixed did not have temperature ranges that overlapped.

In the experiments, three liquid crystals were mixed together and were applied to a transparent 0.003 inch mylar substrate. The liquid crystals were then covered with black paint and polyurathane varnish. The black background was required to absorb the light transmitted through the liquid crystals; the polyurathane varnish sealed the black paint. Sealing the system in this manner allowed repeated use of the liquid crystal system. Figure 5 displays the liquid crystal sheet encased in the holders used in the test cells.

Prior to experimental trials, the crystals were calibrated using the Rosemount Constant Temperature Bath following the procedure of

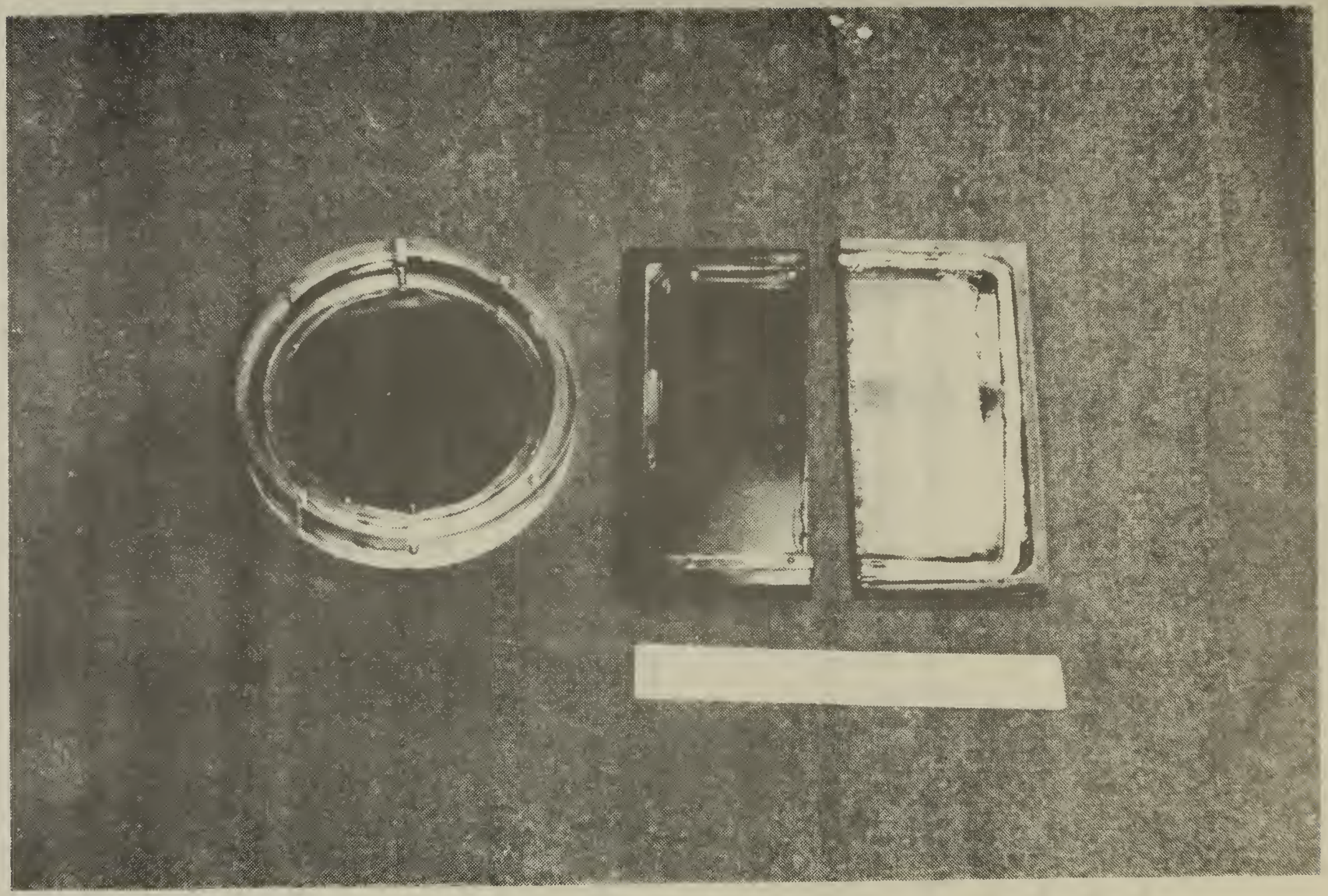

Figure 5. Liquid Crystal Holders

Petrovic [14]. The following liquid crystals were calibrated and subsequently used in experimental trials:

Table 1

Manufacturer	Designation	Red	Green	Blue
National Cash Register	R-27	26.7°C	27.9°C	28.9°C
Hoffman-LaRoche	Rochrome	29.9°C	31.5°C	34.2°C
National Cash Register	R-37	35.7°C	37.0°C	38.5°C
National Cash Register	R-53	50.5°C	52.1°C	53.3°C

Data were collected at specified times after application of power by photographing the isotherms displayed on the liquid crystal sheet. Distances from the probe center to an isotherm (color band) under consideration were easily measured from the photographs.

B. EXPERIMENTAL PROCEDURE

The agar solution was prepared by adding 3.0 grams of DIFCO "BACTO-AGAR" powder to 997 grams of boiling distilled water. When the powdered agar had thoroughly dissolved, a 100 ml. sample was taken to fill the resistivity test cell which was used to determine the variation of resistivity with temperature (see Appendix A). Prior to jelling, the remaining agar solution was poured into one of the probe test cells. The liquid crystal sheet was positioned and the probe located such that a probe diameter was in the plane of the liquid crystals. The entire apparatus was then cooled for approximately six hours to achieve a uniform temperature in the agar. At that time the initial agar temperature was recorded, the generator circuit was connected, and power was applied. Photographs of the liquid crystal sheet were taken through the agar at specified times, thus recording the color change in the liquid crystals. Distances were

measured directly from the pictures and were scaled with respect to the probe radius to form a nondimensional distance.

All quantities were nondimensionalized to allow general application of the data. The following nondimensional quantities were used (5):

$$R = \frac{r_i}{r_o} \qquad \text{Distance}$$

$$\tau = \frac{\alpha t}{r_o^2} \qquad \text{Time}$$

$$\theta = \frac{T - T_o}{T_o} \qquad \text{Temperature}$$

$$G_o = \left(\frac{I}{A}\right)^2 \frac{\rho_o r_o^2}{k T_o} \qquad \text{Power}$$

$$\tilde{\rho} = 1 + m\theta \qquad \text{Resistivity}$$

where

A = surface area of the probe (cm^2)
  for the sphere $4\pi r_o^2$
  for the cylinder $2\pi r_o L$

r_i = distance from the probe center to the outer edge of the isotherm (color band) under consideration (cm)

r_o = probe radius (cm)

α = thermal diffusivity (cm^2/sec)

t = time (sec)

T = isotherm temperature (°C)

T_o = initial agar temperature (°C)

I = radio frequency current (amps)

ρ_o = initial agar resistivity (ohm-cm)

k = thermal conductivity (W/cm °K)

Using a constant temperature-power ratio (θ/G_o), curves were plotted for distance (R) versus time (τ) based on the solution of the finite difference equations for the probe geometry under investigation (Equations 8 or 11). The curves were then compared to the experimental data points of nondimensional isotherm location (R) at various times (τ). An uncertainty analysis was conducted and is presented in Appendix D.

V. EXPERIMENTAL RESULTS

A. SPHERICAL PROBE

Figure 6 is a series of photographs of the growth of the radial temperature field around the spherical probe at nondimensional times of 1.5, 3.1, 6.2, and 12.5 (corresponding to times of 60, 120, 240, and 480 seconds for a spherical probe of radius 0.24 cm.). In Figure 6c, the isotherms used in data collection are labeled for reference. The temperature-color relationships used in data collection were:

Liquid Crystal	Temperature	Color
R-27	27.9°C	Green
Rochrome	29.9°C	Red
R-37	37.0°C	Green

The R-53 appeared on the photograph at large times, but was not actually used in data reduction and comparison with theory. Values of nondimensional radius (R) and time (τ) were plotted for comparison with the theoretical curves based on temperature-power ratios (θ/G_o). Figures 7 and 8 are representative of the comparisons. The dotted lines are the uncertainty limits, which are discussed in Appendix D. Experimental results were within 8% of the theoretical values. Thus, the spherical theory, taking into account variable resistivity, was verified by the experimental procedure of using liquid crystals to determine thermal changes.

Figure 6a
Tau = 1.5 t = 60 sec.

Figure 6b
Tau = 3.1 t = 120 sec.

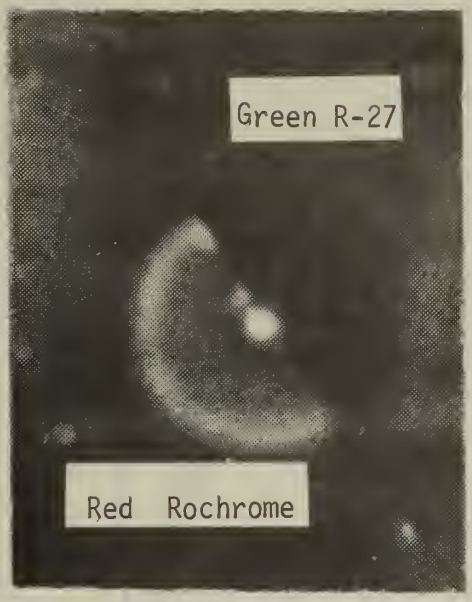

Figure 6c
Tau = 6.2 t = 240 sec.

Figure 6d
Tau = 12.5 t = 480 sec.

Figure 6. Spherical transient temperature field growth with probe diameter of 0.241 cm.

Figure 7

Nondimensional isotherm radii
vs.
nondimensional time for a spherical
probe of diameter 0.482 cm.
Data set I

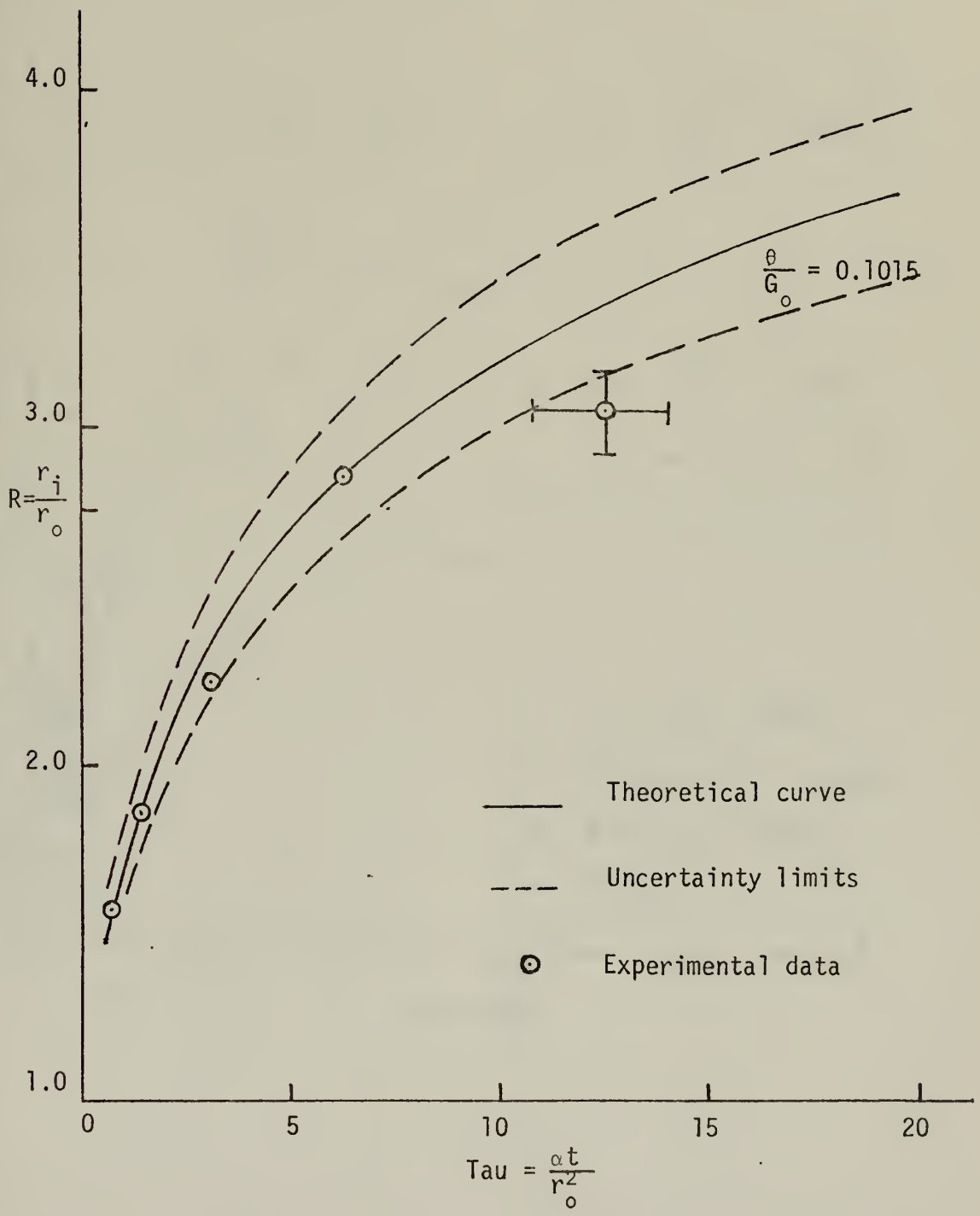

Figure 8

Nondimensional isotherm radii
vs.
nondimensional time for a spherical
probe of diameter 0.482 cm
using three liquid crystals.
Data set J

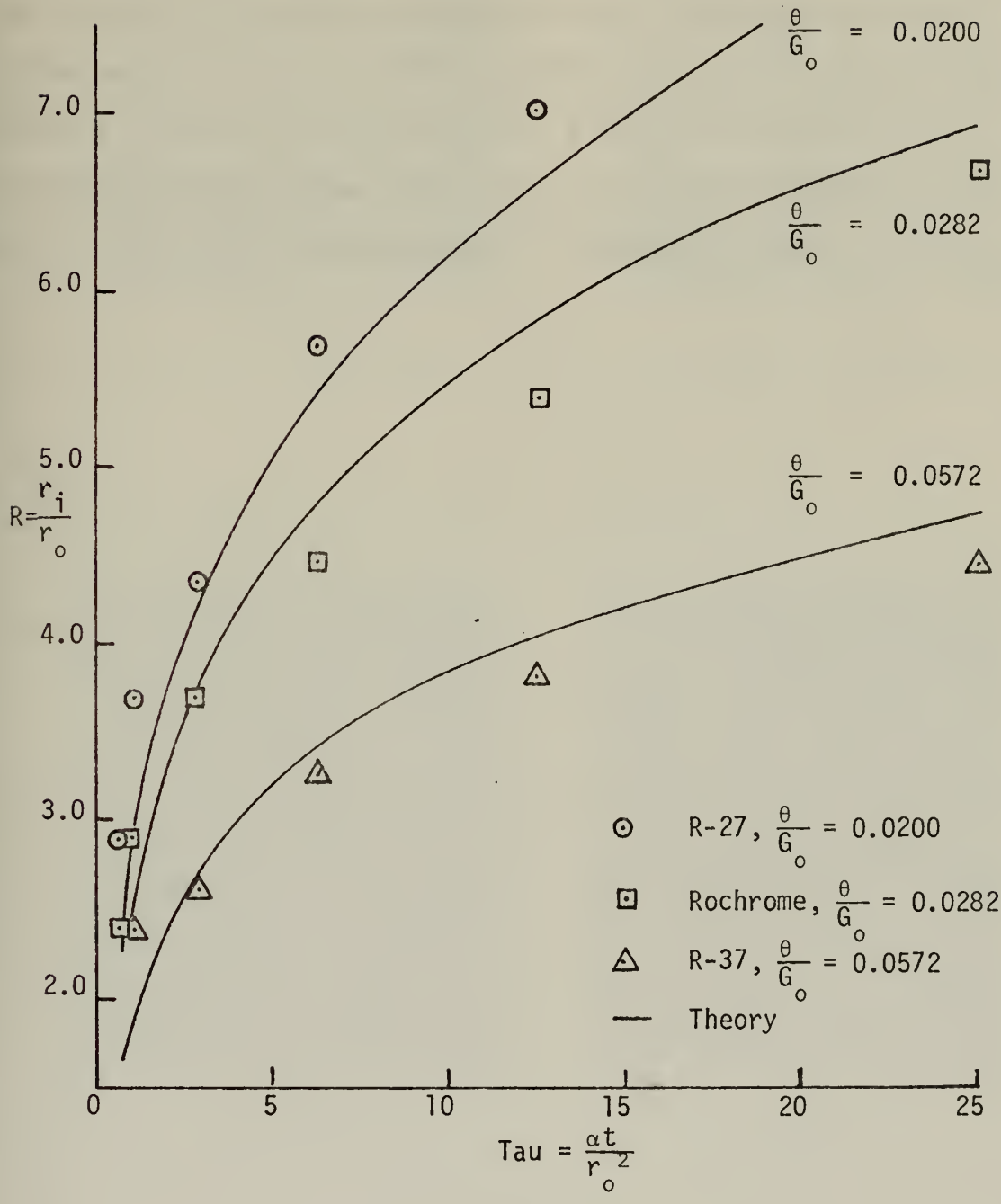

B. CYLINDRICAL PROBE

Figures 9, 10, and 11 display the experimentally determined transient temperature field at nondimensional times of 4.2, 6.25, 9.3, and 12.5 (corresponding to times of 40, 60, 90, and 120 seconds for a cylindrical probe of radius 0.12 cm.). The length to diameter ratios used were 4, 10, and 20 in Figures 9, 10, and 11, respectively. Values of distance (R) were plotted as a function of time (τ) for constant temperature-power ratios (θ/G_o), as seen in Figures 12, 13, and 14. The solid lines represent the theoretical curves.

Figure 9a
Tau = 4.2 t = 40 sec.

Figure 9b
Tau = 6.2 t = 60 sec.

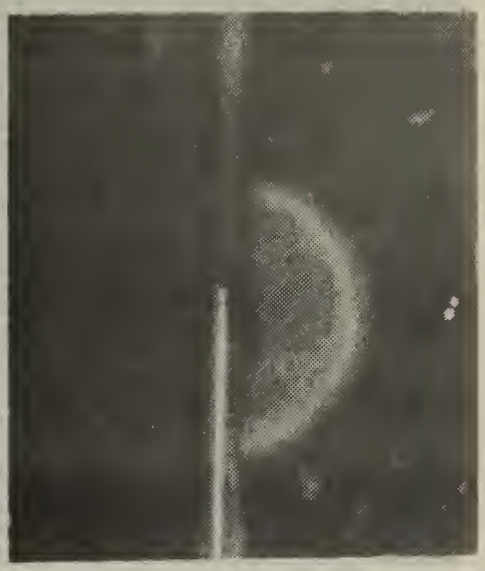

Figure 9c
Tau = 9.3 t = 90 sec.

Figure 9d
Tau = 12.5 t = 120 sec.

Figure 9. Cylindrical transient temperature field growth, L/D = 4, probe diameter = 0.241 cm.

Figure 10a
Tau = 4.2 t = 40 sec.

Figure 10b
Tau = 6.2 t = 60 sec.

Figure 10c
Tau = 9.3 t = 90 sec.

Figure 10d
Tau = 12.5 t = 120 sec.

Figure 10. Cylindrical transient temperature field growth, L/D = 10, probe diameter = 0.241 cm.

Figure 11a
Tau = 4.2 t = 40 sec.

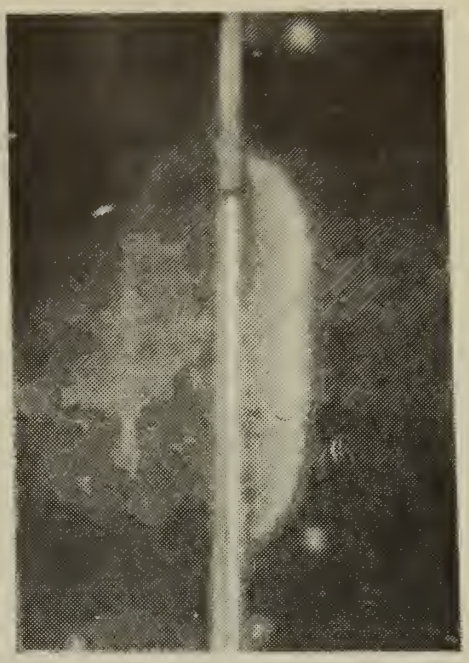

Figure 11b
Tau = 6.2 t = 60 sec.

Figure 11c
Tau = 9.3 t = 90 sec.

Figure 11d
Tau = 12.5 t = 120 sec.

Figure 11. Cylindrical transient temperature field growth, L/D = 20, probe diameter = 0.241 cm.

Figure 12
Nondimensional isotherm radii
vs.
nondimensional time for a cylindrical
probe with L/D = 4 and diameter = 0.241 cm.
Data set M

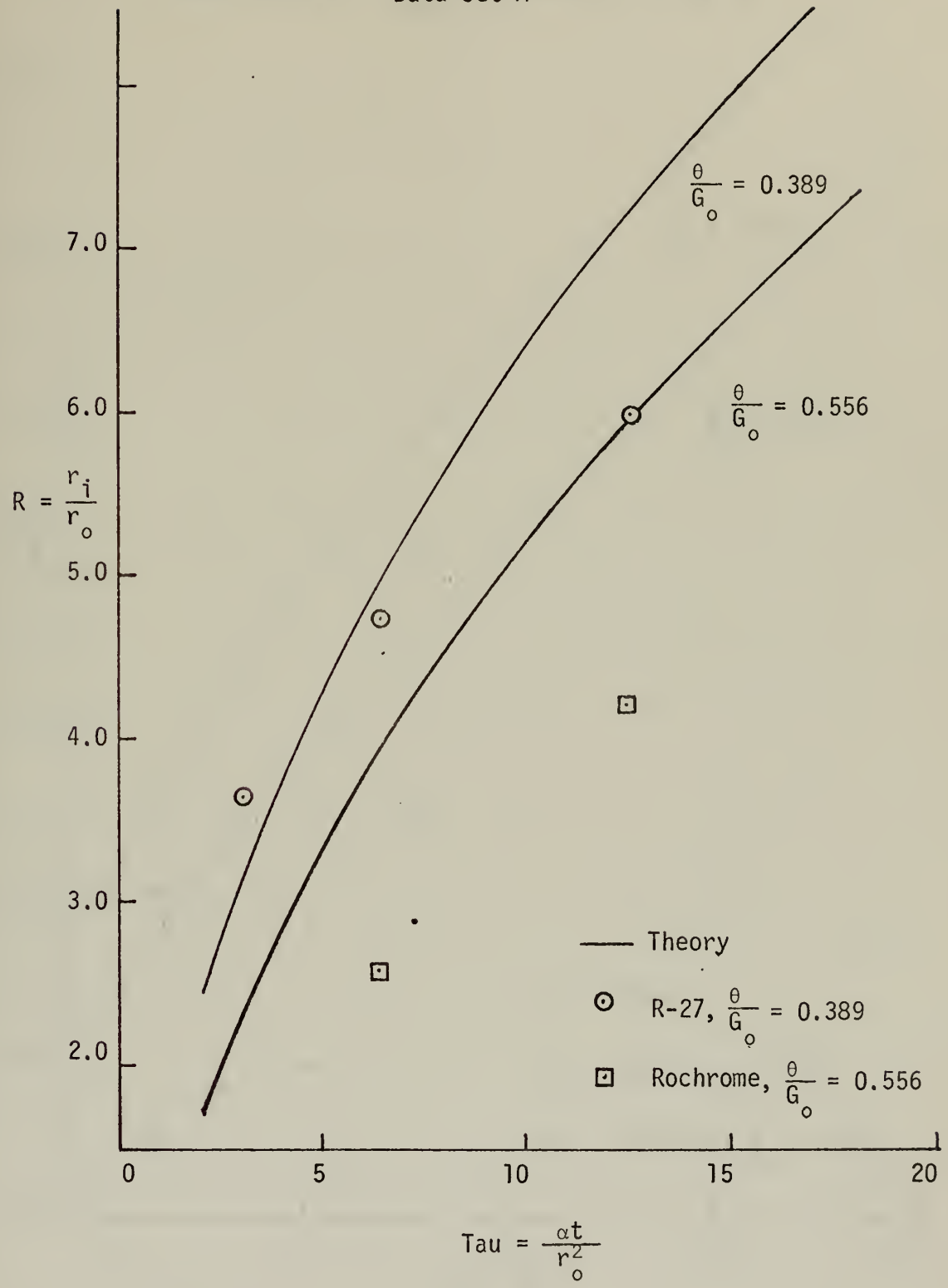

Figure 13
Nondimensional isotherm radii
vs.
nondimensional time for a cylindrical
probe with L/D = 10 and diameter = 0.241 cm.
Data set L

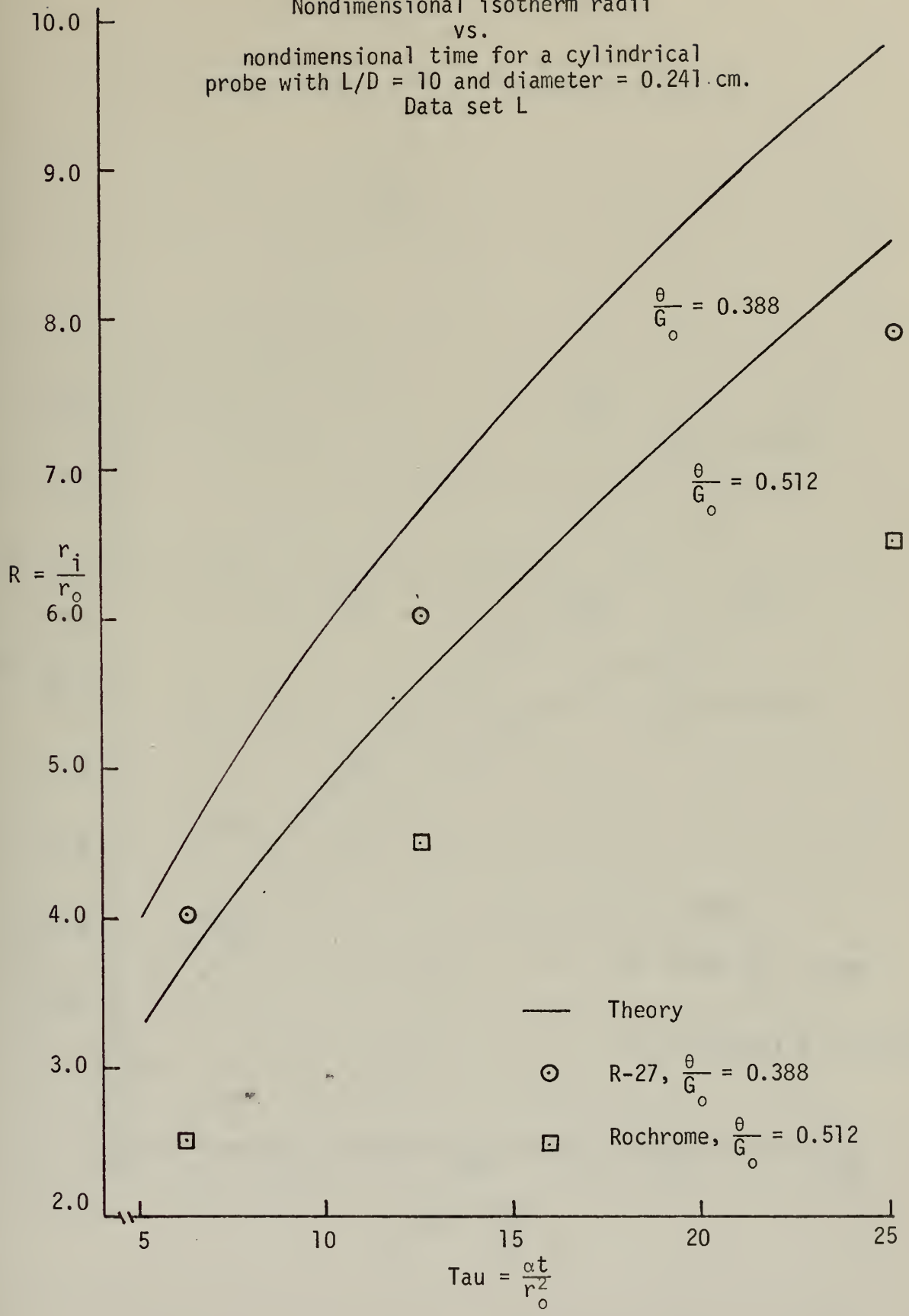

Figure 14
Nondimensional isotherm radii
vs.
nondimensional time for a cylindrical
probe with L/D = 20 and diameter = 0.241 cm.
Data set K

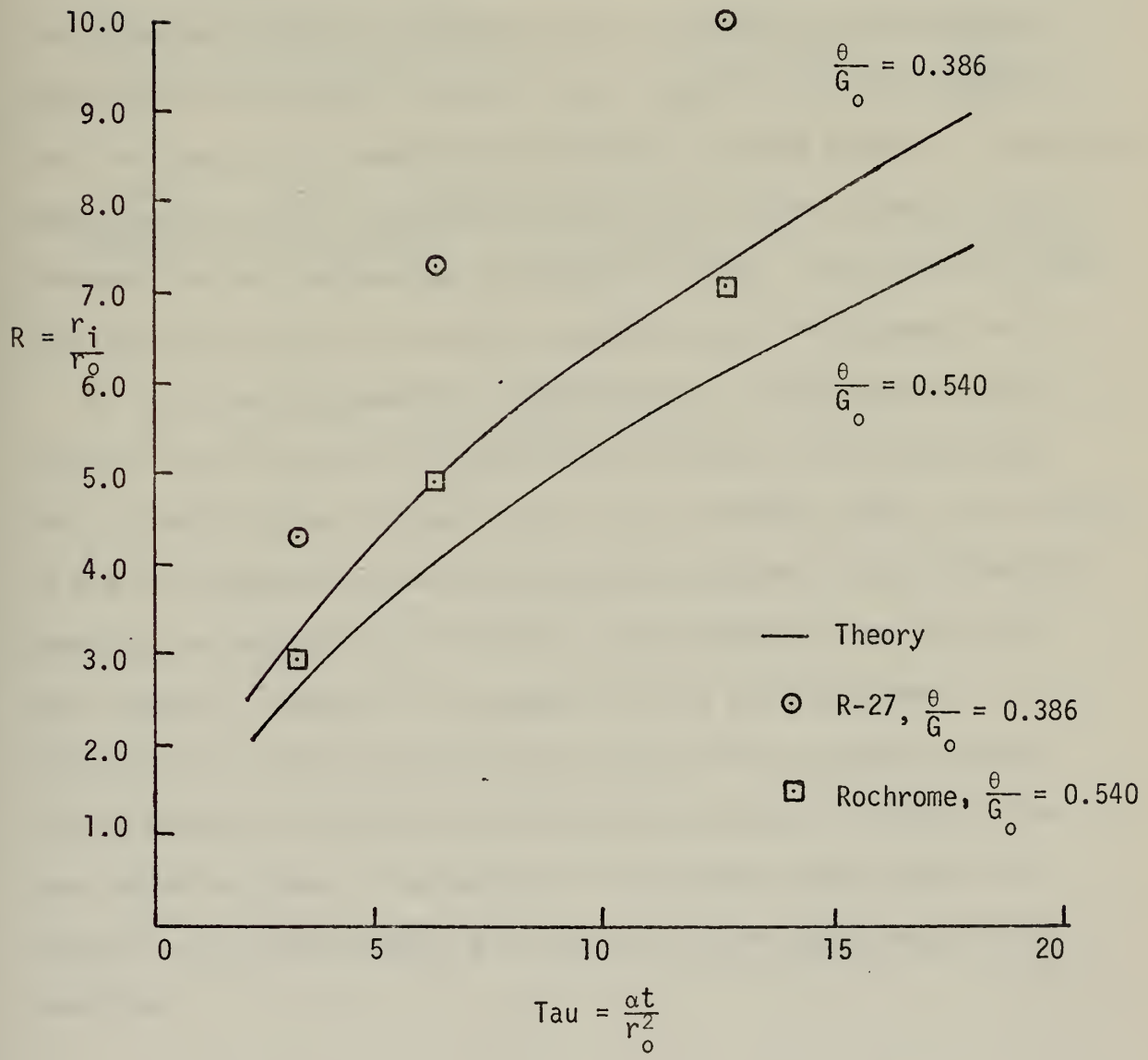

VI. DISCUSSION OF RESULTS

A serious difficulty in modeling the radio frequency probe in tissue has previously been an inability to accurately map the thermal area surrounding the probe. Thermocouples and thermistors have either been placed inside the probe tip, where they actually measured the probe temperature, or placed in the medium, where they acted as thermal sinks. The use of liquid crystals, as demonstrated in this thesis, now allows an accurate, continuous display of specific temperatures depending on the crystal in use. Liquid crystals provide a flexible tool for temperature measurement regardless of probe geometry. Figure 15 shows liquid crystals indicating isotherms which were caused by radio frequency current between two nonsymmetric probes. As can be seen, the liquid crystals react to provide a complete map of the thermal region.

In the spherical geometry, the experimental values were in good agreement with the theory as modified for variable resistivity (8%). The cylindrical data and theory were not in agreement (30%). As a result of the poor agreement between theory and experiment in the cylindrical geometry, an examination of the flux lines emanating from the probe was conducted. Appendix C discusses the flux plots obtained. Figure 16 is a flux plot showing only the lines of constant current. As can be seen, the direction of the current lines is changed in the area above the probe. The bending of the current lines results in a higher local current density with greater heating than theoretically predicted.

Figure 15
Liquid crystals map a
nonsymmetric thermal region

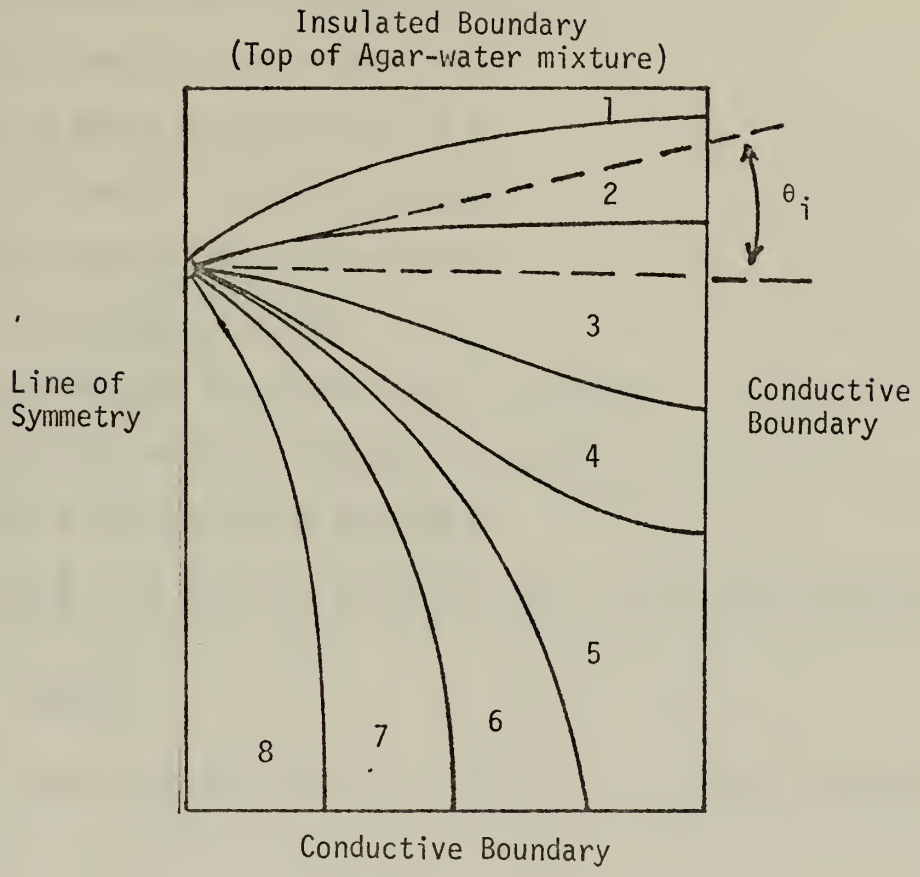

Figure 16. Constant current lines emanating from a cylindrical probe based on teledeltus plot of the isopotentials in plane perpendicular to probe axis

An approximation was derived to account for the increased current density. Due to symmetry of the problem, only half the probe-cell system was modeled. The following parameters were defined:

Number of flow tubes (for half field) = b

Current flow (for half field) = I/2

Half the probe surface area = $\pi r_o L$

Angle subtended by the ith flow tube = ϕ_i

Surface area of the ith flow tube at the probe surface = $\phi_i r_o L$

Current flow per flow tube = I/2b = constant

Current flux in the ith flow tube = $I/2b\phi_i r_o L$

Recall that I was previously defined as

$I = \frac{I}{A}$, or for this situation, the local current density is

$$I_i = \frac{I}{2b\phi_i r_o L}$$

The local power parameter is $G_i = \frac{I_i^2 \rho_o r_o^2}{k T_o}$ or after substitution for I_i^2,

$$G_i = \frac{\pi^2}{b^2 \phi_i^2} G_o$$

From Figure 16, $\phi = 14°$, b = 8 which yields $G_i = 2.58\ G_o$. Applying this correction to the nondimensional temperature-power term (θ/G_o) shifts the theoretical curve so that experimental data more closely approximate the theory (Figure 17).

Since the degree of current density is influenced by probe depth, the correction factor must be determined for each experiment.

Examination of Figure 18 demonstrates the strong end effects on the finite cylindrical probe. The cylindrical theory (Equation 11) was

Figure 17
Comparison of experimental data with
original theoretical curve and
corrected theoretical curve

Cylindrical probe L/D = 20

Data set K

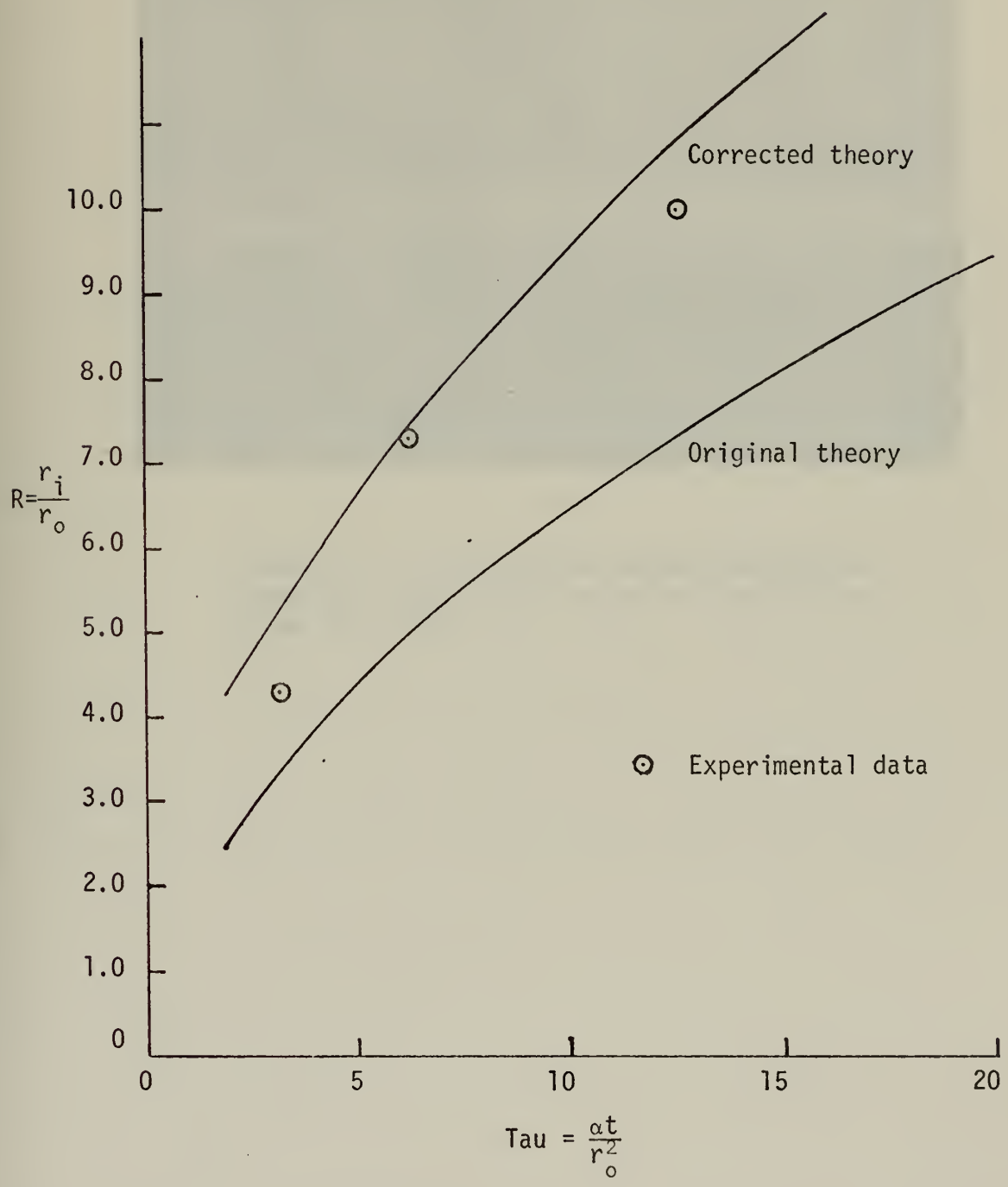

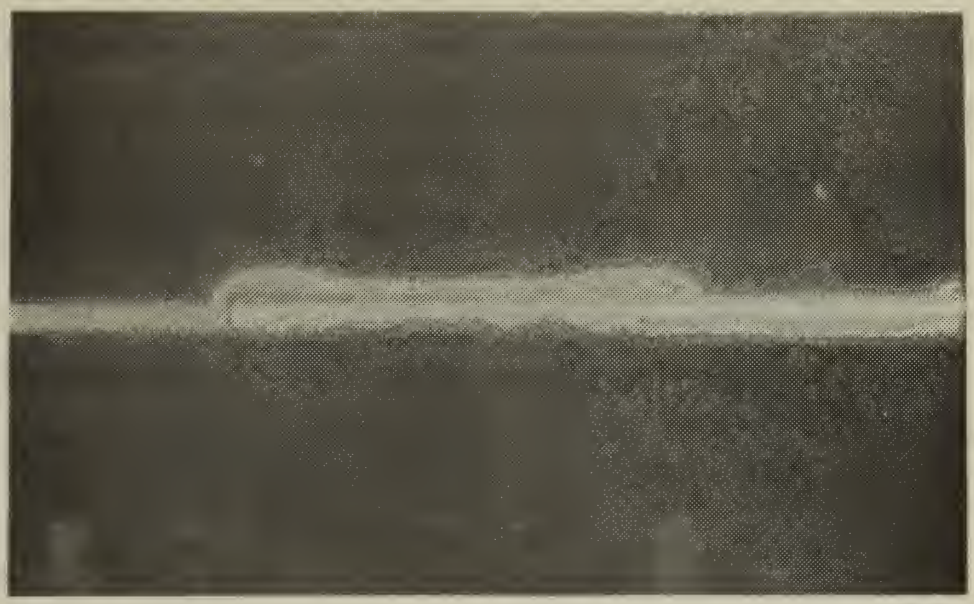

Figure 18. Liquid crystals demonstrating the pronounced edge effects caused by a cylindrical probe (L/D = 20)

based on an infinite cylindrical probe with no end effects. The figures show the strong thermal fields at the probe ends developing before the effects at the probe center are observed. With time, the conduction of heat in the agar tended to reduce the thermal gradient between the probe ends and its midpoint, with the resultant growth as shown in Figure 11. A possible explanation for the early observation of thermal fields at the probe ends is that radio frequency current density is higher at sharp corners than at plane surfaces. The higher current density results in greater heating.

By using a probe with a small surface area, resulting in high current density, it was possible to observe boiling in the agar. Since the liquid crystals used in the experiments were active in temperature ranges below the boiling temperature of the agar, no data were taken on boiling. However, Figure 19 is a photograph taken of the boiling phenomenon. It was of interest to observe formation of a bubble as the agar was heated to boiling. When rising, the bubble traveled until it encountered a cool region; the bubble then collapsed. This boiling is analogous to that occurring in actual surgery. The reason for controlling the probe tip temperature is readily apparent when observing the deterioration of the jelled agar as bubbles rise randomly towards the surface; the analogy in surgery being unpredictable physiological damage.

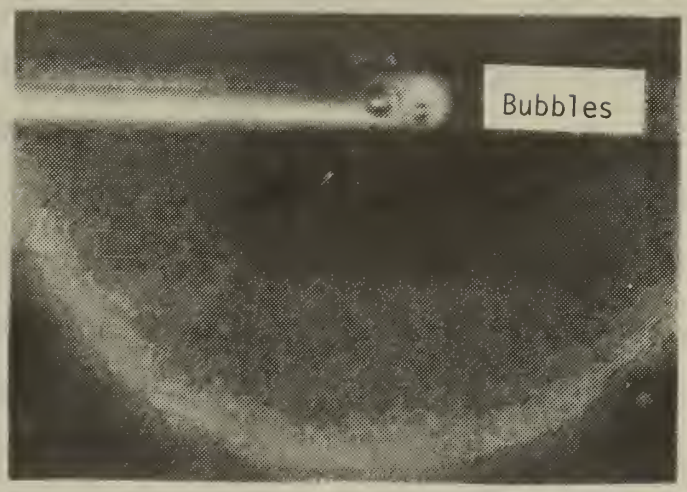

Figure 19. Boiling of the agar-water mixture caused by excessive probe tip temperature

VII. CONCLUSIONS AND RECOMMENDATIONS

A. CONCLUSIONS

The use of liquid crystals for mapping regions surrounding heated surgical probes has been clearly demonstrated. When accuracy on the order of 1.0°C is sufficient, liquid crystals provide a continuous picture of thermal changes as displayed in Figures 20, 21, 22, and 23. Through the use of liquid crystals, the spherical theory developed by Gengler [5] has been verified. On the other hand, Gengler's cylindrical theory has been shown to require further work in order to account for the finite cylindrical probe with its strong end effects.

It is most probable that an actual radio frequency surgical probe would be constructed with a length to diameter ratio in the range of two to five [1, 2, 15, 16]. Clearly, a theoretical treatment for an infinite cylinder would break down at these small length to diameter ratios. As a demonstration of this fact, an equivalent surface area for a spherical probe was determined based on the surface area of the cylindrical probe with a length to diameter ratio of four. Figure 24 is a comparison of the cylindrical theory, the spherical theory, and the experimental data. Relationships between the cylindrical and the spherical parameters have been derived based on the fact that the cylindrical surface area equals the spherical surface area ($2\pi r_{cyl} L = 4\pi r^2_{sphere}$).

$$(G_o)_{cyl} = \frac{I^2 \rho_o r^2_{cyl}}{k T_o} \qquad (G_o)_{sphere} = \frac{I^2 \rho_o r^2_{sphere}}{k T_o}$$

Figure 20. Color photograph of liquid crystals in thermal field of cylindrical probe (L/D = 4). Current flux = 0.414 amps/cm^2

Figure 21. Color photograph of liquid crystals in thermal field of cylindrical probe (L/D = 10). Current flux = 0.414 amps/cm^2

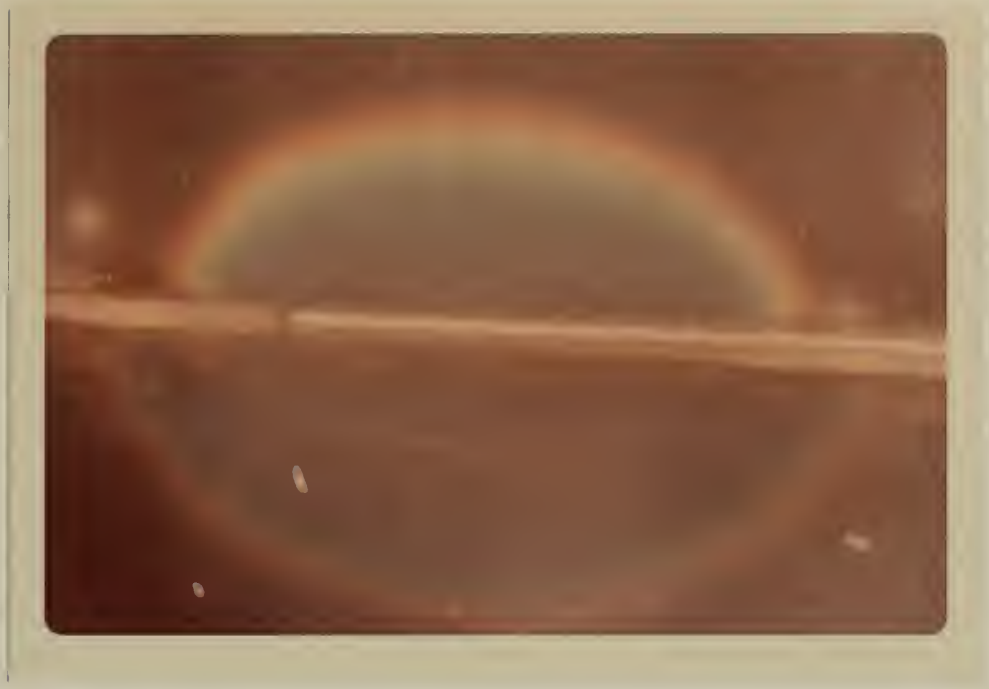

Figure 22. Color photograph of liquid crystals in thermal field of cylindrical probe (L/D = 20). Current flux = 0.414 amps/cm^2.

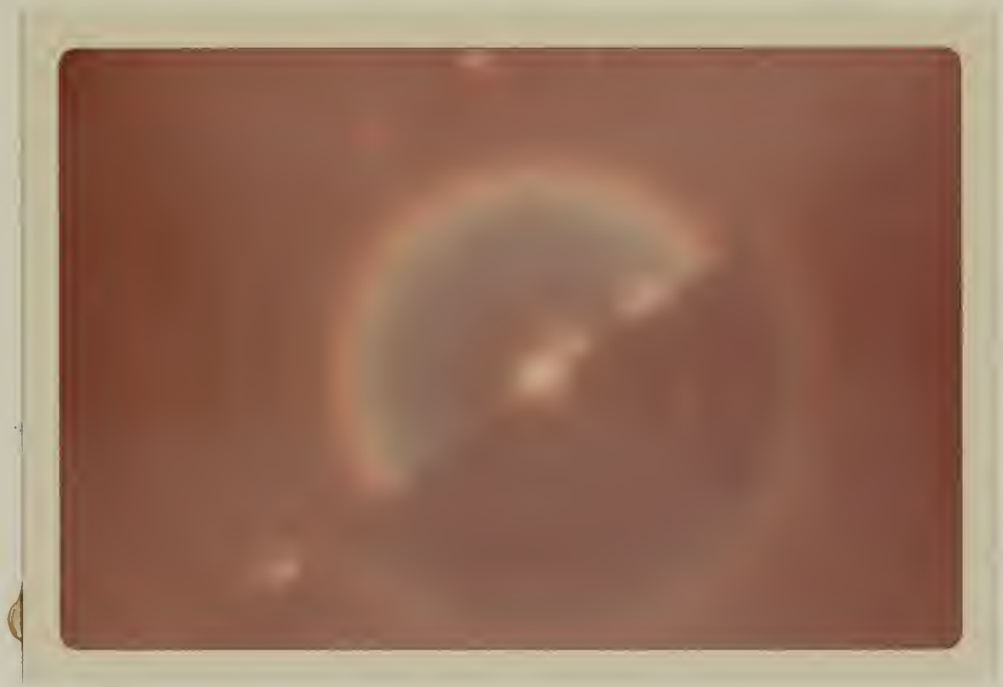

Figure 23. Color photograph of liquid crystals in thermal field of spherical probe

Figure 24
Comparison of cylindrical data (L/D = 4) and cylindrical theory with spherical theory and scaled cylindrical data

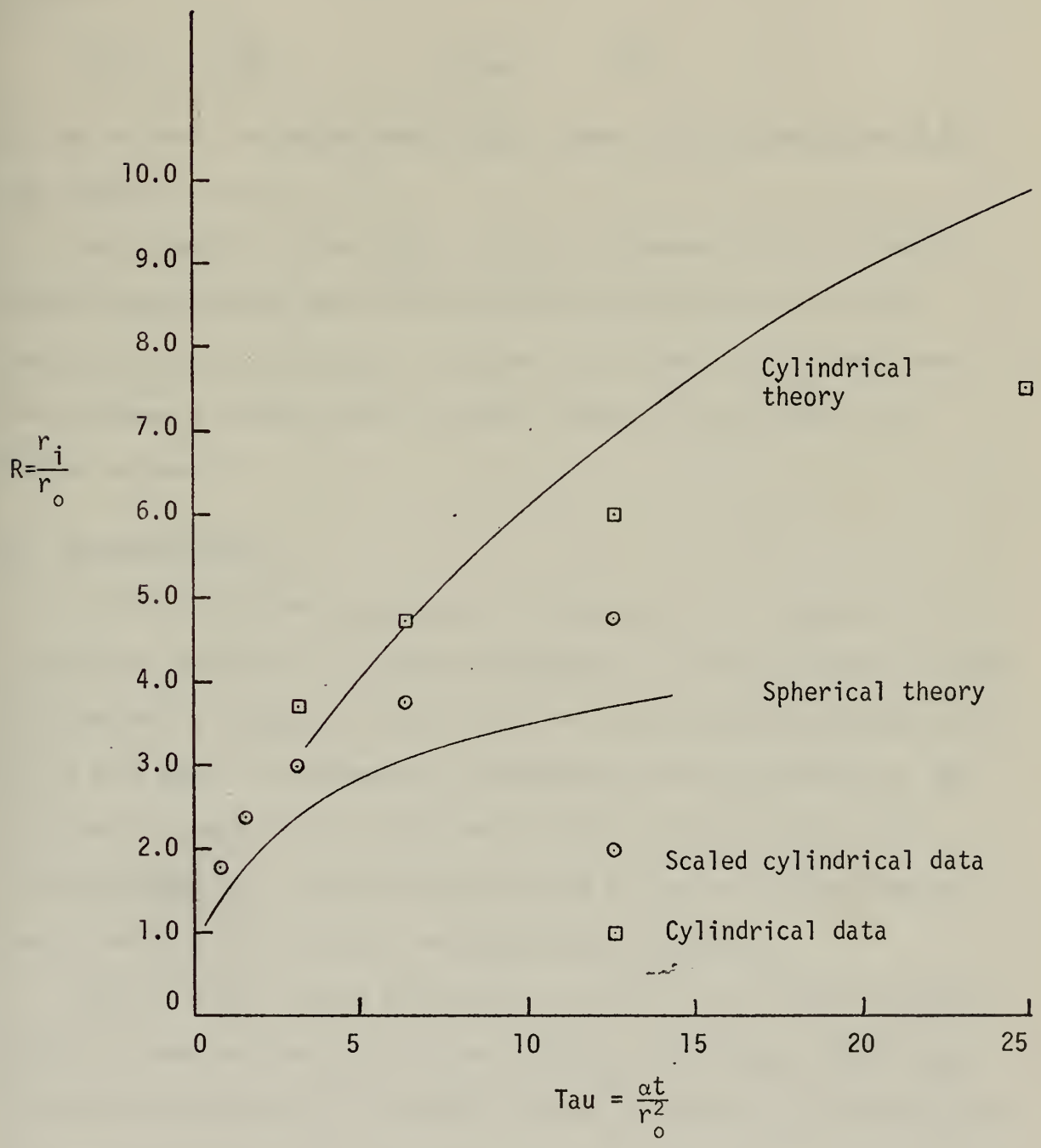

$$\frac{(G_o)_{cyl}}{(G_o)_{sphere}} = \frac{r^2_{cyl}}{r^2_{sphere}}$$

but $r^2_{sphere} = r_{cyl}L/2$ from the equivalence of surface areas. Therefore,

$$(G_o)_{sphere} = 4(G_o)_{cyl}$$

Similarly,

$$R_{sphere} = \frac{R_{cyl}}{2} \qquad \tau_{sphere} = \frac{\tau_{cyl}}{4}$$

As can be seen, the experimental data is more closely approximated by the spherical theory.

The cylindrical probe with a length to diameter ratio of 20 most closely approximated the infinite probe of the cylindrical theory. Use of the correction factor to account for current path changes near the air-agar interface, tends to bring theory and experiment into better agreement.

B. RECOMMENDATIONS

Further work, both experimental and theoretical, is needed for the cylindrical geometry. Of particular interest are the cylindrical probes with length to diameter ratios of five or less since actual probes will be in this range. Experimental investigations into the effect of the air-agar interface with varying probe depths would demonstrate the analogous effects of lesion creation close to the skull; both the air-agar interface and the skull are essentially insulators.

Liquid crystals placed perpendicular to the axis of the cylindrical probe and running from the air-agar surface to the bottom of the agar could effectively map the distorted thermal region due to the insulated air-agar surface.

Studies of various tissues should be conducted to fully catalogue tissue electrical properties. Such a catalogue would allow the surgeon to theoretically determine current strength and duration for a particular lesion size prior to the actual surgery.

Some refinement in the spherical experimentation would reduce uncertainty. The major uncertainties were in the thermophysical properties of the agar.

A method of retaining the liquid crystals in the plane of a diameter of the probe is required. This is particularly difficult when using the cylindrical probe. Placing the substrate in tension in its holder only succeeds temporarily. The substrate of mylar eventually stretched and sagged. Without having the liquid crystals in the diametral plane, true distances cannot be measured for scaling with respect to the probe radius.

A better potentiometer is required for controlling the RFG-2AV generator output. The control provided by the manufacturer had excessive play. This was partially overcome by careful selection of meter scales during experimentation.

Use of a 35mm camera with a through the lense light meter system is suggested for taking data. Most data for this study was recorded using the industrial Polaroid film. When used under artificial light, the film is very slow (ASA 24); colors are not well defined which is critical when using liquid crystals. The net result with the color Polaroid is a poor reproduction of the liquid crystal colors. Using 35mm black and white or tungsten corrected color film gives highly satisfactory results when used with the proper light meter settings. Cameras using Polaroid film are often moved during film insertion and removal. The slightest movement results in an unfocused picture at the short distances

normally used in photographing the probe area. With a 35mm camera, there is a minimum of movement during the shutter release and film winding processes. The actual time for inserting and removing the Polaroid film limits the data that can be taken; this is most true at small times. Using a 35mm camera, with the fast film advance time, allows more frequent data recording.

A study should be conducted to determine the feasibility of mixing more than three liquid crystals without a loss of color brilliance. The required separation of temperature ranges should be determined since the closer the temperature ranges, the more crystals could theoretically be mixed. This would yield more data for each experimental trial. The temperature ranges, however, must be far enough apart so that each color band is displayed clearly.

APPENDIX A: RESISTIVITY

BACKGROUND

Initially, thermal and electrical properties of the 99.7 percent water/0.3 percent agar solution were unknown. It was decided to investigate the electrical resistivity of the solution since thermal properties could be correlated with the solution's water content [10]. A test cell, pictured in Figure 25, was designed and manufactured for use in the resistivity investigation. To prevent a standing wave in the resistivity test cell, the test cell length could not be an integral or a quarter wavelength of the 500 kilohertz signal used in the experiments. Using the relationship between frequency (f), wavelength (λ), and the speed of light in air related to the speed of light in water (n),

$$\lambda = \frac{3 \times 10^8}{n\ f} \quad \text{meters}$$

the wavelength was determined and the test cell designed to prevent standing waves.

A plexiglass tube, 13 cm. in length with 2.5 cm. ID, was used as the test cell due to the insulating properties of plexiglass at the power levels used. Copper plugs were machined to fit tightly into the cylinder with the area of the plug ends known. A BLH two-inch, constantan-chromel needle thermocouple was introduced through the wall of the plexiglass cylinder midway between the copper ends. To prevent leakage of air into the container, a seal of neoprene rubber was provided between the test cell and the thermocouple shaft. During the experimental trials, the test cell was filled with hot agar solution.

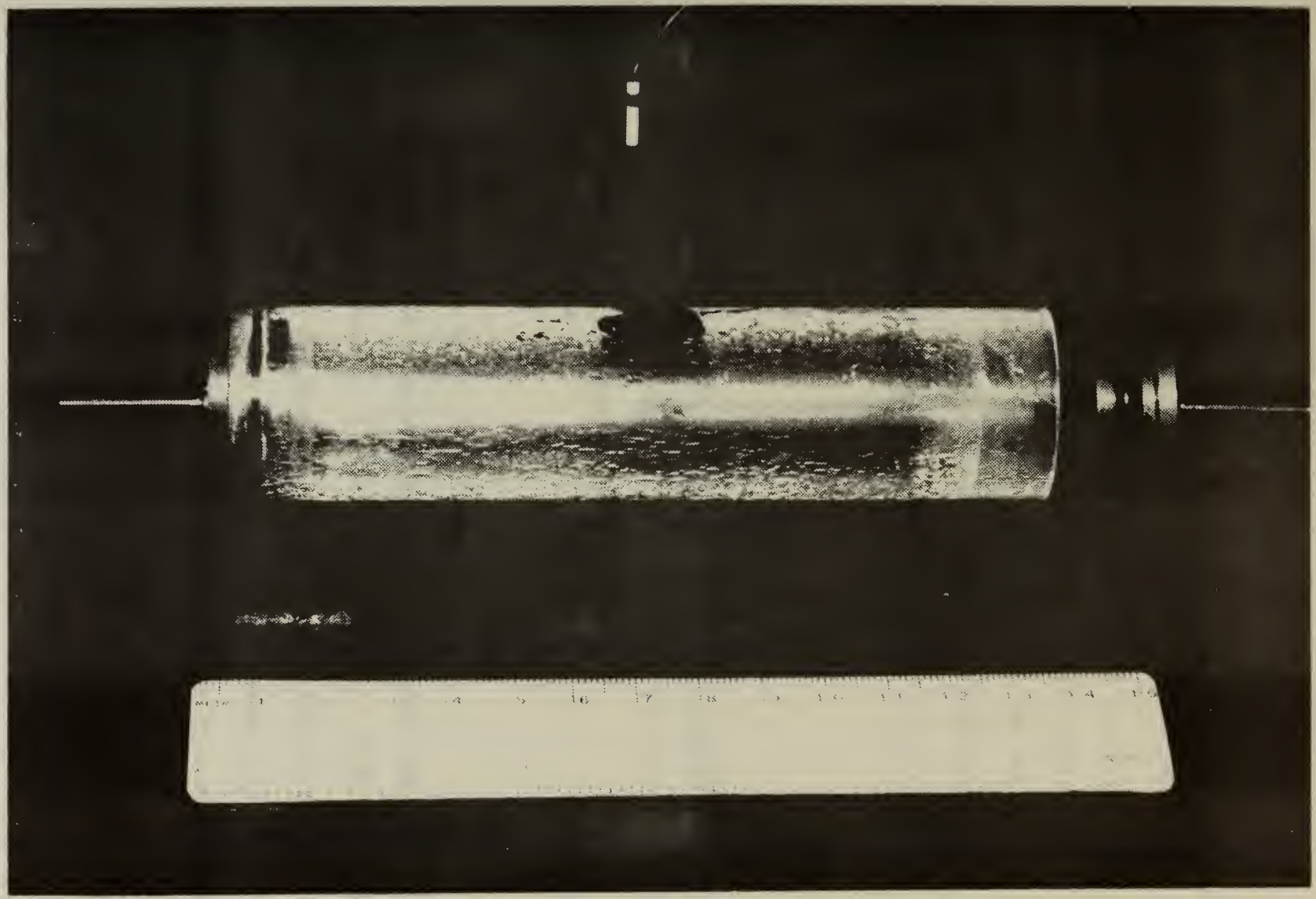

Figure 25. The resistivity test cell with attached thermocouple

By carefully capping the test cell, no air was trapped inside. The capped cylinder was placed in the generator circuit shown in Figure 26.

Voltage was applied across the circuit for one minute when collecting data. One minute was chosen since no change in voltage drop occurred after this time. Determination of resistivity was accomplished by recording voltages across the circuit and the ten ohm resistor along with the distance between the surfaces of the copper plugs. The voltage drop across the resistor yielded circuit current from Kirchoff's Law:

$$I = \frac{E}{R_{10}}$$

The resistance of the cylinder was determined by dividing this current into the voltage drop across the cylinder. Resistivity is related to resistance by the area to length ratio:

$$\rho = \frac{A}{L} R$$

It was thus possible to calculate resistivity.

At the same time the voltage readings were recorded, the needle thermocouple was read via the millivolt potentiometer. Data were taken as the test cell cooled and again as the cell was heated in a controllable oven (Figure 27). Early experimental trials showed a wide variation in agar resistivity (Figure 28). To reduce all plots to a common scale, two nondimensional quantities were introduced:

$$\theta = \frac{T - T_o}{T_o} \qquad \text{Temperature}$$

$$\tilde{\rho} = \frac{\rho}{\rho_o} \qquad \text{Resistivity}$$

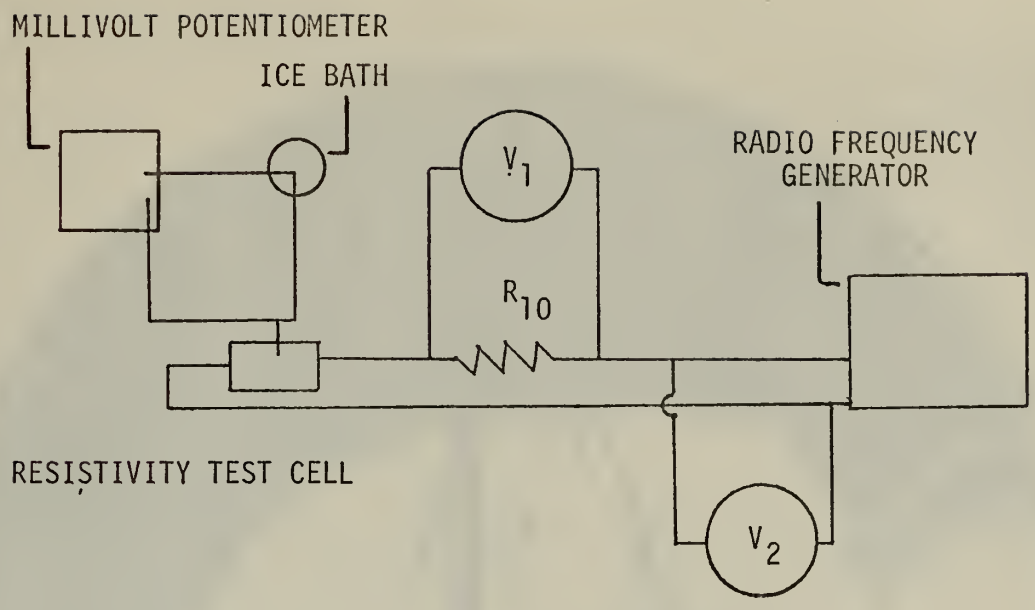

Voltmeter V_1 measured voltage drop across the ten ohm resistor from which circuit current was determined.

Voltmeter V_2 measured circuit voltage which was used in conjunction with circuit current to determine resistivity test cell resistance.

Resistivity Test Cell Circuitry
Figure 26

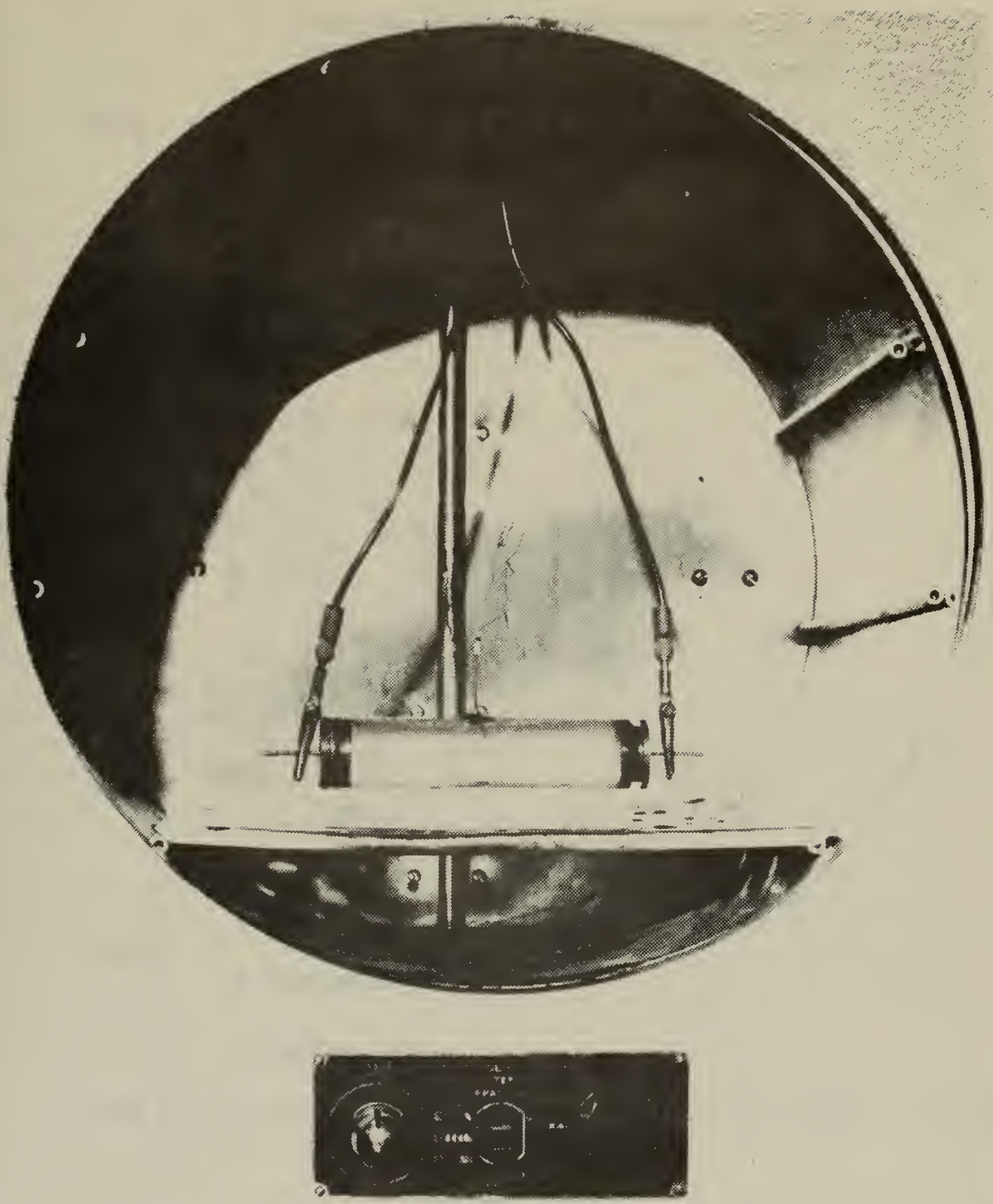

Figure 27. The resistivity test cell in the oven for the heating phase of resistivity data collection

Figure 28
Variation in resistivity values
as a function of temperature

Data sets A-H

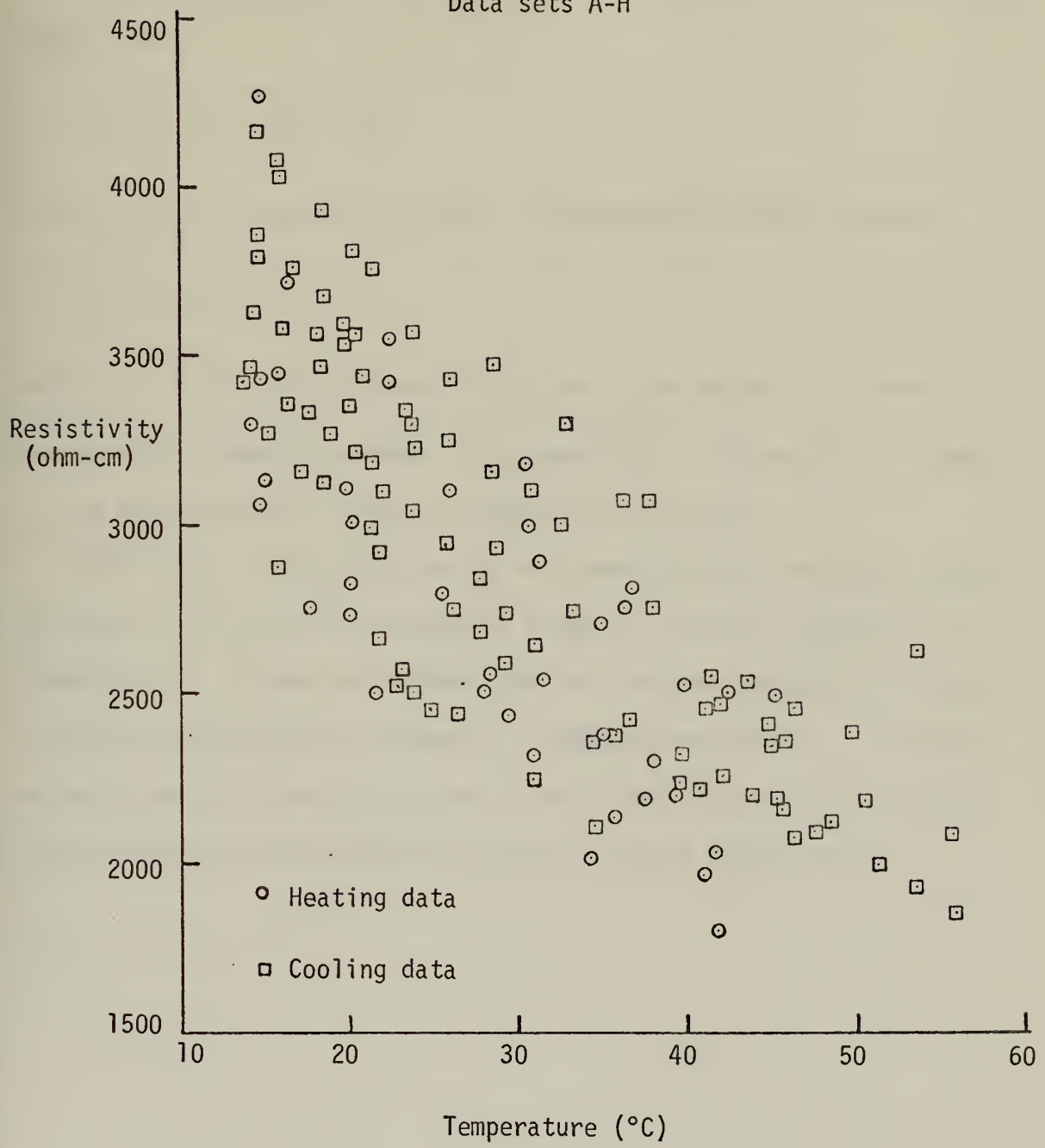

where the subscript indicates the initial conditions of the experimental trial. In this way, the plots had common points of origin.

A linear curve was fit to each set of data points. In dimensional form,

$$\rho = \rho_o + \gamma (T - T_o)$$

where γ was the slope of the curve. Nondimensionalizing yielded

$$\tilde{\rho} = 1 + m\theta$$

where $m = \frac{\gamma T_o}{\rho_o}$, the nondimensional slope. The values of m were generated by computer program III (Appendix E). Figure 29 is a sample of the nondimensional curves plotted by this program.

As a result of this portion of the investigation, the great change in resistivity over the temperature range of interest (15-60°C) was demonstrated. It was determined that the programs written by Gengler [5] required modification to reflect the changing resistivity. This was accomplished by incorporating the slope of the linear curve from the resistivity data into computer programs I and II (Appendix E).

Figure 29
Agar-water mixture nondimensional resistivity as a function of nondimensional heating and cooling temperatures

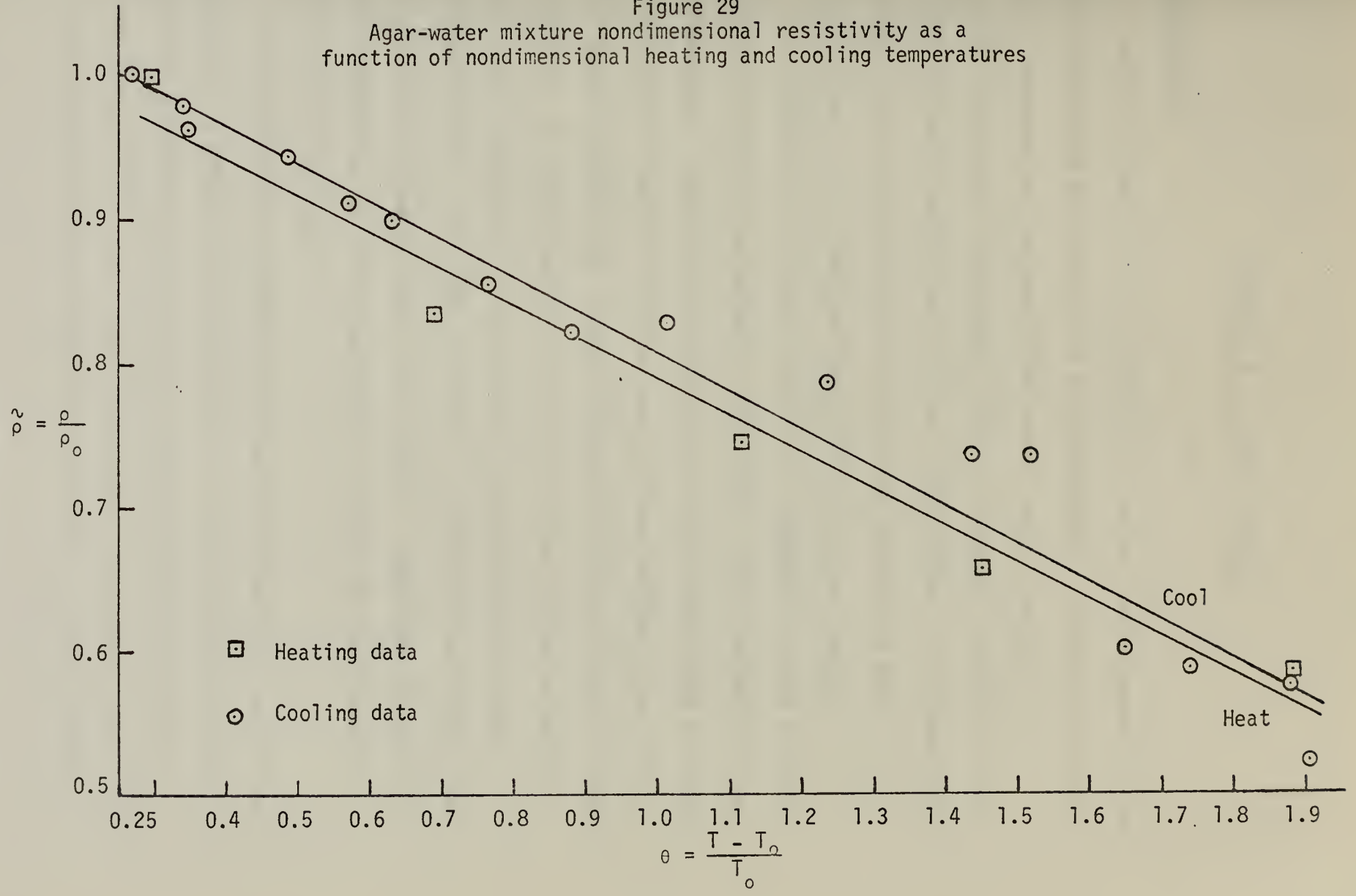

APPENDIX B: LIQUID CRYSTALS

BACKGROUND

Matter can exist in solid, liquid, or gaseous state depending upon the temperature and pressure of the surroundings. In the solid state, most compounds are composed of an ordered array of molecules in a crystal structure. When heated, the crystal begins to deform as the molecules absorb energy and leave the "ground state." The temperature at which the deformation begins is known as the melting point [17]; it is normally a well-defined characteristic of the compound.

In 1888 Reinitzer noticed that not all compounds changed directly from solid state to an isotropic liquid [18]. The intermediate phase, a "mesophase," exhibited characteristics of both crystalline structure and isotropic liquid. Thus, the name of these substances was coined as liquid crystals [18]. Lehmann continued Reinitzer's work in liquid crystals. He classified the crystals into three categories based on molecular orientation; the categories are smectic, nematic, and cholesteric [17]. Only the cholesteric crystals will be discussed as it is the only type utilized in this report. Interested readers may find information on smectic and nematic crystals in the literature [16, 17, 18, 19, 20].

The cholesteric mesophase has the molecules' long axis parallel and coplanar. A model for this structure is a deck of cards, each card with one corner bent up such that a slight rotation of the entire stack results [18]. The average displacement of adjacent layers is fifteen minutes of arc per layer [21] with each layer on the order of

1000 Å thick [22]. The rotation is due to the stretched out non-symmetric shape of the crystal molecule [23].

The helical rotation of the cholesteric liquid crystal gives rise to its optical properties. When transmitting polarized light, the helical layers cause the light to be rotated to the left with rotations of fifty degrees per millimeter. This property is known as being optically active. By way of comparison, quartz, one of the most optically active materials in nature, has a rotation of twenty degrees per millimeter for polarized light. Another property of the cholesteric liquid crystals is circular dichroism which is a function of temperature, material, and the angle of the incident light. The incident beam of unpolarized white light is split into two components. One component is rotated clockwise while the other component is rotated counter-clockwise. The result is that one component is reflected while the other is transmitted. To absorb the transmitted beam, a black background is required behind the liquid crystals. Circular dichroism is the characteristic that gives cholesteric liquid crystals their iridescent colors. This characteristic should not be confused with the birefringence or double defraction of white light by the cholesteric liquid crystals (Figure 30). Birefringence is often used as a test for the cholesteric mesophase [21]. In the material the incident beam is divided into two polarized components which are vibrating at right angles to each other and are travelling at different speeds. They are, therefore, refracted at different angles and emerge as two beams of perpendicularly polarized light. The rotary power of the birefringent cholesteric mesophase is as much as 1800 degrees per centimeter when light is transmitted along the optical axis normal to a thin sheet [23, 24]. The thickness of the

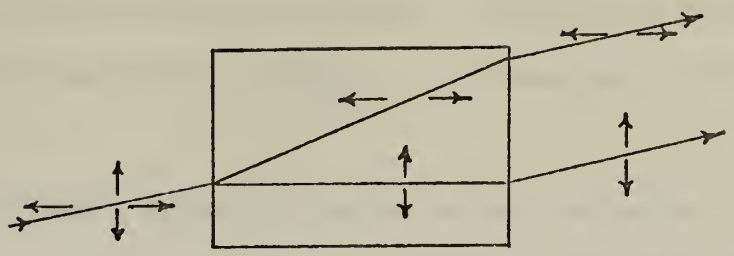

Birefringence: In the material, the incident beam of light is divided into two polarized components vibrating at right angles to each other and traveling at different speeds. They are, therefore, refracted at different angles and emerge as two beams of perpendicularly polarized light

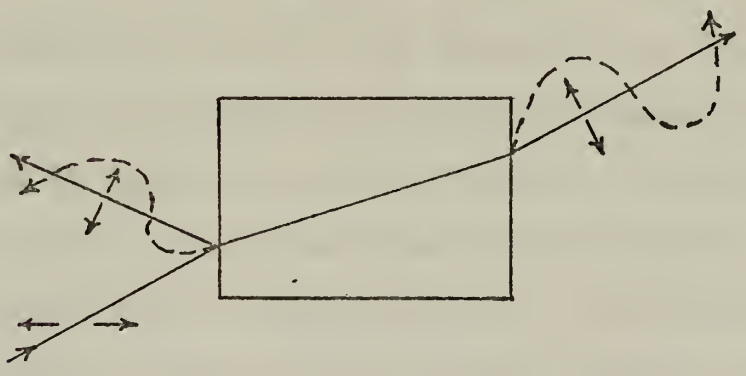

Circular dichroism: The incident beam of unpolarized light is split into two components, one rotating clockwise and the other rotating counterclockwise. The result is that one is reflected while the other is transmitted.

Figure 30

cholesteric film does not alter the predominant wavelength of the reflected light as it is rotated; however, the angle of incidence and the angle of observation both effect the wavelength of the reflected light.

The most striking changes in the cholesteric mesophase are those due to temperature changes. This mesophase is made temperature sensitive by the narrow band of optical reflection which is associated with a change in crystal structure. Cholesteric liquid crystals are also sensitive to organic compounds, shear, and electromagnetic radiation at high frequencies and power levels. Depending on composition, cholesteric liquid crystals span a range from -20 to 250 degrees C [25]. Any specific compound may have its range narrowed to as little as one degree or increased to six degrees by varying the compound ingredients [26]. If heated far beyond its temperature range and allowed to cool, the transition colors occur at lower temperatures, similar to a magnet being heated above the Curie temperature [21]. If not thermally shocked as just described, the transition colors remain invariant with temperature; the material may be repeatedly recycled. Not all cholesteric liquid crystals react with the same color changes; some display all colors of the spectrum starting with red to yellow to green to blue, while others may change directly from red to blue.

Cholesteric liquid crystals will deteriorate in several days if not insulated from dust and organic materials. National Cash Register Company has been successful with encapsulating the cholesteric liquid crystals in spheres 5 to 30 microns in diameter [23]. The result of the microencapsulation process is a long life with little deterioration from contamination. The NCR process reduces the angle dependence of the

crystal as far as color is concerned although resolution is degraded and response time is increased approximately ten percent [22]. The microencapsulated crystals are used in industry since they are not readily contaminated; they were used in this experiment.

Liquid crystals have many engineering applications. In temperature measurement, cholesteric liquid crystals are primarily used. Guidelines for use of liquid crystals in thermal mapping may be summarized as follows:

a) The heat capacity of the object should be greater than that of the liquid crystals;

b) The size of the object must be great enough to resolve the colors of the liquid crystals;

c) The rate of temperature change must be slow enough for the liquid crystal to follow. (A maximum time of about 0.2 seconds.);

d) The temperature range under study must be within the range of the liquid crystal;

e) The surface of the object must be capable of holding liquid crystals unless an adhesive backing is used;

f) The surface must be black to display the liquid crystals;

g) The temperature pattern must be correlated with another material property such as voids present in nondestructive testing or power dissipated per unit area.

APPLICATION AND CALIBRATION

Reference 27 lists many techniques for application of liquid crystals; in this investigation, a commercial artist's air brush was utilized. Three crystals, designated R-27, R-37, and R-53, were mixed equally. After standing overnight, the cholesteric substances tended to separate from excess water. The water was carefully removed leaving a more concentrated liquid crystal which resulted in a more brilliant color display. The concentrated mixture was sprayed onto the transparent substrate in three thin coats, allowing adequate drying time for each coat. To prevent any absorption of moisture from the environment, drying was conducted under a 40 watt lamp. After the three coats of liquid crystals were dried, two coats of black paint were applied. Testors Flat Black Spray Enamel was used since it contained no chemical which might have reacted with the crystals to cause a shift in the color-temperature relationship. The black paint was required to absorb the light transmitted through the liquid crystal, as only a small portion of the light was reflected. To provide a watertight system, a layer of polyurathane varnish was applied over the black paint and along each edge of the substrate. Thus, the crystals were sealed from all contaminants.

A second type of liquid crystal, designated ROCHROME, was also used during the experiments. Rochrome, manufactured by Hoffman-LaRoche, consists of liquid crystals sandwiched between a layer of mylar and a black adhesive backing. Rochrome is cut to the desired shape and applied directly to the object under study. Again, the edges were sealed to prevent water contamination and separation of the Rochrome from the surface. The surfaces to which the Rochrome and the liquid crystals were applied in this investigation were mylar and glass. The mylar was used with the

probe apparatus while the glass was used during the calibration procedure.

Calibration was conducted using the Rosemount Engineering Company Variable Temperature Bath (Model 913A) in conjunction with its commutating bridge and platinum resistance standard thermometer.

National Cash Register liquid crystals (R-27, R-37, and R-53) were prepared by spraying them onto a glass slide, coating with black paint, and sealing with polyurathane varnish. Rochrome was prepared by sticking a small piece to the slide and sealing the edges with polyurathane. The slides were placed in the bath at approximately one-third of the bath's depth and close to the center of the bath diameter. Effects of the bath container edges were thus minimized. The bath temperature was raised slowly as the slides were observed. To minimize variations between observers, the same observer read the slide colors while an assistant operated the equipment during all calibration procedures.

As the temperature was raised, the liquid crystals reacted, each at its own temperature level. When the slide had turned one color, i.e. red to green, the commutating bridge reading was recorded; then the temperature of the bath was increased to determine the next color change. A conversion table was used to convert the bridge readings to temperature. The uncertainty in this temperature-color calibration procedure was calculated to be ±0.5°C which agrees with Reference 27. Table B-1 lists the crystals used and their calibration temperature-color relationships.

Table B-1

Crystal	Red	Green	Blue
R-27	26.7°C	27.9°C	28.9°C
Rochrome	29.9°C	31.5°C	34.2°C
R-37	35.7°C	37.0°C	38.5°C
R-53	50.5°C	52.1°C	53.3°C

APPENDIX C: FLUX PLOTS

Gengler's theoretical analysis of the cylindrical probe modeled the probe as an infinite cylinder with negligible end effects; the current flow should have been a one-dimensional problem. With the experimental cylindrical probe, end effects were pronounced, prompting an investigation of current paths in the probe vicinity. The area of interest was within ten probe diameters. The problem was approached in two phases. First, the horizontal plane was examined using TRUMP [28, 29], a computer code, while in the second phase, teledeltus paper was used to depict the isopotentials in the vertical plane.

TRUMP solved the general partial differential equation $\nabla^2\theta = 0$. It was postulated that the radio frequency potential steady state condition was established instantaneously with power application. A nodal network was constructed for use with TRUMP (Figure 31). Due to symmetry of the probe-cell system, only one quadrant of the system was modeled. Three cylindrical probes, with length to diameter ratios of 4, 10, and 20 were used with two sets of boundary conditions. The first boundary conditions approximated a small finite cylinder inside an infinite cylinder by the use of two conductive sides of the nodal boundaries for the outer cylinder wall and two insulated sides of the nodal boundaries for the endcaps of the outer cylinder. Figures 32, 33, and 34 are plots of the isopotentials and lines of constant current for each probe length to diameter ratio. Inspection of these figures in the area within ten probe diameters, shows the current lines orthogonal to the probe surface. It was, therefore, expected that the current flow

Probe (L/D = 20)

1	11	21	31	41	51	61	71	81	91	101	111	121	131
10	20	30	40	50	60	70	80	90	100	110	120	130	140

Figure 31
TRUMP nodal network

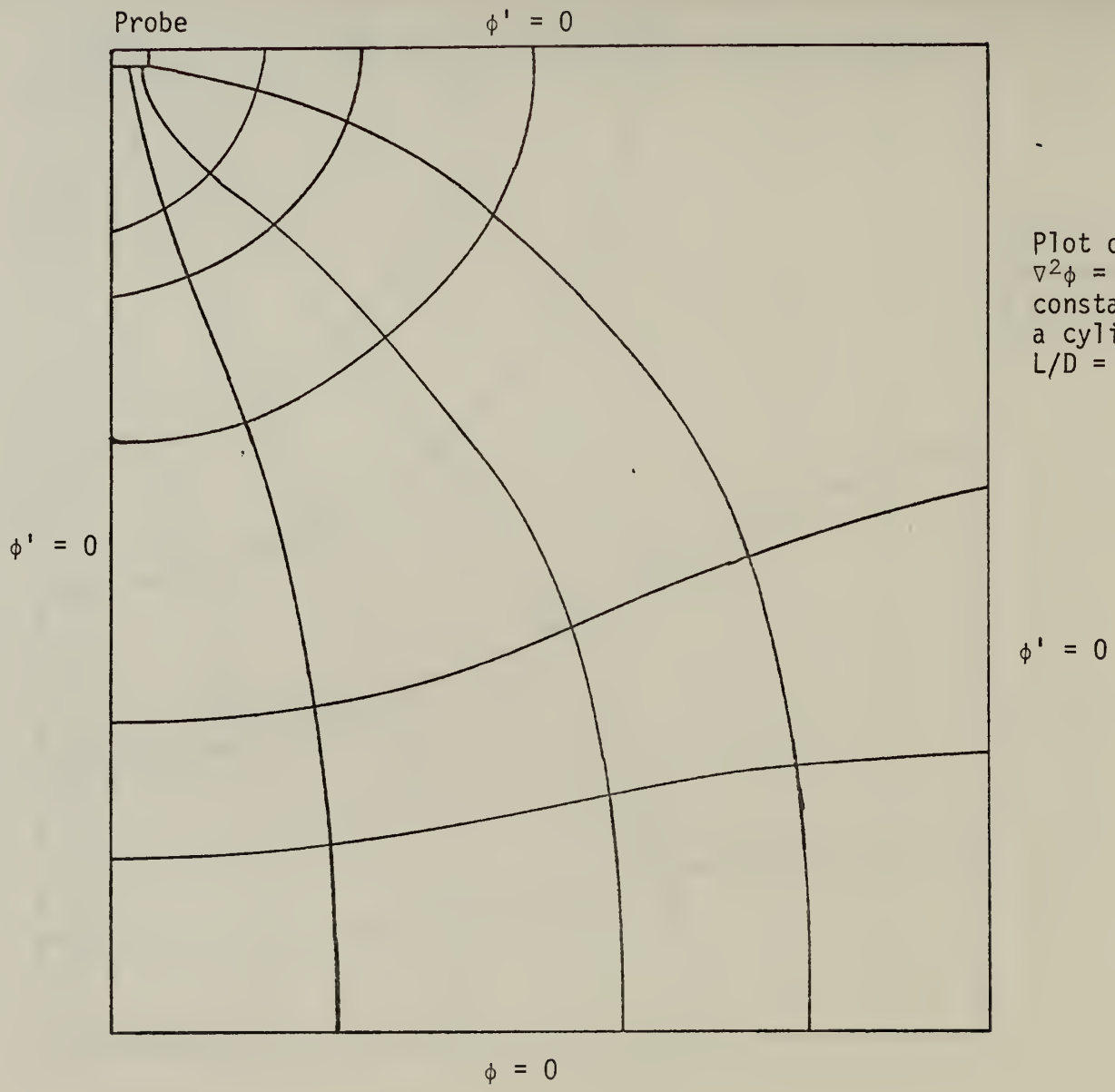

Figure 32

Plot of TRUMP solution of $\nabla^2\phi = 0$. Isopotentials and constant current lines for a cylindrical probe with L/D = 4.

$\phi = 0$ (Conductive Boundary)

$\phi' = 0$ (Insulated Boundary)

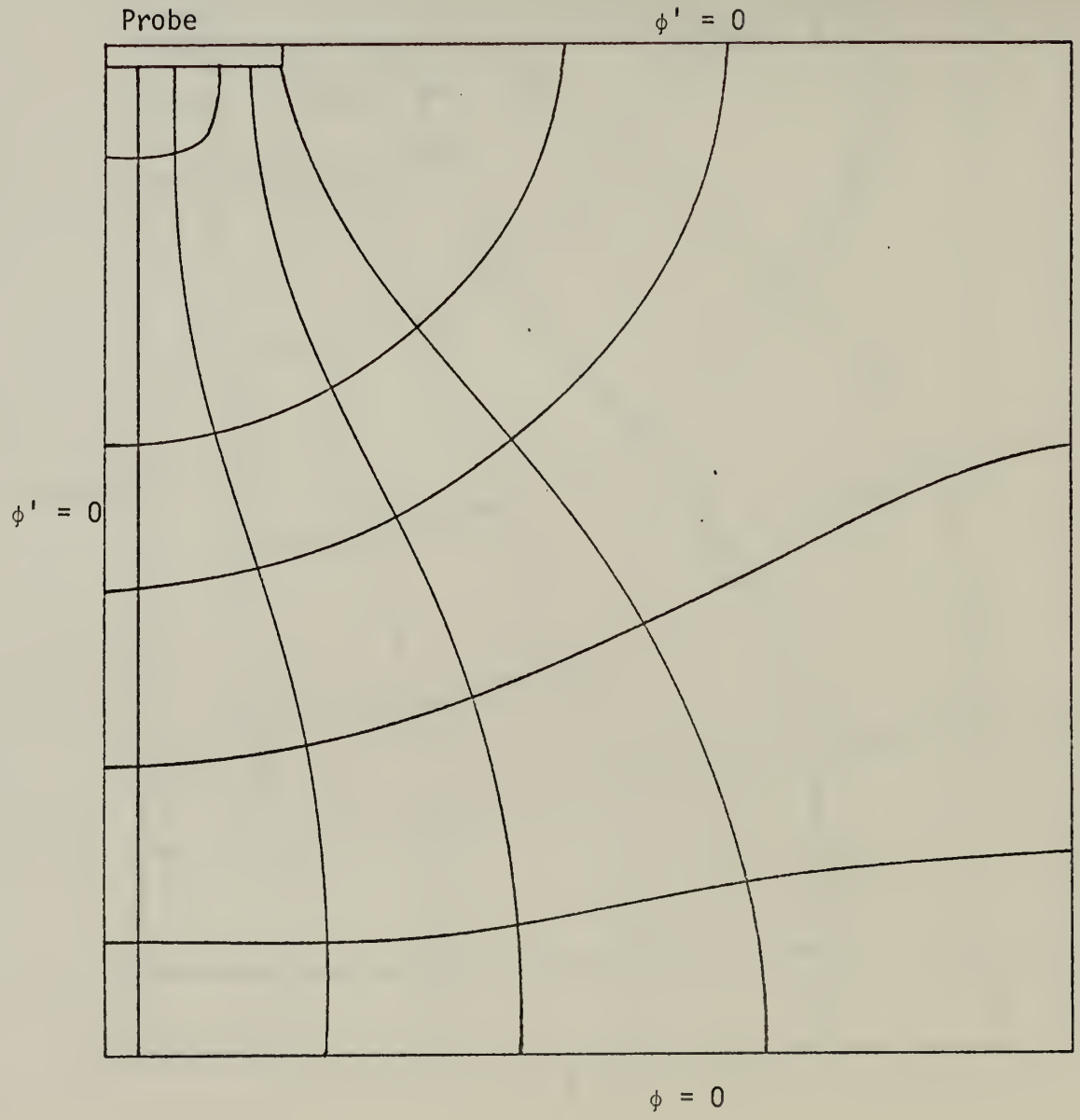

Figure 33

Plot of TRUMP solution of $\nabla^2\phi = 0$. Isopotentials and constant current lines for a cylindrical probe with L/D = 10.

$\phi = 0$ (Conductive Boundary)

$\phi' = 0$ (Insulated Boundary)

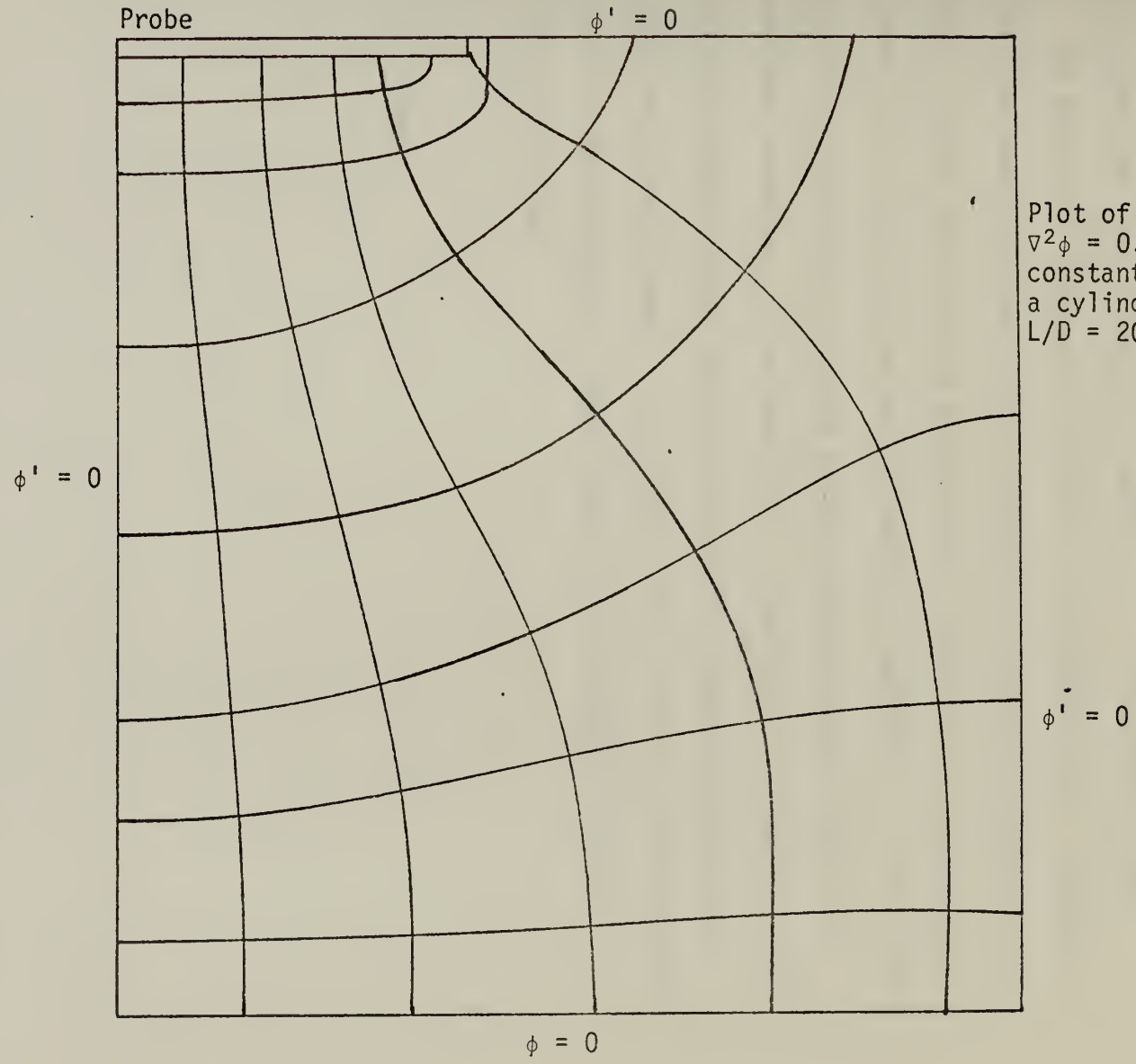

Figure 34

Plot of TRUMP solution of $\nabla^2\phi = 0$. Isopotentials and constant current lines for a cylindrical probe with L/D = 20.

$\phi = 0$ (Conductive Boundary)

$\phi' = 0$ (Insulated Boundary)

and the resultant thermal problem would be one dimensional. For comparison, a second set of boundary conditions surrounded the probe with conductive surfaces. Figures 35, 36, and 37 display the isopotentials and constant current lines for this situation.

The second portion of current path investigation was undertaken when experimental data did not agree with the theory. As stated earlier, in this second phase, isopotentials in the vertical plane were examined using the same sets of boundary conditions as in the first phase.

The probe-cell system was scaled on teledeltus paper. Boundary conditions were simulated using conductive silver paint and metallic tape. Figures 38 and 39 are plots of the isopotentials and constant current lines under the two sets of boundary conditions. It is seen that the insulated agar surface caused current to bend towards the conductive boundary. Since heating is a function of current per unit area, the higher current density resulted in higher heating effects in the experimental model. The higher heating effects were the major cause for the difference between theory and experiment with the cylindrical probe.

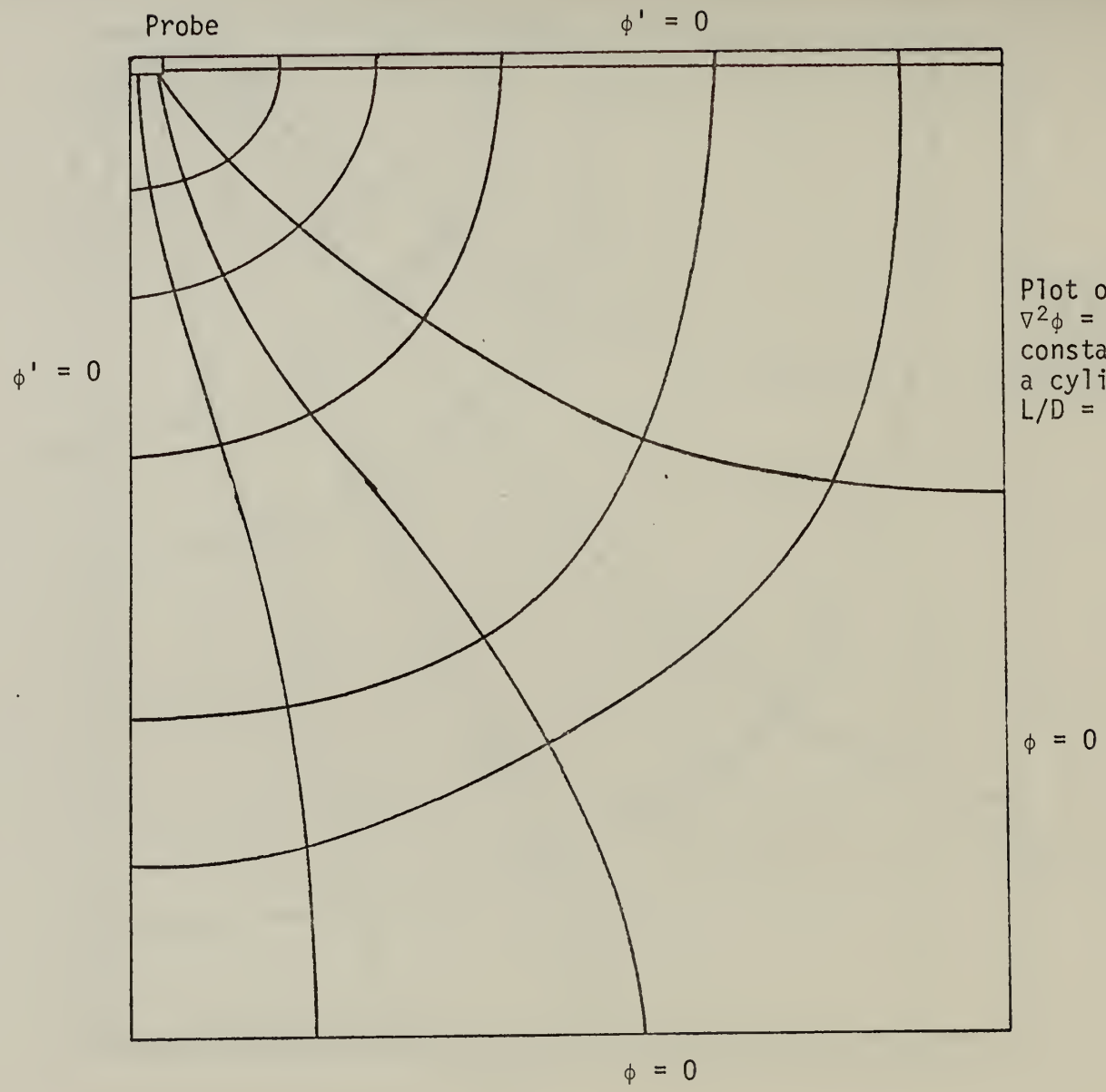

Figure 35

Plot of TRUMP solution of $\nabla^2\phi = 0$. Isopotentials and constant current lines for a cylindrical probe with L/D = 4.

$\phi = 0$ (Conductive Boundary)

$\phi' = 0$ (Insulated Boundary)

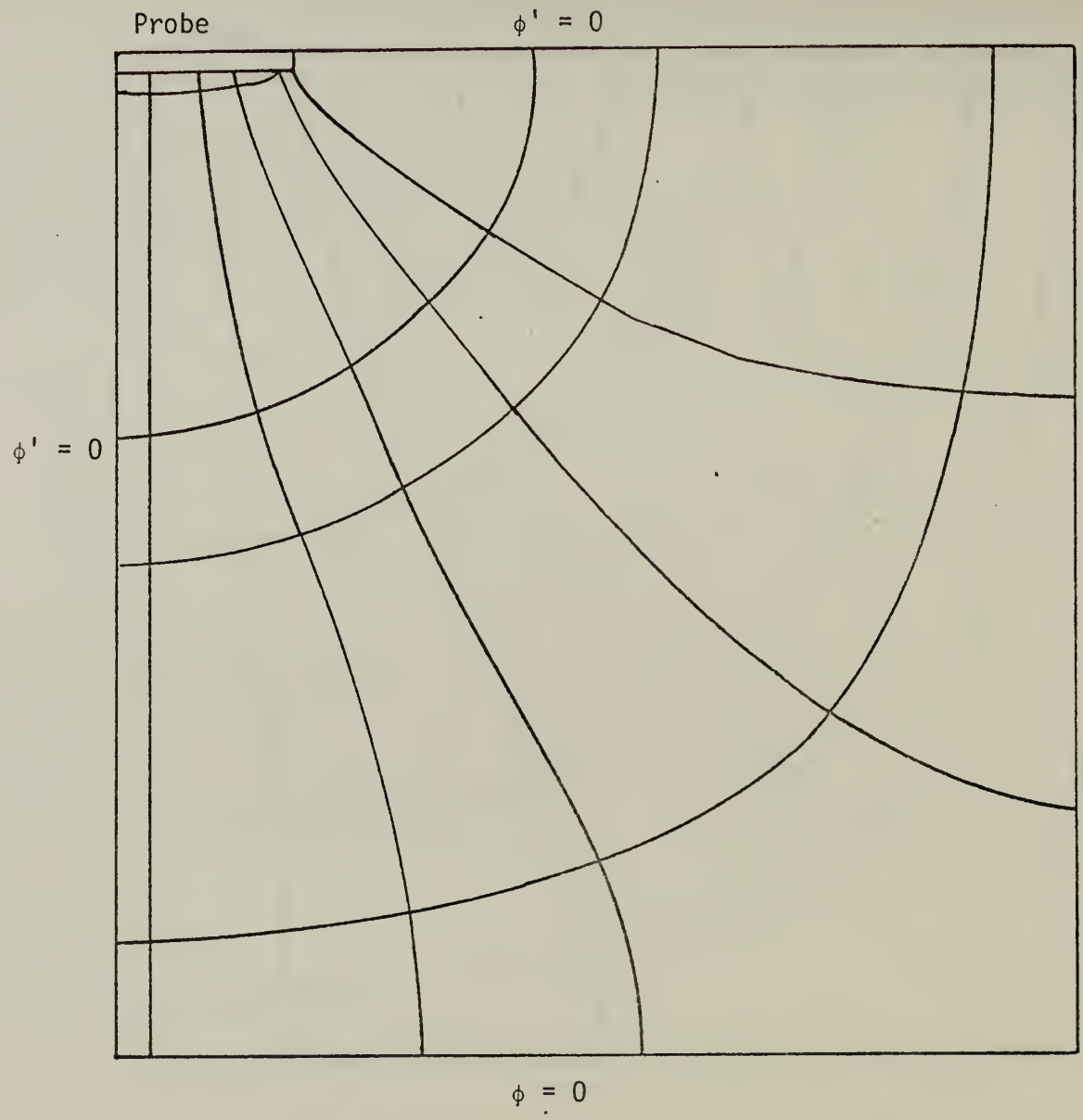

Figure 36

Plot of TRUMP solution of $\nabla^2\phi = 0$. Isopotentials and constant current lines for a cylindrical probe with L/D = 10.

$\phi = 0$ (Conductive Boundary)

$\phi' = 0$ (Insulated Boundary)

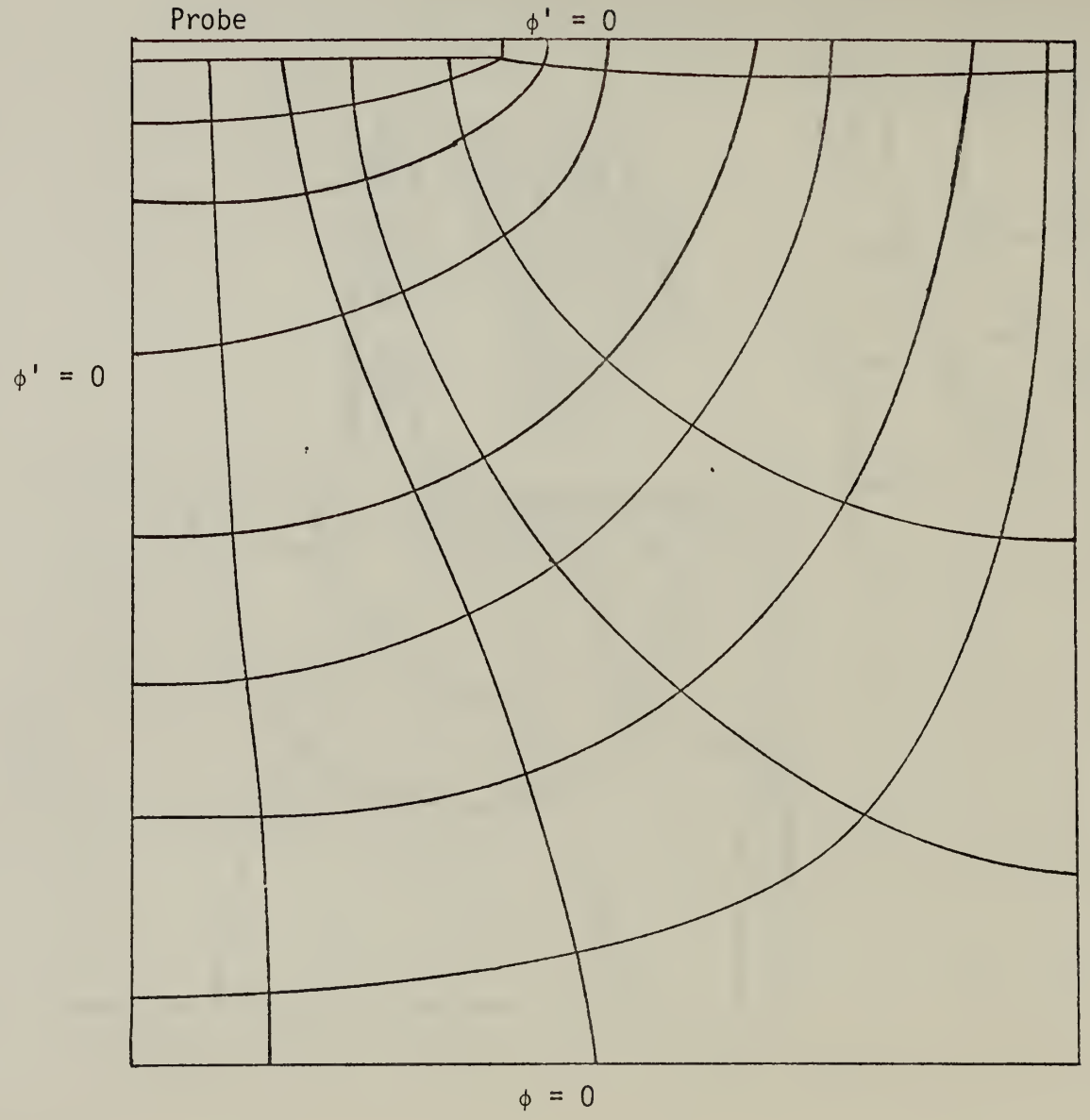

Figure 37

Plot of TRUMP solution of $\nabla^2\phi = 0$. Isopotentials and constant current lines for a cylindrical probe with L/D = 20.

$\theta = 0$ (Conductive Boundary)

$\theta' = 0$ (Insulated Boundary)

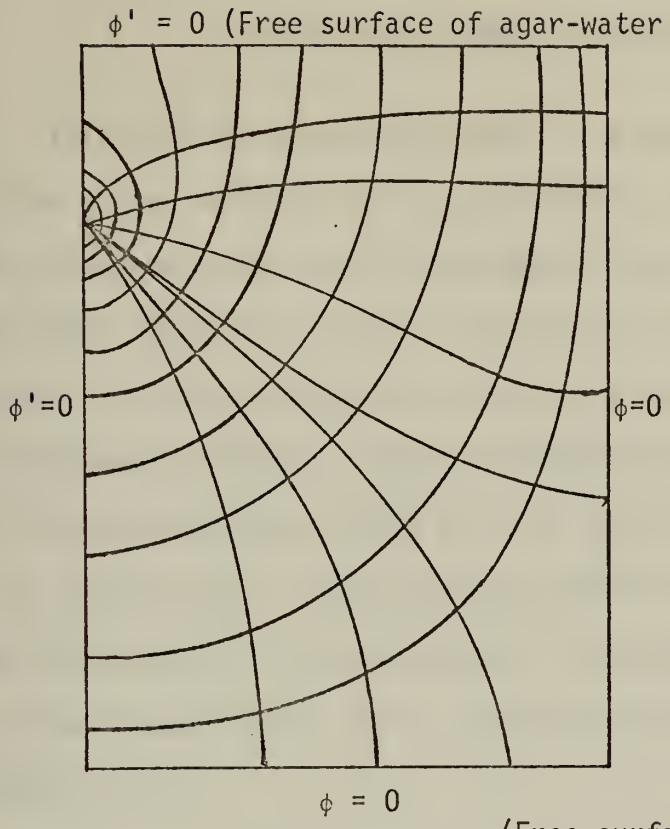

Figure 38

Teledeltus plot of isopotentials and constant current lines in a plane perpendicular to the cylindrical probe axis.

Free surface of agar-water mixture acting as an insulator.

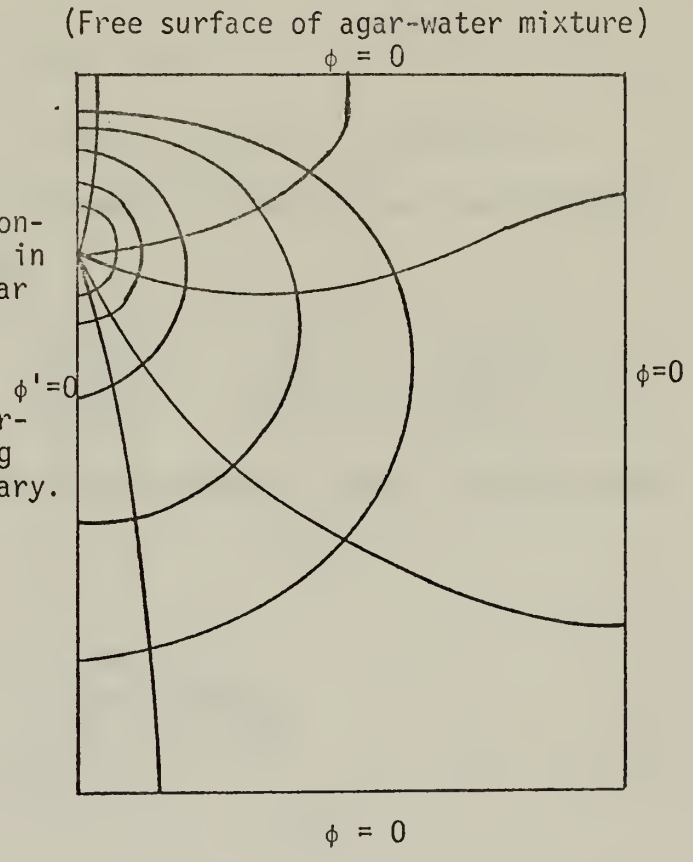

Figure 39
Teledeltus plot of isopotentials and constant current lines in a plane perpendicular to the cylindrical probe axis.

Free surface of agar-water mixture acting as conductive boundary.

APPENDIX D: SAMPLE UNCERTAINTY ANALYSIS

Reference 30 categorizes error in experimental investigation as fixed error, variable error, and mistakes. Fixed error is defined as a constant error such as equipment consistently reading low. Variable error is caused by variations in sensors, an example of which is having two different observers taking readings in separate experimental trials. Finally, mistakes may occur during experiments by reading the wrong scale, etc. If it is assumed that the error, i.e. uncertainty, of each primary variable has the same probability of occurrence, it is then possible to calculate the overall uncertainty in each value. As an example, define P, the result of some experiment as,

$$P = P(x_1, x_2, x_3, \ldots x_n)$$

If ω_p is the uncertainty in P, and ω_1, ω_2, ω_3, $\ldots\omega_n$ are the uncertainty in each primary independent variable, then the relative uncertainty in P is defined as

$$\frac{\omega_p}{P} = \sqrt{\left(\frac{\omega_1}{x_1}\right)^2 + \left(\frac{\omega_2}{x_2}\right)^2 + \left(\frac{\omega_3}{x_3}\right)^2 + \ldots + \left(\frac{\omega_n}{x_n}\right)^2} \qquad (D\text{-}1)$$

In the experimental trials on the spherical probe, the quantities calculated were

$$G_o = \frac{I^2\rho_o}{16\pi^2 r_o^2 k\, T_o} = \frac{V^2\rho_o}{16\pi^2 r_o^2 k\, T_o R_{10}^2}$$

$$\theta = \frac{T - T_o}{T_o} \qquad \tau = \frac{\alpha t}{r_o^2}$$

$$R = \frac{r_p}{r_{o_p}}$$

Deriving the expressions for the relative uncertainty in each quantity

$$\frac{\omega_{G_o}}{G_o} = \left[\left(\frac{2\omega_V}{V}\right)^2 + \left(\frac{\omega_{\rho_o}}{\rho_o}\right)^2 + \left(\frac{2\omega_{r_o}}{r_o}\right)^2 + \left(\frac{\omega_k}{K}\right)^2 + \left(\frac{\omega_{T_o}}{T_o}\right)^2 + \left(\frac{2\omega_{R_e}}{R_e}\right)^2\right]^{1/2}$$

$$\frac{\omega_\theta}{\theta} = \left[\left(\frac{\omega_T}{T - T_o}\right)^2 + \left(\frac{\omega_{T_o}}{T - T_o}\right)^2\right]^{1/2}$$

$$\frac{\omega_R}{R} = \left[\left(\frac{\omega_{r_p}}{r_p}\right)^2 + \left(\frac{\omega_{r_{o_p}}}{r_{o_p}}\right)^2\right]^{1/2}$$

$$\frac{\omega_\tau}{\tau} = \left[\left(\frac{\omega_\alpha}{\alpha}\right)^2 + \left(\frac{\omega_t}{t}\right)^2 + \left(\frac{2\omega_{r_o}}{r_o}\right)^2\right]^{1/2}$$

For all independent variables except resistivity ρ_o it was possible to estimate the uncertainty either directly from observing equipment (voltage, current) or from available tables (α, k). For resistivity it was necessary to calculate uncertainty using

$$\rho_o = \left(\frac{V}{I}\right)\left(\frac{A}{L}\right) = \frac{V_{cct} - V_R}{V_R}\left(\frac{R_{10}}{L}\right)\left(\frac{\pi D^2}{4}\right)$$

Following the example of Equation D-1,

$$\frac{\omega_{\rho_o}}{\rho_o} = \left[\left(\frac{\omega_{V_{cct}}}{V_{cct} - V_R} \right)^2 + \left(\frac{\omega_{V_R}}{V_{cct} - V_R} \right)^2 + \left(\frac{\omega_{V_{cct}}}{V_{cct}} \right)^2 + \left(\frac{\omega_{R_{10}}}{R_{10}} \right)^2 + \left(\frac{2\omega_D}{D} \right)^2 + \left(\frac{\omega_L}{L} \right)^2 \right]^{1/2}$$

Table D-1 lists values of uncertainty for each independent variable and the value of the variable used in the calculations. The following values were calculated for uncertainty:

$$\frac{\omega_{\rho_o}}{\rho_o} = 0.036 \ (3.6\%)$$

$$\frac{\omega_{G_o}}{G_o} = 0.1217 \ (12.2\%)$$

$$\frac{\omega_\theta}{\theta} = 0.019 \ (1.9\%)$$

$$\frac{\omega_R}{R} = 0.029 \ (2.9\%)$$

$$\frac{\omega_\tau}{\tau} = 0.102 \ (10.2\%)$$

To obtain uncertainty in the quantity θ/G_o the following relationship was used

$$\frac{\omega_{\theta/G_o}}{\theta/G_o} = \left[\left(\frac{\omega_\theta}{\theta} \right)^2 + \left(\frac{\omega_{G_o}}{G_o} \right)^2 \right]^{1/2}$$

Using the values above,

$$\frac{\omega_{\theta/G_o}}{\theta/G_o} = 0.123 \ (12.3\%)$$

As may be seen from the last column of Table D-1, the largest uncertainties arise from the thermophysical properties, i.e. thermal conductivity (k), thermal diffusivity (α), and resistivity (ρ_o).

Table D-1

Quantity x_i	Uncertainty ω_i	Percent Uncertainty
V_{cct} = 80.0 volts	0.0025 volts	0
V_R = 0.118 volts	0.0025 volts	0.02
D = 2.540 cm	0.025 cm	0
L = 11.95 cm	0.025 cm	0
R_{10} = 10.0 ohms	0.3 ohms	0.03
V = 0.60 volts	0.0025 volts	0
r_o = 0.241 cm	0.001 cm	0
T_o = 23.0 °C	0.25 °C	0.01
T = 37.0 °C	0.10 °C	0
r_{o_p} = 0.380 cm	0.01 cm	0.02
r_p = 0.90 cm	0.01 cm	0.01
t = 30.0 sec	0.025 sec	0
k = 0.628 W/m°K	0.0628 W/m°K	10.0
α = 0.001512 m^2/sec	0.0001512 m^2/sec	10.0
ρ_o = 3250.0 ohm-cm	117.0 ohm-cm	3.60

APPENDIX E

```
C       COMPUTER PROGRAM I
C       PROGRAM FOR THE INSULATED SPHERE.
C
C
C       MODIFIED TO REFLECT CHANGING RESISTIVITY
C
C
C
C       TET REPRESENTS THE NONDIMENSIONAL TEMPERATURE.
C       BETA IS THE BLOOD FLOW TERM.
C       G IS THE NONDIMENSIONAL POWER TERM.
C       DR IS DELTA RADIUS.
C       EM REPRESENTS THE M IN THE STABILITY CRITERIA.
C       DELTAU REPRESENTS NONDIMENSIONAL TIME CHANGE.
        DIMENSION TET(500,2),TT(500,2),RHO(500)
        ITIME=0
        READ(5,100)BETA,DR,GO,AM,LI,IH
100     FORMAT(3F10.4,F10.6,2I10)
        WRITE(6,150)BETA,DR,GO,AM,LI,IH
150     FORMAT('1',6X,'BETA = ',F4.2,/,7X,'DR = ',F6.4,/,7X,'G
       AO' = ',F6.1,/,7X,'SMALL M =',F10.6,/,7X,'LI = ',I3,/,7X
       B,'HI = ',I4.//)
        TET(1,1)=0.0
        WRITE(6,2000)
2000    FORMAT('1',T4,'TEMPERATURE DISTRIBUTION AT SPECIFIED T
       AIME AND RADIAL LOCATIONS',//,9X,'TIME (TAU)',1X,'LOCAT
       BION (R)',3X,'TEMPERATURE (THETA)/POWER (GO)')
        S=AM*DR**2*GO
        EM=1.0/(2.0+BETA*DR**2-S)
        DELTAU=EM*DR**2
        DO 10 K=1,IH
10      TET(K,1)=0.0
50      DO 200 I=LI,IH
        TET(IH+1,1)=TET(IH-1,1)
        TET(LI-1,1)=TET(LI+1,1)
        X=FLOAT(I)
200     TET(I,2)=EM*((1.-1./X)*TET(I-1,1)+(1.+1./X)*TET(I+1,1)
       B)+TET(I,1)*(1.-2.*EM+(EM*DR**2*AM*GO)/(X*DR)**4)+(GO*E
       CM*DR**2)/(X*DR)**4
        ITIME=ITIME+1
        TIME=FLOAT(ITIME)
        TAU=TIME*DELTAU
        IF(ITIME.GT.1000) GO TO 90
        IF(ITIME.GT.100) GO TO 70
        ITEST=ITIME/20*20
        GO TO 80
70      ITEST=ITIME/50*50
        GO TO 80
90      ITEST=ITIME/100*100
80      J=0
        DO 60 J=LI,IH
        Y=FLOAT(J)
        R=Y*DR
        IF((ITIME-ITEST).NE.0) GO TO 60
        TT(J,2)=TET(J,2)/GO
        WRITE(6,220) TAU,R,TT(J,2)
220     FORMAT(' ',F15.4,7X,F6.3,5X,E15.7)
60      TET(J,1)=TET(J,2)
        IF(ITIME.GT.4000)STOP
        GO TO 50
          END
```

```
C      COMPUTER PROGRAM II
C      PROGRAM FOR THE INSULATED CYLINDER
C
C      MODIFIED FOR VARIABLE RESISTIVITY
C
C      TET REPRESENTS THE NONDIMENSIONAL TEMPERATURE.
C      BETA IS THE BLOOD FLOW TERM.
C      G IS THE NONDIMENSIONAL POWER TERM.
C      DR IS DELTA RADIUS.
C      EM REPRESENTS THE M IN THE STABILITY CRITERIA.
C      DELTAU REPRESENTS NONDIMENSIONAL TIME CHANGE.
       DIMENSION TET(500,2),TT(500,2)
       ITIME=0
       READ(5,100)BETA,DR,GO,AM,LI,IH
100    FORMAT(3F10.4,F10.6,2I10)
       WRITE(6,150)BETA,DR,GO,AM,LI,IH
150    FORMAT('1',6X,'BETA = ',F4.2,/,7X,'DR = ',F6.4,/,7X,'G
      AO = ',F6.3,/,7X,'SMALL M = ',F10.6,/,7X,'LI = ',I3,/,'
      BHI = ',I4,//)
       WRITE(6,2000)
2000   FORMAT('1',T4,'TEMPERATURE DISTRIBUTION AT SPECIFIED T
      AIME AND RADIAL LOCATIONS',//,9X,'TIME (TAU)',1X,'LOCAT
      BION (R)',3X,'TEMPERATURE (THETA)/POWER (GO)')
       EM=1.0/(2.0-BETA*DR**2-AM*GO)
       DELTAU=EM*DR**2
       DO 10 K=1,IH
10     TET(K,1)=0.0
50     DO 200 I=LI,IH
       TET(IH+1,1)=TET(IH-1,1)
       TET(LI-1,1)=TET(LI+1,1)
       X=I
200    TET(I,2)=EM*((1.-1./(2.*X))*TET(I-1,1)+(1.+1./(2.*X))*
      ATET(I+1,1))+(1.-BETA*EM*DR**2-2.*EM+(AM*GO*EM)/X**2)*T
      BET(I,1)+(GO*EM)/X**2
       ITIME=ITIME+1
       TAU=ITIME*DELTAU
       IF(ITIME.GT.1000) GO TO 90
       IF(ITIME.GT.100) GO TO 70
       ITEST=ITIME/20*20
       GO TO 80
70     ITEST=ITIME/50*50
       GO TO 80
90     ITEST=ITIME/100*100
80     J=0
       DO 60 J=LI,IH
       R=J*DR
       IF((ITIME-ITEST).NE.0) GO TO 60
       TT(J,2)=TET(J,2)/GO
       WRITE(6,220)TAU,R,TT(J,2)
220    FORMAT(' ',F15.4,7X,F6.3,5X,E15.7)
60     TET(J,1)=TET(J,2)
       IF(ITIME.GT.4000)STOP
       GO TO 50
        END
```

```
C       PROGRAM NUMBER III
C       PROGRAM TO FIT AND PLOT CURVES FOR RESISTIVITY AND
C       TEMPERATURE DATA.  SUBROUTINE LSQPL2 IS CALLED TO FIT
C       THE CURVES TO DATA.  SUBROUTINE DRAW IS USED TO PLOT
C       THESE CURVES AND THE DATA POINTS.  ALL ARGUMENTS FOR
C       LSQPL2 MUST BEGIN WITH D EXCEPT M AND KM.
C       FOR  ALL DRAW THE FOLLOWING NOTATION IS USED
C       M=NUMPTS. THE NUMBER OF POINTS
C       TEMP=NONDIMENSIONAL TEMPERATURE (X)
C       RES=RESISTIVITY (Y)
C       DX REPRESENTS NONDIMENSIONAL TEMPERATURE---THETA.
C       DF2 IS RESISTIVITY
        IMPLICIT REAL*8(D)
        REAL*8 TITLE(10)/10*' '/
        REAL*8 ITITLE
        REAL*8 LABEL/'          '/
        REAL LABEL2/4HHEAT/
        REAL LABEL1/4HCOOL/
        DIMENSION DX(100),DF2(100),DWI(100),DY(100),DELY(100),
       ADB(100),DSB(100),THET(100),TEMP(100),RES(100),B(100),Y
       B(100),ITITLE(12),DTHET(100),DRES(100),THETA(100)
        READ(5,9)(ITITLE(I),I=1,12)
9       FORMAT(A8)
        DO 100 J=1,2
        READ(5,1)M,KM,XCAL,YCAL
1       FORMAT(2I10,2F10.1)
        WRITE(6,2)M,KM,YCAL,XCAL
2       FORMAT(30H1 THE NUMBER OF DATA POINTS IS ,I10,/,30HO T
       AHE MAXIMUM DEGREE OF FIT IS ,I10,/,21HO THE Y-AXIS SCA
       BLE IS ,F10.1,21HO IN DEGREES PER INCH ,/,21HO THE X-AX
       CIS SCALE IS ,F10.1,20HO IN OHM-CM PER INCH )
        READ(5,3)(DX(I),DF2(I),I=1,M)
3       FORMAT(2F10.1)
        READ(5,11)TO
11      FORMAT(F5.1)
        WRITE(6,12)TO
12      FORMAT(34HO THE INITIAL TEMPERATURE (TO) WAS,F5.1,9HOI
        DTO=TO
        DO 7 I=1,M
        DRES(I)=DF2(I)/DF2(1)
        DTHET(I)=(DX(I)-DTO)/DTO
7       DWI(I)=1.0000000
        WRITE(6,4)
4       FORMAT(14X,45HODIMENSIONAL VALUES    NONDIMENSIONAL VA
       BLUES ,/,9X,51H TEMPERATURE  RESISTIVITY       THETA
       C  RHO-PRIME ,/,9X,24H (DEGREES C)     (OHM-CM) ,//)
        WRITE(6,6)(DX(I),DF2(I),DTHET(I),DRES(I),I=1,M)
6       FORMAT(12X,F6.1,7X,F6.1,8X,F8.6,5X,F8.6)
        CALL LSQPL2(M,KM,DTHET,DRES,DWI,DY,DELY,DB,DSB,TITLE)
        DO 15 I=1,KM
15      B(I)=DB(I)
        DO 8 I=1,M
        Y(I)=DY(I)
        THETA(I)=DTHET(I)
8       RES(I)=DRES(I)
        IF(J.EQ.2) GO TO 101
99      CALL DRAW(M,THETA,RES,1,5,LABEL,ITITLE,XCAL,YCAL,0,0,0
       A,0,8,11,1,LAST)
        CALL DRAW(M,THETA,Y,2,0,LABEL2,ITITLE,XCAL,YCAL,0,0,0,
       A0,8,11,1,LAST)
        WRITE(6,13) LAST
13      FORMAT(8HO LAST = ,I3)
        GO TO 100
101     CALL DRAW(M,THETA,RES,2,4,LABEL,ITITLE,XCAL,YCAL,0,0,0
       A,0,8,11,1,LAST)
        CALL DRAW(M,THETA,Y,3,0,LABEL1,ITITLE,XCAL,YCAL,0,0,0,
       A0,8,11,1,LAST)
        WRITE(6,104)LAST
104     FORMAT(8HO LAST = ,I3)
100     CONTINUE
        STOP
        END
```

APPENDIX F

TEMPERATURE AND RESISTIVITY VALUES
DATA SET A

HEATING CONDITIONS

THE NUMBER OF DATA POINTS IS 5
THE MAXIMUM DEGREE OF FIT IS 1
THE Y-AXIS SCALE IS 0.10 IN DEGREES PER INCH
THE X-AXIS SCALE IS 1.00 IN OHM-CM PER INCH
THE INITIAL TEMPERATURE (TO) WAS 21.00IN DEG C

DIMENSIONAL VALUES		NONDIMENSIONAL VALUES	
TEMPERATURE (DEGREES C)	RESISTIVITY (OHM-CM)	THETA	RHO-PRIME
27.5	2753.6	0.309524	1.000000
31.3	2508.5	0.490476	0.910989
37.5	2508.5	0.785714	0.910989
44.0	2014.9	1.095238	0.731733
51.4	1800.1	1.447619	0.653726

COEFFICIENTS OF THE POWER SERIES EXPANSION
Y(X)=B(1)+B(2)*X+B(3)*X**2...

B(1)= 1.09146D 00 B(2)=-3.02738D-01

ESTIMATES OF ERROR FOR THE COEFFICIENTS

ERRB(1)=9.288D-02 ERRB(2)=1.008D-01
SUM SQ DEV = 1.023D-03 F-RATIO = 9.028D 00
CHISQ= 5.993D-03 DEG OF FREEDOM = 3.

I	X(I)	F2(I)	Y(I)	DELY(I)
1	0.310	1.00000000D 00	9.9775817D-01	-2.2418303D-03
2	0.490	9.1098925D-01	9.4297694D-01	3.1987691D-02
3	0.786	9.1098925D-01	8.5359704D-01	-5.7392208D-02
4	1.095	7.3173300D-01	7.5989231D-01	2.8159305D-02
5	1.448	6.5372603D-01	6.5321307D-01	-5.1295695D-04

TEMPERATURE AND RESISTIVITY VALUES
DATA SET A

COOLING CONDITIONS

THE NUMBER OF DATA POINTS IS 9
THE MAXIMUM DEGREE OF FIT IS 1
THE Y-AXIS SCALE IS 0.10 IN DEGREES PER INCH
THE X-AXIS SCALE IS 1.00 IN OHM-CM PER INCH
THE INITIAL TEMPERATURE (TO) WAS 21.00IN DEG C

DIMENSIONAL VALUES		NONDIMENSIONAL VALUES	
TEMPERATURE (DEGREES C)	RESISTIVITY (OHM-CM)	THETA	RHO-PRIME
25.2	2870.5	0.200000	1.000000
29.9	2687.9	0.423810	0.936387
31.2	2645.9	0.485714	0.921756
32.7	2546.3	0.557143	0.887058
33.6	2508.5	0.600000	0.873890
34.6	2453.8	0.647619	0.854834
35.9	2418.7	0.709524	0.842606
40.8	2242.2	0.942857	0.781118
44.7	2102.7	1.128571	0.732520

COEFFICIENTS OF THE POWER SERIES EXPANSION
Y(X)=B(1)+B(2)*X+B(3)*X**2...

B(1)= 1.05463D 00 B(2)=-2.91728D-01

ESTIMATES OF ERROR FOR THE COEFFICIENTS

ERRB(1)=1.928D-02 ERRB(2)=2.818D-02
SUM SQ DEV = 4.170D-05 F-RATIO = 1.071D 02
CHISQ= 4.352D-04 DEG OF FREEDOM = 7.

I	X(I)	F2(I)	Y(I)	DELY(I)
1	0.200	1.00000000D 00	9.9627984D-01	-3.7201594D-03
2	0.424	9.3638739D-01	9.3098836D-01	-5.3990293D-03
3	0.486	9.2175579D-01	9.1292901D-01	-8.8267779D-03
4	0.557	8.8705800D-01	8.9209131D-01	5.0353033D-03
5	0.600	8.7388957D-01	8.7958868D-01	5.6991168D-03
6	0.648	8.5483365D-01	8.6569688D-01	1.0863226D-02
7	0.710	8.4260582D-01	8.4763753D-01	5.0317150D-03
8	0.943	7.8111827D-01	7.7956769D-01	-1.5505811D-03
9	1.129	7.3252047D-01	7.2538965D-01	-7.1308133D-03

TEMPERATURE AND RESISTIVITY VALUES
DATA SET B

HEATING CONDITIONS

THE NUMBER OF DATA POINTS IS 5
THE MAXIMUM DEGREE OF FIT IS 1
THE Y-AXIS SCALE IS 0.10 IN DEGREES PER INCH
THE X-AXIS SCALE IS 1.00 IN OHM-CM PER INCH
THE INITIAL TEMPERATURE (TO) WAS 23.00IN DEG C

DIMENSIONAL VALUES		NONDIMENSIONAL VALUES	
TEMPERATURE (DEGREES C)	RESISTIVITY (OHM-CM)	THETA	RHO-PRIME
26.2	3723.4	0.139130	1.000000
32.2	3422.1	0.400000	0.919079
40.4	2997.6	0.756522	0.805071
46.0	2753.6	1.000000	0.739539
52.0	2508.4	1.260870	0.673685

COEFFICIENTS OF THE POWER SERIES EXPANSION
Y(X)=B(1)+B(2)*X+B(3)*X**2...

B(1)= 1.03617D 00 B(2)=-2.93393D-01

ESTIMATES OF ERROR FOR THE COEFFICIENTS

ERRB(1)=1.533D-02 ERRB(2)=1.875D-02
SUM SQ DEV = 3.424D-05 F-RATIO = 2.449D 02
CHISQ= 2.218D-04 DEG OF FREEDOM = 3.

I	X(I)	F2(I)	Y(I)	DELY(I)
1	0.139	1.0000000D 00	9.9534654D-01	-4.6534639D-03
2	0.400	9.1907934D-01	9.1880931D-01	-2.7002533D-04
3	0.757	8.0507063D-01	8.1420844D-01	9.1378018D-03
4	1.000	7.3953913D-01	7.4277369D-01	3.2345616D-03
5	1.261	6.7368534D-01	6.6623647D-01	-7.4488742D-03

TEMPERATURE AND RESISTIVITY VALUES
DATA SET B

COOLING CONDITIONS

THE NUMBER OF DATA POINTS IS 19
THE MAXIMUM DEGREE OF FIT IS 1
THE Y-AXIS SCALE IS 0.10 IN DEGREES PER INCH
THE X-AXIS SCALE IS 1.00 IN OHM-CM PER INCH
THE INITIAL TEMPERATURE (TO) WAS 23.00IN DEG C

DIMENSIONAL VALUES		NONDIMENSIONAL VALUES	
TEMPERATURE (DEGREES C)	RESISTIVITY (OHM-CM)	THETA	RHO-PRIME
24.1	3872.4	0.047826	1.000000
24.7	3850.4	0.073913	0.994319
25.7	3764.8	0.117391	0.972214
26.5	3743.9	0.152174	0.966816
28.3	3662.9	0.230435	0.945899
29.4	3585.3	0.278261	0.925860
30.0	3547.7	0.304348	0.916150
31.0	3492.8	0.347826	0.901973
32.5	3394.7	0.413043	0.876640
35.7	3226.3	0.552174	0.833153
38.0	3136.6	0.652174	0.809989
40.3	3079.5	0.752174	0.795243
42.0	2971.3	0.826087	0.767302
46.2	2822.5	1.008696	0.728876
48.0	2753.6	1.086957	0.711084
51.4	2546.2	1.234783	0.657525
53.5	2527.2	1.326087	0.652619
56.3	2453.8	1.447826	0.633664
59.6	2384.6	1.591304	0.615794

COEFFICIENTS OF THE POWER SERIES EXPANSION
Y(X)=B(1)+B(2)*X+B(3)*X**2...

B(1)= 9.96853D-01 B(2)=-2.59982D-01

ESTIMATES OF ERROR FOR THE COEFFICIENTS

ERRB(1)=2.404D-02 ERRB(2)=2.947D-02
SUM SQ DEV = 1.840D-04 F-RATIO = 7.784D 01
CHISQ= 4.787D-03 DEG OF FREEDOM = 17.

I	X(I)	F2(I)	Y(I)	DELY(I)
1	0.048	1.0000000D 00	9.8441862D-01	-1.5581376D-02
2	0.074	9.9431877D-01	9.7763649D-01	-1.6682284D-02
3	0.117	9.7221361D-01	9.6633292D-01	-5.8806934D-03
4	0.152	9.6681644D-01	9.5729007D-01	-9.5263750D-03
5	0.230	9.4589918D-01	9.3694365D-01	-8.9555299D-03
6	0.278	9.2585993D-01	9.2450973D-01	-1.3501984D-03
7	0.304	9.1615019D-01	9.1772759D-01	1.5774039D-03
8	0.348	9.0197294D-01	9.0642403D-01	4.4510941D-03
9	0.413	8.7663981D-01	8.8946868D-01	1.2828875D-02
10	0.552	8.3315257D-01	8.5329728D-01	2.0144712D-02
11	0.652	8.0998864D-01	8.2729908D-01	1.7310444D-02
12	0.752	7.9524326D-01	8.0130088D-01	6.0576240D-03
13	0.826	7.6730193D-01	7.8208482D-01	1.4782893D-02
14	1.009	7.2887615D-01	7.3460986D-01	5.7337062D-03
15	1.087	7.1108357D-01	7.1426344D-01	3.1798741D-03
16	1.235	6.7752505D-01	6.7583132D-01	1.8306273D-02
17	1.326	6.5261853D-01	6.5209384D-01	-5.2469423D-04
18	1.448	6.3366388D-01	6.2044386D-01	-1.3220020D-02
19	1.591	6.1579382D-01	5.8314210D-01	-3.2651727D-02

TEMPERATURE AND RESISTIVITY VALUES
DATA SET C

HEATING CONDITIONS

THE NUMBER OF DATA POINTS IS 5
THE MAXIMUM DEGREE OF FIT IS 1
THE Y-AXIS SCALE IS 0.10 IN DEGREES PER INCH
THE X-AXIS SCALE IS 1.00 IN OHM-CM PER INCH
THE INITIAL TEMPERATURE (TO) WAS 22.50IN DEG C

DIMENSIONAL VALUES		NONDIMENSIONAL VALUES	
TEMPERATURE (DEGREES C)	RESISTIVITY (OHM-CM)	THETA	RHO-PRIME
24.8	3428.4	0.102222	1.000000
29.5	3110.6	0.311111	0.907304
35.4	2799.1	0.573333	0.816445
41.3	2544.3	0.835556	0.742125
47.8	2299.9	1.124444	0.670838

COEFFICIENTS OF THE POWER SERIES EXPANSION
Y(X)=B(1)+B(2)*X+B(3)*X**2...

B(1)= 1.01512D 00 B(2)=-3.18632D-01

ESTIMATES OF ERROR FOR THE COEFFICIENTS

ERRB(1)=3.256D-02 ERRB(2)=4.701D-02
SUM SQ DEV = 1.755D-04 F-RATIO = 4.595D 01
CHISQ= 1.059D-03 DEG OF FREEDOM = 3.

I I	X(I) X(I)	F2(I) F2(I)	Y(I) Y(I)	DELY(I) DELY(I)
1	0.102	1.00000000D 00	9.82551580-01	-1.7448425D-02
2	0.311	9.0730370D-01	9.1599281D-01	8.6891120D-03
3	0.573	8.1644499D-01	8.3244032D-01	1.5995330D-02
4	0.836	7.4212461D-01	7.4888783D-01	6.7632205D-03
5	1.124	6.7083771D-01	6.5683847D-01	-1.3999237D-02

TEMPERATURE AND RESISTIVITY VALUES
DATA SET C

COOLING CONDITIONS

THE NUMBER OF DATA POINTS IS 21
THE MAXIMUM DEGREE OF FIT IS 1
THE Y-AXIS SCALE IS 0.10 IN DEGREES PER INCH
THE X-AXIS SCALE IS 1.00 IN OHM-CM PER INCH
THE INITIAL TEMPERATURE (TO) WAS 22.50IN DEG C

DIMENSIONAL VALUES		NONDIMENSIONAL VALUES	
TEMPERATURE (DEGREES C)	RESISTIVITY (OHM-CM)	THETA	RHO-PRIME
23.5	3463.8	0.044444	1.000000
25.2	3428.4	0.120000	0.989780
25.8	3359.8	0.146667	0.969975
26.2	3359.8	0.164444	0.969975
27.1	3326.5	0.204444	0.960361
28.4	3261.8	0.262222	0.941683
30.0	3199.6	0.333333	0.923725
31.0	3169.4	0.377778	0.915007
31.6	3082.1	0.404444	0.889803
33.3	3026.4	0.480000	0.873723
35.3	2921.0	0.568889	0.843293
37.2	2822.7	0.653333	0.814914
39.2	2730.7	0.742222	0.788354
40.8	2644.6	0.813333	0.763497
46.7	2415.9	1.075556	0.697471
49.5	2315.8	1.200000	0.668572
52.0	2253.5	1.311111	0.650586
53.9	2194.5	1.395556	0.633553
55.6	2152.2	1.471111	0.621341
57.5	2085.2	1.555556	0.601998
61.0	1986.3	1.711111	0.573445

COEFFICIENTS OF THE POWER SERIES EXPANSION
Y(X)=B(1)+B(2)*X+B(3)*X**2...

B(1)= 1.00608D 00 B(2)=-2.68473D-01

ESTIMATES OF ERROR FOR THE COEFFICIENTS
ERRB(1)=2.339D-02 ERRB(2)=2.634D-02
SUM SQ DEV = 1.733D-04 F-RATIO = 1.039D 02
CHISQ= 5.050D-03 DEG OF FREEDOM = 19.

I	X(I)	F2(I)	Y(I)	DELY(I)
1	0.044	1.00000000D 00	9.9414846D-01	-5.8515376D-03
2	0.120	9.8978001D-01	9.7386386D-01	-1.5916152D-02
3	0.147	9.6997517D-01	9.6670459D-01	-3.2705851D-03
4	0.164	9.6997517D-01	9.6193174D-01	-8.0434331D-03
5	0.204	9.6036145D-01	9.5119283D-01	-9.1686220D-03
6	0.262	9.4168255D-01	9.3568107D-01	-6.0014703D-03
7	0.333	9.2372539D-01	9.1658968D-01	-7.1357053D-03
8	0.378	9.1500664D-01	9.0465756D-01	-1.0349077D-02
9	0.404	8.8980311D-01	8.9749829D-01	7.6951848D-03
10	0.480	8.7372250D-01	8.7721369D-01	3.4911861D-03
11	0.569	8.4329349D-01	8.5334945D-01	1.0055955D-02
12	0.653	8.1491426D-01	8.3067842D-01	1.5764164D-02
13	0.742	7.8835383D-01	8.0681418D-01	1.8460349D-02
14	0.813	7.6349674D-01	7.8772279D-01	2.4226050D-02
15	1.076	6.9747099D-01	7.1732328D-01	1.9852295D-02
16	1.200	6.6857209D-01	6.8391334D-01	1.5341256D-02
17	1.311	6.5058606D-01	6.5408305D-01	3.4969836D-03
18	1.396	6.3355275D-01	6.3141202D-01	-2.1407282D-03
19	1.471	6.2134072D-01	6.1112741D-01	-1.0213311D-02
20	1.556	6.0199781D-01	5.8845639D-01	-1.3541420D-02
21	1.711	5.7344535D-01	5.4669397D-01	-2.6751383D-02

TEMPERATURE AND RESISTIVITY VALUES
DATA SET D

HEATING CONDITIONS

THE NUMBER OF DATA POINTS IS 5
THE MAXIMUM DEGREE OF FIT IS 1
THE Y-AXIS SCALE IS 0.10 IN DEGREES PER INCH
THE X-AXIS SCALE IS 1.00 IN OHM-CM PER INCH
THE INITIAL TEMPERATURE (TO) WAS 19.00IN DEG C

DIMENSIONAL VALUES		NONDIMENSIONAL VALUES	
TEMPERATURE (DEGREES C)	RESISTIVITY (OHM-CM)	THETA	RHO-PRIME
24.7	4271.7	0.300000	1.000000
32.2	3551.6	0.694737	0.831425
40.3	3182.6	1.121053	0.745043
46.5	2810.8	1.447368	0.658005
54.8	2496.5	1.884211	0.584428

COEFFICIENTS OF THE POWER SERIES EXPANSION
Y(X)=B(1)+B(2)*X+B(3)*X**2...

B(1)= 1.04268D 00 B(2)=-2.55996D-01

ESTIMATES OF ERROR FOR THE COEFFICIENTS

ERRB(1)=7.167D-02 ERRB(2)=5.862D-02
SUM SQ DEV = 6.349D-04 F-RATIO = 1.907D 01
CHISQ= 3.980D-03 DEG OF FREEDOM = 3.

I	X(I)	F2(I)	Y(I)	DELY(I)
1	0.300	1.00000000D 00	9.6588252D-01	-3.4117482D-02
2	0.695	8.3142543D-01	8.6483137D-01	3.3405945D-02
3	1.121	7.4504296D-01	7.5569614D-01	1.0653179D-02
4	1.447	6.5800501D-01	6.7216052D-01	1.4155514D-02
5	1.884	5.8442775D-01	5.6033059D-01	-2.4097156D-02

TEMPERATURE AND RESISTIVITY VALUES
DATA SET D

COOLING CONDITIONS

THE NUMBER OF DATA POINTS IS 19
THE MAXIMUM DEGREE OF FIT IS 1
THE Y-AXIS SCALE IS 0.10 IN DEGREES PER INCH
THE X-AXIS SCALE IS 1.00 IN OHM-CM PER INCH
THE INITIAL TEMPERATURE (TC) WAS 19.00IN DEG C

DIMENSIONAL VALUES		NONDIMENSIONAL VALUES	
TEMPERATURE (DEGREES C)	RESISTIVITY (OHM-CM)	THETA	RHO-PRIME
24.1	4166.1	0.268421	1.000000
24.0	4166.1	0.263158	1.000000
25.5	4065.7	0.342105	0.975901
25.7	4017.2	0.352632	0.964259
28.2	3923.7	0.484211	0.941816
29.9	3791.3	0.573684	0.910036
31.0	3749.1	0.631579	0.899906
33.5	3551.6	0.763158	0.852500
35.7	3407.8	0.878947	0.817983
38.3	3442.7	1.015789	0.826360
42.5	3275.4	1.236842	0.786203
48.4	3066.7	1.442105	0.736108
47.6	3066.7	1.515789	0.736108
50.4	2498.0	1.652632	0.599602
52.0	2461.5	1.736842	0.590840
54.7	2408.6	1.878947	0.578143
55.6	2358.0	1.936842	0.565997
55.3	2189.2	1.910526	0.525479
57.8	2120.3	2.042105	0.508941

COEFFICIENTS OF THE POWER SERIES EXPANSION
Y(X)=B(1)+B(2)*X+B(3)*X**2...

B(1)= 1.07062D 00 B(2)=-2.64046D-01

ESTIMATES OF ERROR FOR THE COEFFICIENTS

ERRB(1)=5.741D-02 ERRB(2)=4.532D-02
SUM SQ DEV = 7.197D-04 F-RATIO = 3.395D 01
CHISQ= 2.039D-02 DEG OF FREEDOM = 17.

I	X(I)	F2(I)	Y(I)	DELY(I)
1	0.268	1.0000000D 00	9.9973970D-01	-2.6030080D-04
2	0.263	1.0000000D 00	1.0011294D 00	1.1294136D-03
3	0.342	9.7590072D-01	9.8028370D-01	4.3829747D-03
4	0.353	9.6425914D-01	9.7750427D-01	1.3245129D-02
5	0.484	9.4181609D-01	9.4276141D-01	9.4532068D-04
6	0.574	9.1003576D-01	9.1913626D-01	9.1004975D-03
7	0.632	8.9990639D-01	9.0384940D-01	3.9430164D-03
8	0.763	8.5249994D-01	8.6910654D-01	1.6606603D-02
9	0.879	8.1798325D-01	8.3853283D-01	2.0549580D-02
10	1.016	8.2636039D-01	8.0240025D-01	-2.3960135D-02
11	1.237	7.8620292D-01	7.4403224D-01	-4.2170679D-02
12	1.442	7.3610811D-01	6.8983338D-01	-4.6274729D-02
13	1.516	7.3610811D-01	6.7037738D-01	-6.5730731D-02
14	1.653	5.9960155D-01	6.3424480D-01	3.4643259D-02
15	1.737	5.9084035D-01	6.1200937D-01	2.1169020D-02
16	1.879	5.7814263D-01	5.7448708D-01	-3.6555431D-03
17	1.937	5.6599698D-01	5.5920023D-01	-6.7967500D-03
18	1.911	5.2547947D-01	5.6614880D-01	4.0669333D-02
19	2.042	5.0894122D-01	5.3140594D-01	2.2464721D-02

TEMPERATURE AND RESISTIVITY VALUES
DATA SET E

HEATING CONDITIONS

THE NUMBER OF DATA POINTS IS 5
THE MAXIMUM DEGREE OF FIT IS 1
THE Y-AXIS SCALE IS 0.10 IN DEGREES PER INCH
THE X-AXIS SCALE IS 1.00 IN OHM-CM PER INCH
THE INITIAL TEMPERATURE (TO) WAS 22.50IN DEG C

DIMENSIONAL VALUES		NONDIMENSIONAL VALUES	
TEMPERATURE (DEGREES C)	RESISTIVITY (OHM-CM)	THETA	RHO-PRIME
25.7	3451.0	0.142222	1.000000
35.7	3105.5	0.586667	0.899884
41.0	2894.7	0.822222	0.838800
44.7	2710.6	0.986667	0.785453
49.5	2529.6	1.200000	0.733005

COEFFICIENTS OF THE POWER SERIES EXPANSION
Y(X)=B(1)+B(2)*X+B(3)*X**2...

B(1)= 1.04182D 00 B(2)=-2.54679D-01

ESTIMATES OF ERROR FOR THE COEFFICIENTS

ERRB(1)=1.692D-02 ERRB(2)=2.036D-02
SUM SQ DEV = 3.281D-05 F-RATIO = 1.565D 02
CHISQ= 1.893D-04 DEG OF FREEDOM = 3.

I	X(I)	F2(I)	Y(I)	DELY(I)
1	0.142	1.0000000D 00	1.0055945D 00	5.5945479D-03
2	0.587	8.9988409D-01	8.9240367D-01	-7.4804221D-03
3	0.822	8.3880035D-01	8.3241250D-01	-6.3878439D-03
4	0.987	7.8545349D-01	7.9053188D-01	5.0783871D-03
5	1.200	7.3300493D-01	7.3620026D-01	3.1953310D-03

TEMPERATURE AND RESISTIVITY VALUES
DATA SET E

COOLING CONDITIONS

THE NUMBER OF DATA POINTS IS 9
THE MAXIMUM DEGREE OF FIT IS 1
THE Y-AXIS SCALE IS 0.10 IN DEGREES PER INCH
THE X-AXIS SCALE IS 1.00 IN OHM-CM PER INCH
THE INITIAL TEMPERATURE (TO) WAS 22.50IN DEG C

DIMENSIONAL VALUES		NONDIMENSIONAL VALUES	
TEMPERATURE (DEGREES C)	RESISTIVITY (OHM-CM)	THETA	RHO-PRIME
24.3	3796.6	0.080000	1.000000
26.4	3674.0	0.173333	0.967708
27.5	3559.0	0.222222	0.937418
29.5	3522.3	0.311111	0.927751
30.5	3416.4	0.355556	0.899858
32.0	3382.6	0.422222	0.890955
33.0	3316.8	0.466667	0.873624
33.3	3284.9	0.480000	0.865222
63.5	2627.1	1.822222	0.691961

COEFFICIENTS OF THE POWER SERIES EXPANSION
Y(X)=B(1)+B(2)*X+B(3)*X**2...

B(1)= 9.73366D-01 B(2)=-1.62877D-01

ESTIMATES OF ERROR FOR THE COEFFICIENTS

ERRB(1)=3.445D-02 ERRB(2)=5.010D-02
SUM SQ DEV = 4.706D-04 F-RATIO = 1.057D 01
CHISQ= 4.657D-03 DEG OF FREEDOM = 7.

I	X(I)	F2(I)	Y(I)	DELY(I)
1	0.080	1.0000000D 00	9.6033601D-01	-3.9663989D-02
2	0.173	9.6770795D-01	9.4513418D-01	-2.2573768D-02
3	0.222	9.3741769D-01	9.3717132D-01	-2.4637119D-04
4	0.311	9.2775115D-01	9.2269339D-01	-5.0577603D-03
5	0.356	8.9985777D-01	9.1545442D-01	1.5596652D-02
6	0.422	8.9095507D-01	9.0459597D-01	1.3640904D-02
7	0.467	8.7362377D-01	8.9735700D-01	2.3733234D-02
8	0.480	8.6522151D-01	8.9518531D-01	2.9963799D-02
9	1.822	6.9196123D-01	6.7656853D-01	-1.5392701D-02

TEMPERATURE AND RESISTIVITY VALUES
DATA SET F

HEATING CONDITIONS

THE NUMBER OF DATA POINTS IS 5
THE MAXIMUM DEGREE OF FIT IS 1
THE Y-AXIS SCALE IS 0.10 IN DEGREES PER INCH
THE X-AXIS SCALE IS 1.00 IN OHM-CM PER INCH
THE INITIAL TEMPERATURE (TO) WAS 22.50IN DEG C

DIMENSIONAL VALUES		NONDIMENSIONAL VALUES	
TEMPERATURE (DEGREES C)	RESISTIVITY (OHM-CM)	THETA	RHO-PRIME
24.2	3298.8	0.075556	1.000000
30.0	2009.1	0.333333	0.912180
38.0	2559.3	0.688889	0.775828
44.8	2381.3	0.991111	0.721869
49.0	2197.8	1.177778	0.666242

COEFFICIENTS OF THE POWER SERIES EXPANSION
Y(X)=B(1)+B(2)*X+B(3)*X**2...

B(1)= 1.011910 00 B(2)=-3.010450-01

ESTIMATES OF ERROR FOR THE COEFFICIENTS

ERRB(1)=3.607D-02 ERRB(2)=4.687D-02
SUM SQ DEV = 2.179D-04 F-RATIO = 4.125D 01
CHISQ= 1.360D-03 DEG OF FREEDOM = 3.

I	X(I)	F2(I)	Y(I)	DELY(I)
1	0.076	1.00000000D 00	9.8916102D-01	-1.0838983D-02
2	0.333	9.1218019D-01	9.1155822D-01	-6.2196487D-04
3	0.689	7.7582757D-01	8.0451988D-01	2.8692310D-02
4	0.991	7.2186856D-01	7.1353730D-01	-8.3312616D-03
5	1.178	6.6624227D-01	6.5734217D-01	-8.9001007D-03

TEMPERATURE AND RESISTIVITY VALUES
DATA SET F

COOLING CONDITIONS

THE NUMBER OF DATA POINTS IS 12
THE MAXIMUM DEGREE OF FIT IS 1
THE Y-AXIS SCALE IS 0.10 IN DEGREES PER INCH
THE X-AXIS SCALE IS 1.00 IN OHM-CM PER INCH
THE INITIAL TEMPERATURE (TO) WAS 22.50IN DEG C

DIMENSIONAL VALUES		NONDIMENSIONAL VALUES	
TEMPERATURE (DEGREES C)	RESISTIVITY (OHM-CM)	THETA	RHO-PRIME
24.0	3630.9	0.066667	1.000000
25.0	3581.6	0.111111	0.986422
25.5	3574.1	0.133333	0.984356
27.9	3465.7	0.240000	0.954502
29.8	3330.9	0.324444	0.917376
33.5	3206.2	0.488889	0.883032
38.2	2906.9	0.697778	0.800600
43.0	2743.9	0.911111	0.755708
51.0	2449.4	1.266667	0.674599
55.0	2348.6	1.444444	0.646837
60.5	2183.8	1.688889	0.601449
65.5	2077.7	1.911111	0.572227

COEFFICIENTS OF THE POWER SERIES EXPANSION
Y(X)=B(1)+B(2)*X+B(3)*X**2...

B(1)= 1.00200D 00 B(2)=-2.42002D-01

ESTIMATES OF ERROR FOR THE COEFFICIENTS

ERRB(1)=3.175D-02 ERRB(2)=3.181D-02
SUM SQ DEV = 3.350D-04 F-RATIO = 5.786D 01
CHISQ= 5.607D-03 DEG OF FREEDOM = 10.

I	X(I)	F2(I)	Y(I)	DELY(I)
1	0.067	1.00000000D 00	9.8586368D-01	-1.4136322D-02
2	0.111	9.8642210D-01	9.7510801D-01	-1.1314087D-02
3	0.133	9.8435650D-01	9.6973018D-01	-1.4626316D-02
4	0.240	9.5450164D-01	9.4391658D-01	-1.0585056D-02
5	0.324	9.1737586D-01	9.2348082D-01	6.1049610D-03
6	0.489	8.8303176D-01	8.8368486D-01	6.5310099D-04
7	0.698	8.0060040D-01	8.3313323D-01	3.2532827D-02
8	0.911	7.5570795D-01	7.8150603D-01	2.5798084D-02
9	1.267	6.7459858D-01	6.9546071D-01	2.0862127D-02
10	1.444	6.4683687D-01	6.5243805D-01	5.6011774D-03
11	1.689	6.0144868D-01	5.9328189D-01	-8.1667866D-03
12	1.911	5.7222727D-01	5.3950356D-01	-3.2723708D-02

TEMPERATURE AND RESISTIVITY VALUES
DATA SET G

HEATING CONDITIONS

THE NUMBER OF DATA POINTS IS 5
THE MAXIMUM DEGREE OF FIT IS 1
THE Y-AXIS SCALE IS 0.10 IN DEGREES PER INCH
THE X-AXIS SCALE IS 1.00 IN OHM-CM PER INCH
THE INITIAL TEMPERATURE (T0) WAS 15.00IN DEG C

DIMENSIONAL VALUES		NONDIMENSIONAL VALUES	
TEMPERATURE (DEGREES C)	RESISTIVITY (OHM-CM)	THETA	RHO-PRIME
25.0	3134.0	0.666667	1.000000
30.3	2822.8	1.020000	0.900702
39.0	2439.1	1.600000	0.778271
47.3	2188.5	2.153333	0.698309
51.4	2031.9	2.426667	0.648341

COEFFICIENTS OF THE POWER SERIES EXPANSION
Y(X)=B(1)+B(2)*X+B(3)*X**2...

B(1)= 1.11070D 00 B(2)=-1.94223D-01

ESTIMATES OF ERROR FOR THE COEFFICIENTS

ERRB(1)=4.886D-02 ERRB(2)=2.862D-02
SUM SQ DEV = 2.156D-04 F-RATIO = 4.605D 01
CHISQ= 1.276D-03 DEG OF FREEDOM = 3.

1	0.667	1.00000000D 00	9.8122036D-01	-1.8779641D-02
2	1.020	9.0070198D-01	9.1259474D-01	1.1892766D-02
3	1.600	7.7827058D-01	7.9994515D-01	2.1674569D-02
4	2.153	6.9830887D-01	6.9247485D-01	-5.8340231D-03
5	2.427	6.4834078D-01	6.3938711D-01	-8.9536710D-03

TEMPERATURE AND RESISTIVITY VALUES
DATA SET G

COOLING CONDITIONS

THE NUMBER OF DATA POINTS IS 10
THE MAXIMUM DEGREE OF FIT IS 1
THE Y-AXIS SCALE IS 0.10 IN DEGREES PER INCH
THE X-AXIS SCALE IS 1.00 IN OHM-CM PER INCH
THE INITIAL TEMPERATURE (TO) WAS 15.00IN DEG C

DIMENSIONAL VALUES		NONDIMENSIONAL VALUES	
TEMPERATURE (DEGREES C)	RESISTIVITY (OHM-CM)	THETA	RHO-PRIME
23.0	3416.5	0.533333	1.000000
24.7	3253.6	0.646667	0.952320
28.0	3105.5	0.866667	0.908971
30.7	2970.3	1.046667	0.869399
35.5	2732.3	1.366667	0.799737
39.0	2587.2	1.600000	0.757266
45.5	2371.3	2.033333	0.694073
50.8	2217.0	2.386667	0.648910
56.3	2069.0	2.753333	0.605591
63.2	1917.5	3.213333	0.561247

COEFFICIENTS OF THE POWER SERIES EXPANSION
Y(X)=B(1)+B(2)*X+B(3)*X**2...

B(1)= 1.04624D 00 B(2)=-1.62031D-01

ESTIMATES OF ERROR FOR THE COEFFICIENTS

ERRB(1)=5.445D-02 ERRB(2)=2.922D-02
SUM SQ DEV = 5.236D-04 F-RATIO = 3.074D 01
CHISQ= 7.122D-03 DEG OF FREEDOM = 8.

I	X(I)	F2(I)	Y(I)	DELY(I)
1	0.533	1.0000000D 00	9.5982118D-01	-4.0178821D-02
2	0.647	9.5231963D-01	9.4145771D-01	-1.0861910D-02
3	0.867	9.0897117D-01	9.0581099D-01	-3.1601795D-03
4	1.047	8.6939851D-01	8.7664549D-01	7.2469802D-03
5	1.367	7.9973657D-01	8.2479571D-01	2.5059133D-02
6	1.600	7.5726621D-01	7.8698857D-01	2.9722365D-02
7	2.033	6.9407288D-01	7.1677533D-01	2.2702445D-02
8	2.387	6.4890970D-01	6.5952453D-01	1.0614822D-02
9	2.753	6.0559052D-01	6.0011332D-01	-5.4771997D-03
10	3.213	5.6124689D-01	5.2557926D-01	-3.5667635D-02

TEMPERATURE AND RESISTIVITY VALUES
DATA SET H

HEATING CONDITIONS

THE NUMBER OF DATA POINTS IS 5
THE MAXIMUM DEGREE OF FIT IS 1
THE Y-AXIS SCALE IS 0.10 IN DEGREES PER INCH
THE X-AXIS SCALE IS 1.00 IN OHM-CM PER INCH
THE INITIAL TEMPERATURE (T0) WAS 7.50IN DEG C

DIMENSIONAL VALUES		NONDIMENSIONAL VALUES	
TEMPERATURE (DEGREES C)	RESISTIVITY (OHM-CM)	THETA	RHO-PRIME
24.7	3062.9	2.293333	1.000000
30.0	2744.0	3.000000	0.895883
40.7	2316.8	4.426667	0.756407
45.4	2142.7	5.053333	0.699566
50.7	1970.0	5.760000	0.643181

COEFFICIENTS OF THE POWER SERIES EXPANSION
Y(X)=B(1)+B(2)*X+B(3)*X**2...

B(1)= 1.21594D 00 B(2)=-1.01526D-01

ESTIMATES OF ERROR FOR THE COEFFICIENTS

ERRB(1)=5.413D-02 ERRB(2)=1.258D-02
SUM SQ DEV = 1.566D-04 F-RATIO = 6.512D 01
CHISQ= 9.317D-04 DEG OF FREEDOM = 3.

I	X(I)	F2(I)	Y(I)	DELY(I)
1	2.293	1.0000000D 00	9.8310763D-01	-1.6892365D-02
2	3.000	8.9588299D-01	9.1136272D-01	1.5479733D-02
3	4.427	7.5640733D-01	7.6651921D-01	1.0111887D-02
4	5.053	6.9956577D-01	7.0289636D-01	3.3305936D-03
5	5.760	6.4318130D-01	6.3115145D-01	-1.2029849D-02

TEMPERATURE AND RESISTIVITY VALUES
DATA SET H

COOLING CONDITIONS

THE NUMBER OF DATA POINTS IS 10
THE MAXIMUM DEGREE OF FIT IS 1
THE Y-AXIS SCALE IS 0.10 IN DEGREES PER INCH
THE X-AXIS SCALE IS 1.00 IN OHM-CM PER INCH
THE INITIAL TEMPERATURE (TO) WAS 7.50IN DEG C

DIMENSIONAL VALUES		NONDIMENSIONAL VALUES	
TEMPERATURE (DEGREES C)	RESISTIVITY (OHM-CM)	THETA	RHO-PRIME
24.0	3267.4	2.200000	1.000000
24.5	3267.4	2.266667	1.000000
25.0	3267.4	2.333333	1.000000
26.5	3147.3	2.533333	0.963243
31.4	2901.0	3.186667	0.887862
37.2	2658.7	3.960000	0.813705
44.5	2364.8	4.933333	0.723756
49.5	2226.4	5.600000	0.681398
65.5	1842.6	7.733333	0.563935
70.5	1757.4	8.400000	0.537859

COEFFICIENTS OF THE POWER SERIES EXPANSION
Y(X)=B(1)+B(2)*X+B(3)*X**2...

B(1)= 1.15284D 00 B(2)=-7.77955D-02

ESTIMATES OF ERROR FOR THE COEFFICIENTS

ERRB(1)=7.009D-02 ERRB(2)=1.450D-02
SUM SQ DEV = 7.999D-04 F-RATIO = 2.880D 01
CHISQ= 1.099D-02 DEG OF FREEDOM = 8.

I	X(I)	F2(I)	Y(I)	DELY(I)
1	2.200	1.00000000D 00	9.8168727D-01	-1.8312735D-02
2	2.267	1.00000000D 00	9.7650090D-01	-2.3499101D-02
3	2.333	1.00000000D 00	9.7131453D-01	-2.8685467D-02
4	2.533	9.6324295D-01	9.5575544D-01	-7.4875103D-03
5	3.187	8.8786191D-01	9.0492905D-01	1.7067140D-02
6	3.960	8.1370509D-01	8.4476720D-01	3.1062116D-02
7	4.933	7.2375589D-01	7.6904626D-01	4.5290368D-02
8	5.600	6.8139805D-01	7.1718260D-01	3.5784546D-02
9	7.733	5.6393463D-01	5.5121889D-01	-1.2715739D-02
10	8.400	5.3785885D-01	4.9935523D-01	-3.8503620D-02

SAMPLE DATA

SPHERICAL PROBE

DATA SET I

T (SEC)	I (AMPS)	TAU	R (CM)	R/RO	R (CM)	R/RO	R (CM)	R/RO
			R-27		ROCHROME		R-37	
30.0	0.050	0.78	1.05	1.62				
60.0	0.050	1.56	1.20	1.85	NOT		NOT	
120.0	0.050	3.12	1.45	2.23				
240.0	0.050	6.25	1.85	2.85	USED		USED	
480.0	0.050	12.50	2.00	3.08				
960.0	0.050	25.00	2.30	3.54				

THETA/GO 0.1260
RESISTIVITY (OHM-CM) 2420.0
ISOTHERM (DEGREE C) 27.9
THE INITIAL TEMPERATURE WAS 19.2 DEGREES C.
THE PROBE RADIUS (ACTUAL) WAS 0.241 CM.
THE PROBE RADIUS IN THE PICTURES WAS 0.650 CM.

SPHERICAL PROBE

DATA SET J

T (SEC)	I (AMPS)	TAU	R (CM)	R/RO	R (CM)	R/RO	R (CM)	R/RO
			R-27		ROCHROME		R-37	
30.0	0.060	0.78	1.10	2.90	0.90	2.37	0.0	0.0
60.0	0.060	1.56	1.40	3.68	1.10	2.90	0.90	2.37
120.0	0.060	3.12	1.65	4.34	1.40	3.68	1.00	2.63
240.0	0.060	6.25	2.15	5.66	1.70	4.47	1.25	3.29
480.0	0.060	12.5	2.65	6.97	2.05	5.40	1.45	3.82
960.0	0.060	25.00	3.30	8.68	2.55	6.71	1.70	4.47

THETA/GO	0.0200	0.0282	0.0572
RESISTIVITY (OHM-CM)	3605.0	3520.0	3190.0
ISOTHERM (DEGREE C)	27.9	29.9	37.0

THE INITIAL TEMPERATURE WAS 23.0 DEGREES C.
THE PROBE RADIUS (ACTUAL) WAS 0.241 CM.
THE PROBE RADIUS IN THE PICTURES WAS 0.38 CM.

SAMPLE DATA

CYLINDRICAL PROBE (L/D=4)

DATA SET K

T (SEC)	I (AMPS)	TAU	R (CM)	R/RO	R (CM)	R/RO	R (CM)	R/RO
			R-27		ROCHROME		R-37	
30.0	0.030	3.11	0.70	3.68	0.0	0.0	NOT	
60.0	0.030	6.23	0.90	4.74	0.50	2.63		
120.0	0.030	12.45	1.15	6.05	0.80	4.21	USED	
240.0	0.030	24.91	1.42	7.47	1.10	5.79		

THETA/GO 0.367 0.501
RESISTIVITY (OHM-CM) 3465.7 3324.9
ISOTHERM (DEGREE C) 27.9 29.9
THE INITIAL TEMPERATURE WAS 22.5 DEGREES C.
THE PROBE RADIUS (ACTUAL) WAS 0.121 CM.
THE PROBE RADIUS IN THE PICTURES WAS 0.19 CM.
THE PROBE LENGTH WAS 0.96 CM.

CYLINDRICAL PROBE (L/D=10)

DATA SET L

T (SEC)	I (AMPS)	TAU	R (CM)	R/RO	R (CM)	R/RO	R (CM)	R/RO
			R-27		ROCHROME		R-37	
60.0	0.090	6.23	0.80	4.00	0.50	2.50	NOT	
120.0	0.090	12.45	1.20	6.00	0.90	4.50	USED	
240.0	0.090	24.91	1.55	7.75	1.30	6.50		

THETA/GO 0.357 0.452
RESISTIVITY (OHM-CM) 3465.7 3324.9
ISOTHERM (DEGREE C) 27.9 29.9
THE INITIAL TEMPERATURE WAS 20.4 DEGREES C.
THE PROBE RADIUS (ACTUAL) WAS 0.121 CM.
THE PROBE RADIUS IN THE PICTURES WAS 0.200 CM.
THE PROBE LENGTH WAS 2.42 CM.

CYLINDRICAL PROBE (L/D=20)

DATA SET M

T (SEC)	I (AMPS)	TAU	R (CM)	R/RO	R (CM)	R/RO	R (CM)	R/RO
			R-27		ROCHROME		R-37	
30.0	0.150	3.11	0.70	4.31	0.48	2.95	0.0	0.0
60.0	0.150	6.23	1.20	7.39	0.80	4.92	0.0	0.0
120.0	0.150	12.45	1.62	9.97	1.15	7.08	0.45	2.77
240.0	0.150	24.91	2.20	13.54	1.62	9.97	0.70	4.31

THETA/GO 0.356 0.489 NOT
RESISTIVITY (OHM-CM) 3551.7 3480.0 USED
ISOTHERM (DEGREE C) 27.9 29.9
THE INITIAL TEMPERATURE WAS 22.5 DEGREES C.
THE PROBE RADIUS (ACTUAL) WAS 0.121 CM.
THE PROBE RADIUS IN THE PICTURES WAS 0.163 CM.
THE PROBE LENGTH WAS 4.84 CM.

REFERENCES

1. Aronow, S., "The Use of Radio Frequency Power in Making Lesions in the Brain," Journal of Neurosurgery, p. 431-438, May, 1960.

2. Fager, C. A., "Use of the Radio Frequency Electrode in Stereotactic Surgery of Parkinson's Disease," Surgical Clinics of North America, v. 45, p. 705-713, 1965.

3. Szekely, E. G., Egyed, J. J., Jacobi, C. G., Moffet, R., Spiegel, E. A., "High Frequency Coagulation by Means of a Stylet Electrode under Temperature Control," Confinia Neurologica, v. 26, p. 146-151, 1966.

4. Van Den Berg, J. W., Van Manen, J., "Graded Coagulation of Brain Tissue," Acta Physiologica et Pharmacologica, v. 10, p. 353-377, 1962.

5. Gengler, P. L., Heat Transfer Analysis of a Radio Frequency Brain Probe, MSME Thesis, Naval Postgraduate School, 1971.

6. U. S. Army Foreign Science and Technology Center FSTC-HT-23-1-67, Liquid Crystals, by I. G. Chistyakov, June 1967.

7. Carpenter, M. B., Whittier, J. R., "Study of Methods for Producing Experimental Lesions of the Central Nervous System with Special Reference to Stereotaxic Technique," Journal of Comparative Neurology, v. 97, p. 73-117, 1954.

8. Groff, J. P., Design and Analysis of a Resistively Heated Surgical Probe, MSME Thesis, Naval Postgraduate School, 1971.

9. Geddes, L. A., Baker, L. E., "The Specific Resistance of Biological Material--A Compendium of Data for the Biomedical Engineer and Physiologist," Medical and Biological Engineering, v. 5, p. 271-293, 1967.

10. Cooper, T. E., Trezek, G. J., "Correlation of Thermal Properties of Some Human Tissue with Water Content," Aerospace Medicine, v. 42, No. 1, p. 24-27, January 1971.

11. Holman, J. P., Heat Transfer, Second Edition, p. 98-103, McGraw-Hill, 1968.

12. Ozisik, M. N., Boundary Value Problems of Heat Conduction, Chap. 9, International Textbook Company, 1968.

13. Crandall, S. H., Engineering Analysis, p. 171-173, McGraw-Hill, 1956.

14. Petrovic, W. K., An Experimental Investigation of the Temperature Field Produced by a Surgical Cryoprobe, MSME Thesis, Naval Postgraduate School, 1972.

15. Feinstein, B., Alberts, W. W., Wright, E. W. Jr., "Implantable Thermistor Electrodes for Radio Frequency Lesion Production," Journal of Neurosurgery, v. 30, p. 313-314, March 1969.

16. Rosomoff, H. L., Carroll, F., Brown, J., Sheptak, P., "Percutaneous Radio Frequency Cervical Cordotomy: Technique," Journal of Neurosurgery, v. 23, p. 639-644, 1965.

17. Gray, G. W., Molecular Structure and the Properties of Liquid Crystals, Academic Press, 1962.

18. Fergason, J. L., Taylor, T. R., Harsch, T. B., "Liquid Crystals and Their Application," Electro-Technology, v. 85, No. 1, p. 41-50, January 1970.

19. Westinghouse Electric Corporation Technical Report, Basic Studies of Liquid Crystals as Related to Electro-optical and Other Devices, by L. C. Scala, G. D. Dixon, and D. F. Ciliberti, August 1970.

20. Battelle Memorial Institute, Liquid Crystals, by G. H. Brown, J. W. Doane, D. L. Fisher, and V. Neff, November 1970.

21. Fergason, J. L., "Liquid Crystals," Scientific American, v. 211, No. 2, p. 76-86, August 1964.

22. Fergason, J. L., Brown, G. H., "Liquid Crystals and Living Systems," Journal of American Oil Chemicals Society, v. 45, No. 3, p. 120-127, March 1968.

23. Fergason, J. L., "Liquid Crystals in Nondestructive Testing," Applied Optics, v. 7, No. 9, p. 1729-1737, September 1968.

24. Subramanyan, S. V., "Optical Reflections from Cholesteric Liquid Crystal Films," Applied Optics, v. 10, No. 2, p. 317-320, February 1971.

25. Fergason, J. L., "Experiments with Cholesteric Liquid Crystals," American Journal of Physics, v. 38, No. 4, p. 425-428, April 1970.

26. Dowden, W. A., "Cholesteric Liquid Crystals: A Review of Developments and Applications," Nondestructive Testing, v. 1, No. 2, p. 99-102, November 1967.

27. Naval Postgraduate School Mechanical Laboratory II Report, Thermal Mapping of Surface Temperatures Using Cholesteric Liquid Crystals, by J. F. Meyer, D. K. MacKenzie, A. H. Wirzburger, June 1972.

28. Lawrence Laboratory Report UCRL-14754, TRUMP, A Computer Program for Transient and Steady State Temperature Distribution in Multidimensional Systems, by A. L. Edwards, July 1, 1969.

29. Erbayram, C., A Computer Program for Solving Transient Heat Conduction Problems, MSME Thesis, Naval Postgraduate School, 1971.

30. Kline, S. J., McClintock, F. A., "Describing Uncertainties in Single Sample Experiments," Mechanical Engineering, v. 75, p. 3, January 1953.

INITIAL DISTRIBUTION LIST

		No. Copies
1.	Defense Documentation Center Cameron Station Alexandria, Virginia 22314	2
2.	Library, Code 0212 Naval Postgraduate School Monterey, California 93940	2
3.	Mechanical Engineering Department Library, Code 59 Naval Postgraduate School Monterey, California 93940	1
4.	Assistant Professor T. E. Cooper, Code 59Cg Department of Mechanical Engineering Naval Postgraduate School Monterey, California 93940	3
5.	LCDR Richard G. Katz 132 Leidig Circle Monterey, California 93940	1

UNCLASSIFIED
Security Classification

DOCUMENT CONTROL DATA · R & D

(Security classification of title, body of abstract and indexing annotation must be entered when the overall report is classified)

ORIGINATING ACTIVITY (Corporate author)

Naval Postgraduate School
Monterey, California 93940

2a. REPORT SECURITY CLASSIFICATION

Unclassified

2b. GROUP

REPORT TITLE

Experimental Investigation of the Heat Transfer Characteristics of a Radio Frequency Surgical Probe

DESCRIPTIVE NOTES (Type of report and inclusive dates)

Master of Science in Mechanical Engineering and Mechanical Engineer

AUTHOR(S) (First name, middle initial, last name)

Richard G. Katz

REPORT DATE	7a. TOTAL NO. OF PAGES	7b. NO. OF REFS
March 1973	114	30

a. CONTRACT OR GRANT NO.	9a. ORIGINATOR'S REPORT NUMBER(S)
b. PROJECT NO.	
c.	9b. OTHER REPORT NO(S) (Any other numbers that may be assigned this report)
d.	

10. DISTRIBUTION STATEMENT

Approved for public release; distribution unlimited.

11. SUPPLEMENTARY NOTES	12. SPONSORING MILITARY ACTIVITY
	Naval Postgraduate School Monterey, California 93940

13. ABSTRACT

Liquid crystals, a material that exhibits brilliant changes in color over narrow temperature bands, have been successfully used to study the temperature field produced by spherical and cylindrical radio frequency surgical probes. An agar-water mixture was used to simulate tissue. Experimental temperature data were obtained by photographing the liquid crystal material through the clear agar. Comparison of experimental data with an existing theoretical solution was excellent, agreeing within 8% for the spherical probe. However, the cylindrical data and cylindrical theory agreed only to within 30%, the large discrepancy being attributed to edge effects.

DD FORM 1 NOV 65 1473 (PAGE 1)
S/N 0101-807-6811

UNCLASSIFIED
Security Classification

A-31408

14. KEY WORDS	LINK A		LINK B		LINK C	
	ROLE	WT	ROLE	WT	ROLE	WT
Radio Frequency Heating						
Surgical Probe						
Heat Transfer						
Liquid Crystals						
Thermal Mapping						

Thesis
K1454
c.1

143837

Katz
Experimental investigation of the heat transfer characteristics of a radio frequency surgical probe.